

**NASA
Technical
Paper
3280**

1992

Equations of Motion of Slung-Load Systems, Including Multilift Systems

Luigi S. Cicolani
and Gerd Kanning
*Ames Research Center
Moffett Field, California*

NASA

National Aeronautics and
Space Administration

Office of Management

Scientific and Technical
Information Program



CONTENTS

	Page
SYMBOLS	v
SUMMARY	1
1. INTRODUCTION	1
Background	1
Equations of Motion for Slung-Load Systems	3
Equations of Motion for Multibody Systems	4
2. SYSTEM DESCRIPTION	5
3. EQUATIONS OF MOTION FOR GENERAL SLUNG-LOAD SYSTEMS	6
Configuration Vectors	6
Kinematics	7
Equations of Motion	7
Simulation Equations for Inelastic Suspensions Using d'Alembert's Principle	8
Simulation Equations for Inelastic Suspension: Explicit Constraint Method	11
Simulation Equations for Inelastic Suspensions from Lagrange's Equations	12
Simulation Equations for Inelastic Suspensions Using Rigid-Body Velocity Coordinates	13
4. APPLICATIONS	14
General Procedure	14
Examples	17
5. APPROXIMATE NONLINEAR MODELS	18
Degenerate Body Approximations	19
Center-of-Gravity Attachments	20
Simplified Helicopter Model	21
6. LINEARIZED EQUATIONS OF MOTION FOR GENERAL SLUNG-LOAD SYSTEMS WITH INELASTIC SUSPENSIONS	24
Applied External Forces	25
Reference Trajectories	26
Linearized Equations from Lagrange's Equation	27
Linearized Equations from d'Alembert's Principle	29
Linearized Equations from Explicit Constraint Method	32
Linearized Equations for Dual-Lift Systems	35
7. CONCLUSIONS	35
APPENDIX A.—SUMMARY OF USEFUL KINEMATIC RELATIONS	37
APPENDIX B.—SIMULATION EQUATIONS FOR SINGLE-POINT SUSPENSIONS	47
APPENDIX C.—SIMULATION EQUATIONS FOR BIFILAR SUSPENSIONS	61
APPENDIX D.—SIMULATION EQUATIONS FOR DUAL-LIFT SYSTEMS	75

APPENDIX E.—SIMULATION EQUATIONS FOR A MULTILIFT SYSTEM WITH PENDANT SUSPENSION	97
APPENDIX F.—LINEARIZED EQUATIONS FOR DUAL-LIFT SYSTEM WITH SPREADER BAR.....	107
REFERENCES.....	121

SYMBOLS

A, B	$6n \times d$ and $6n \times \pi$ matrices of the kinematic relation $v = Au + B\dot{p}$; A, B are the Jacobians, $[\nabla_u^T v]$, $[\nabla_p^T v]$
$AI1, \Lambda$	row partitions of A^{-1} in the case that u is partitioned as $(u1, \dot{\lambda})$; $AI1, \Lambda$ are the Jacobians $[\nabla_v u_1^T]$, $[\nabla_v \dot{\lambda}^T]$
$A1, L$	column partitions of A for elastic suspension with u partitioned as $(u1, \dot{\lambda})$; $A1, L$ are the Jacobians $[\nabla_{u1}^T v]$, $[\nabla_{\dot{\lambda}}^T v]$
$B1, \dots, Bn$	enumerated rigid bodies of a slung-load system
$C1, \dots, Cm$	enumerated cables or straight line links in the suspension of a slung-load system
c	number of constraints imposed by the inelastic suspension on the motion of the system of n rigid bodies
d	number of degrees of freedom of the system of n rigid bodies
D	block-diagonal matrix of the system's rigid-body masses and inertias (eq. (3))
$E_1(\cdot), E_2(\cdot), E_3(\cdot)$	single-axis rotational transformation about i, j, k axes, respectively, through angle (\cdot) (appendix A)
f	list of resultant forces and c.g. moments on each rigid body (eq. (2)), (see note 1 at end of symbols list)
fa	list of resultant aerodynamic forces and c.g. moments on each rigid body (eq. (2); note 1)
fb_a	identical to fa , except that forces are given in body axes (eq. (34))
fc	list of resultant suspension forces and c.g. moments on each rigid body (eq. (2); note 1)
f^*	list of translational and rotational inertia reactions of each rigid body (eq. (3); note 1)
fg	list of gravitational forces on each rigid body
fo	sum of external forces and inertia coupling terms from f^* (eq. (8))
\mathcal{F}_a	reference frame; the subscript a can be any of N for Newtonian space; or $\{1, 2, \dots, n\}$ for rigid-body axes of body $B1, \dots, Bn$; or $\{c1, \dots, cm\}$ for cable axes of cable $C1, \dots, Cm$
FA1, MA1, ...	resultants of all forces and c.g. moments on body $B1, \dots$, due to aerodynamics and rotor
Fb_{va}, Fb_{δ}	matrices of stability and control derivatives for the configuration of n rigid bodies (eq. (36))
FC1, MC1, ...	resultants of all forces and c.g. moments on body $B1, \dots$, due to the suspension
g	gravitational constant
\mathbf{g}	gravity vector
$h1, h2, \dots$	list of forces and c.g. moments per unit tension on each rigid body due to cable attachment $1, \dots, M$ (eq. (10))
H	any basis of the linear vector space containing fc in the case of inelastic suspensions
$H1, H2, \dots$	list of forces and c.g. moments per unit tension due to cable $C1, C2, \dots$, when the cables are attached to two rigid bodies; enumerated columns of the matrix H (eq. (11))
$\{ia, ja, ka\}$	right-handed orthonormal vectors defining a reference frame \mathcal{F}_a
I, O	unit and zero matrices; dimensions are implied by context
$J, J1, Jb, \dots$	inertias measured in body axes; appended symbol indicates the body
$k, k_q, k_{\dot{q}}, k_u$	quadratic velocity term in the equations of motion and its gradients with q, \dot{q}, u
KE	kinetic energy of a system
$K1, c1, \dots, Km, cm$	cable spring constant and damping coefficient for cable $C1, \dots, Cm$
$l01, l1, \dots, lom, lm$	unloaded and loaded cable lengths of cables $C1, \dots, Cm$
m	number of cables and links in the suspension
$m1, J1, \dots, mn, Jn$	masses and inertia matrices of rigid bodies $B1, \dots, Bn$
M	number of attachments of a cable to a rigid body of the system
n	number of rigid bodies in the system
p	suspension parameters that can be controlled; $p = (p_1, \dots, p_\pi)^T$
q	generalized position coordinates of the system; $q = (q_1, \dots, q_d)^T$
$Q, Q_q, Q_{\dot{q}}, Q_u, Q_{\delta}$	generalized forces and their gradients with q, \dot{q}, \dots

$Q, Q_q, Q_{\dot{q}}, Q_u, Q_\delta$	generalized forces and their gradients with q, \dot{q}, \dots
r, v	lists of the inertial c.g. position and Euler attitude angles, and the inertial c.g. velocities and angular velocities of the n rigid bodies (eq. (1); note 1)
R, V	position, velocity vectors relative to inertial space; appended numbers indicate specific points or line segments between points ($\mathbf{R12} = \mathbf{R2} - \mathbf{R1}$, etc.); the star notation $\mathbf{R1}^*, \mathbf{V1}^*, \dots$, indicates the c.g. of body $B1, \dots$
s	suspension force parameters for inelastic suspensions; $s = (s_1, \dots, s_c)^T$
$S(V_a)$	skew-symmetric matrix representing cross-product operation with \mathbf{V} for vectors referred to \mathcal{F}_a (appendix A)
T	matrix of coordinate transformations to convert configuration vectors with inertial components to configuration vectors with body axis components (eq. (35))
$T_{a,b}$	transformation of physical vectors from frame \mathcal{F}_b to frame \mathcal{F}_a ; all transformations are defined from Euler angles (appendix A)
$TC1, \dots, TCm$	cable tensions for cable $C1, \dots, Cm$
u	generalized velocity coordinates of the system of rigid bodies
$(u1, \dot{\lambda})$	generalized velocity coordinates u for the system with elastic suspension separated into $6n - c$ coordinates, $u1$, which define the system with inelastic suspension, and c coordinates, $\dot{\lambda}$, which define the system motion due to suspension stretching
va	configuration velocity with c.g. velocities given relative to the mean wind in body axis components (eq. (34))
VA	velocity vector relative to the mean wind; appended numbers indicate specific point
V0, VA0	reference trajectory velocity relative to ground or mean wind
w	configuration vector of wind velocities (eq. (34))
W0	mean wind velocity
Wi	row list of the axes of rotation of the Euler attitude angles of body Bi (appendix A)
X, X_u, X_v, X_q	configuration vector of inertia-coupling terms in f^* (eq. (3)), and its gradients with u, v, q
α, ω	rigid-body Euler angle triplet (ϕ, θ, ψ) (appendix A) and angular velocity, both relative to inertial space; appended numbers indicate specific body
$\delta, \delta i$	list of controls for the configuration of n bodies, or for body Bi
$\delta r, \delta v, \delta u, \delta q, \dots$	variations r, v, u, q, \dots , from their reference values
ξ, ξ_u	the inertia reaction, $\dot{A}u$, and its gradients with u
ξ_{ij}	c.g. moment per unit tension of cable C_j on body Bi
$()_a$	physical vector given by its coordinates in frame \mathcal{F}_a , the subscript indicates the specific frame (note 2)
$()_o$	quantity evaluated at a reference flight condition
$()^T$	transpose of $()$
\bullet, \times	dot and cross-product operators for physical vectors
∇_z	gradient vector; column of partial derivatives with respect to z , where z is any list of scalar variables defined in context
$\Delta, \Delta i$	variations of $\delta, \delta i$ for their reference value

Notes:

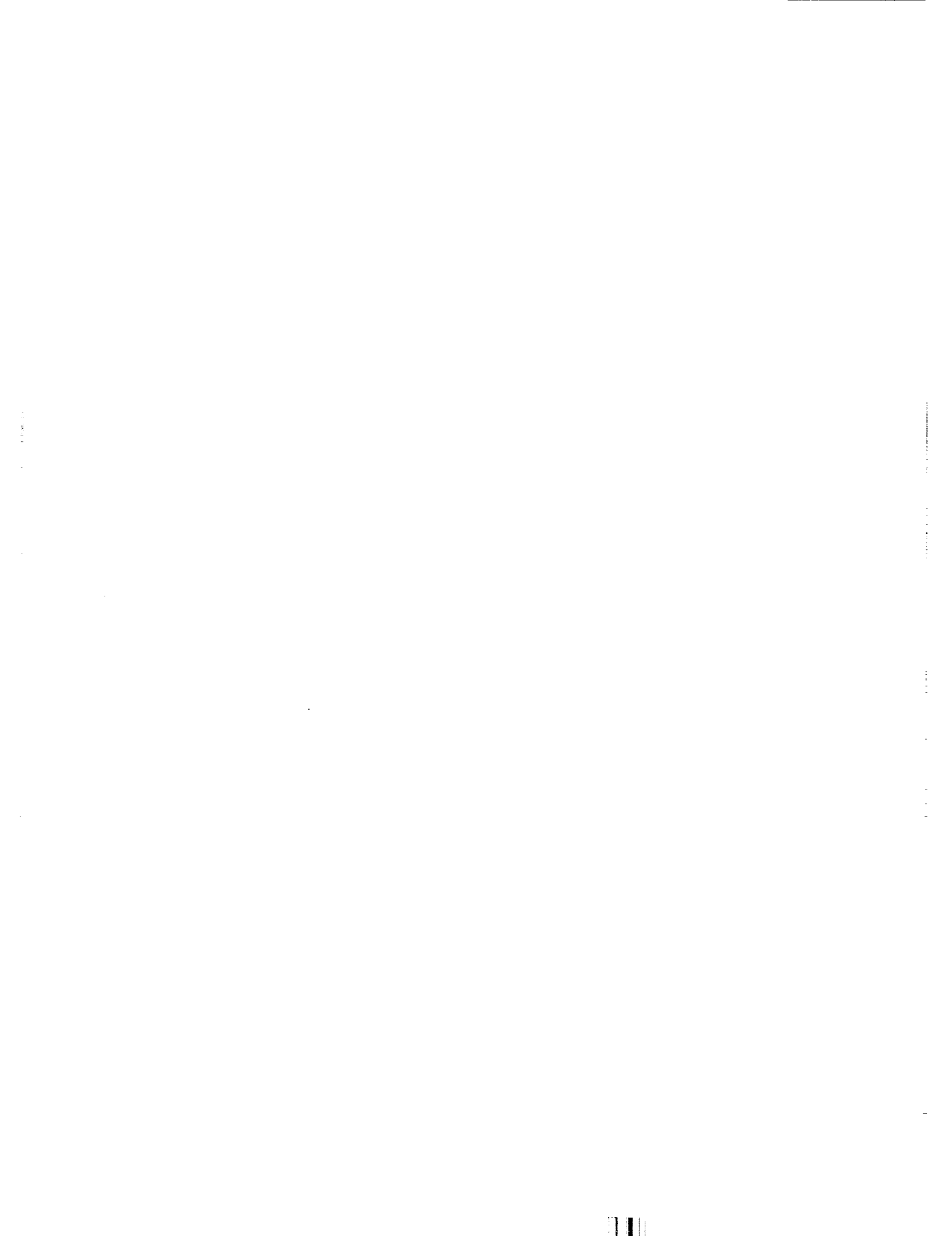
1. Standard axes are adopted for the physical vector elements which make up the configuration vectors $f, fa, fc, f^*, fg, fo, r, v$. Forces and c.g. positions and velocities are given by their inertial components, and the c.g. moments and angular velocities are given by their coordinates in the body axes of their associated rigid body.

2. Boldface symbols indicate physical vectors independent of any reference frame ($\mathbf{R}, \mathbf{V}, \dots$). Vectors given by their coordinates in a frame are in lightface (R_N, V_N, \dots).

The notation follows various rules or habits which provide a succinct treatment of the problem while maintaining physical insight and programmable forms. A degree of notational economy beyond that previously used in work on single-helicopter systems is useful to treat the more complex multilift systems.

First, configuration vectors and matrices are introduced to deal with the general n -body system. These are objects in $6n$ -dimensional space composed of three-dimensional vectors associated with the c.g. and rotational dynamics of the n -constituent bodies. The applications work is done entirely in terms of natural vectors and matrices from three-dimensional rigid-body mechanics. These are the largest objects for which detailed physical insight is readily maintained. Further expansion to scalar components of these objects is strictly avoided in order to avoid the unmanageable number of scalar dynamic terms that can arise in multilift analysis.

Second, the coordinate frames in which vectors are specified are indicated systematically in all equations throughout the text, using subscripts as stated above, in order to maintain a programmable form. Appendix A contains useful relations to account for coordinate frames in the usual relations and operations of vector mechanics; that is, an algebra of transformations is combined with the usual vector mechanics. The result is that the underlying vector-mechanical and transformation-algebraic structure is retained in the working equations for efficient analysis and programming. For example, the dynamic terms in the equations of motion in the applications results consist almost entirely of coordinate transformations and their derivatives, Coriolis effects, and centrifugal accelerations; this mass of terms is stated in a brief, programmable form.



EQUATIONS OF MOTION OF SLUNG-LOAD SYSTEMS, INCLUDING MULTILIFT SYSTEMS

Luigi S. Cicolani and Gerd Kanning
Ames Research Center

SUMMARY

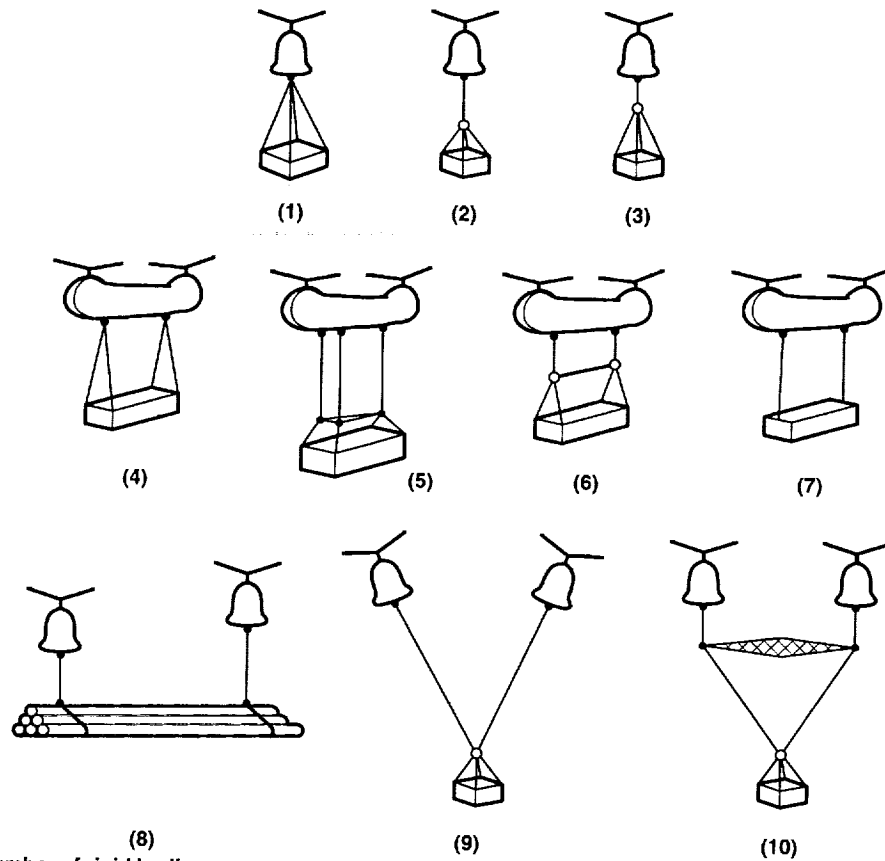
General simulation equations are derived for the rigid body motion of slung-load systems. This work is motivated by an interest in trajectory control for slung loads carried by two or more helicopters. An approximation of these systems consists of several rigid bodies connected by straight-line cables or links. The suspension can be assumed elastic or inelastic. Equations for the general system are obtained from the Newton-Euler rigid-body equations with the introduction of generalized velocity coordinates. Three forms are obtained: two generalize previous case-specific results for single-helicopter systems with elastic and inelastic suspensions, respectively, and the third is a new formulation for inelastic suspensions. The latter is derived from the elastic suspension equations by choosing the generalized coordinates so that motion induced by cable stretching is separated from motion with invariant cable lengths, and by then nulling the stretching coordinates to get a relation for the suspension forces. The result is computationally more efficient than the conventional formulation, is readily integrated with the elastic suspension formulation, and is easily applied to the complex dual-lift and multilift systems. Results are given for two-helicopter systems; three configurations are included and these can be integrated in a single simulation. Equations are also given for some single-helicopter systems, for comparison with the previous literature, and for a multilift system. Equations for degenerate-body approximations (point masses, rigid rods) are also formulated and results are given for dual-lift and multilift systems. Finally, linearized equations of motion are given for general slung-load systems are presented along with results for the two-helicopter system with a spreader bar.

1. INTRODUCTION

Background

Various actual and proposed slung-load systems are illustrated in figure 1. Single-helicopter slung-load operations with the load suspended by cables in various ways from a single attachment point have been common since the 1950s. Such operations were further developed and extensively used during the Vietnam war. Later research during the period 1965-1975 for the Heavy Lift Helicopter was focused on the stabilization of difficult loads, such as the standard 8- by 8- by 20-ft cargo container (MILVAN), by means of suspensions with multiple attachment points and various control devices.

The use of two or more helicopters has been periodically proposed since the early success of single-helicopter operations using suspensions consisting of cables and spreader bars (systems 8-12 in fig. 1) (refs. 1-3). Dual-lift suspensions have received limited flight testing, have been used to carry payloads in a few isolated commercial operations, and have been advocated as an alternative either to developing new helicopters with greater payloads than those of current helicopters (ref. 4), or to obtaining larger-capacity helicopters than those locally available in a given situation. A significant obstacle to further operational development is the complexity of system motion and its guidance and control along any typical maneuvering flight path (ref. 5). Until recently, progress beyond the initial investigation of hover dynamics and control in references 6 and 7 has been hampered by the lack of realistic and comprehensive equations of motion for use in theoretical and simulation studies. Tractability of the equations for analysis and programming and computational efficiency become critical factors for the multilift systems. Whereas the slung-load systems can be viewed simply as a few rigid bodies connected by cables, considerable complexity of the equations of motion (EOMs) arises in applying the classic methods of



n = Number of rigid bodies
c = Number of constraints (inelastic suspension)
d = $6n - c$ = number of degrees of freedom
m = Number of suspension lines

System	n	c	d	m
1	2	3	9	4
2	2	1	11	1
3	2	1	11	5
4	2	3	9	4
5	2	3	9	3
6	2	1	11	7
7	2	2	10	2
8	3	2	16	2
9	3	2	16	2
10	4	4	20	4
11	4	3	21	3
12	5	6	24	6

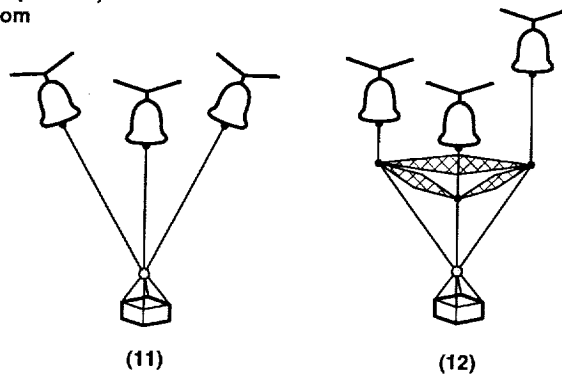


Figure 1. Examples of slung-load systems.

the previous slung-load literature to the multilift systems when the cables are modeled as inelastic.

The approach taken in this paper and in our initial report (ref. 8) is to develop a systematic analytical formulation for general slung-load systems and analytical devices tailored to such systems, which are readily applied to specific cases and yield tractable, efficient equations. The devices include special coordinates that represent the suspension constraints in an inelastic system, and the systematic use of the natural vectors and matrices of rigid-body mechanics in the applications work.

An alternative approach that would circumvent the need for further analysis would be to use one of the commercially available computer programs for the dynamics of general multibody systems. A third potential approach would be to apply the previous derivation techniques to multilift systems by using symbolic digital computations to circumvent the excessive labor and unfavorable error probabilities of extended hand analysis and programming. However, these alternative approaches are designed to accommodate a very large class of dynamic systems, and the results do not provide the insight and computational efficiency achieved here by restricting the class to slung-load systems.

Equations of Motion for Slung-Load Systems

The slung-load systems shown in figure 1 are viewed here as members of a class of systems consisting of rigid bodies connected by massless straight-line links which can be either elastic or inelastic, and which support only forces along the link. These systems are characterized by the mass, inertia, and aerodynamics of the rigid bodies, and the suspension's attachment point locations, unloaded link lengths, and link elastic parameters. The limitations of these class properties in representing the slung-load systems are as follows. The rigid-body assumption excludes flexible loads and helicopter elastic modes; cable mass and aerodynamics are neglected; and cable stretching is neglected in the case of inelastic cables. Despite these limitations, the class properties are expected to suffice for trajectory-control studies in which only low-frequency phenomena are of interest.

Previous derivations of the EOMs for single-helicopter slung-load systems have assumed either inelastic cables (refs. 9-12), or elastic cables (refs. 13-15), or considered both cable models (ref. 16). In most of

these works, the results are specific to particular suspensions, but references 13 and 15 account for a general set of elastic suspensions in which all cables connect two rigid bodies. Early work on the EOMs for multilift systems assumed inelastic cables and yielded only limited results. In reference 17, a general formulation for systems of point masses connected by inelastic cables is given, and reference 18 contains equations for the same approximation of the three-body, dual-lift system 9 of figure 1. In references 6 and 7 linearized hover equations are given for the four-body, dual-lift system 10 of figure 1, assuming a point mass load.

In the above-cited literature, the formulation of the EOMs depends principally on their use for simulation or control analysis. For simulations, the suspension is usually assumed elastic, and the equations are formulated from the Newton-Euler equations for the rigid-body velocity coordinates as, for example, in references 13-15. This method can be readily applied to most of the systems shown in figure 1, including the dual-lift and multilift systems. The forces and moments applied to the configuration by the cables appear explicitly in the equations, and are calculated from the system geometry and from a simple spring model of cable stretching.

In practice, however, cables are relatively stiff, so the rigid-body motion with inelastic cables differs very little from that with elastic cables, and a reduced-order inelastic-cable model is of interest in trajectory-control analysis. Equations of motion for inelastic cables have usually been derived from Lagrange's equations for general dynamical systems. Equations are given for a minimal set of suspension-specific, generalized position coordinates, and the nonworking suspension forces are eliminated, consistent with d'Alembert's principle. These equations require the inverse of a large system matrix and contain lengthy second-order velocity terms in exchange for the reduced system order and eliminated suspension forces. These features obstruct the use of the equations in simulations, but in controls work the objective has usually been to obtain linearized EOMs for the application of linear system theory. Satisfactory results have been obtained for single-helicopter systems by this approach, but results for dual lift have been limited to hover, where the second-order dynamics can be neglected. In addition, modern control design methods are available for aeronautical systems with significant aerodynamic or dynamic nonlinearities based on partial inversion of the nonlinear EOMs. A segment of the dual-lift control literature seeks to apply these methods (refs. 17-21). For this work, a suitable nonlinear model is needed

which is both analytically tractable and computationally efficient.

An alternative, ad-hoc analytical approach for inelastic cables is based on manipulation of the Newton-Euler equations to eliminate cable tensions in a subset of these equations. This subset is combined with kinematic constraint equations to obtain $6n$ equations for the linear and angular accelerations of the system's rigid bodies, where n is the number of bodies. Results have been obtained for single-helicopter systems (ref. 16) and, recently, for dual lift (twin lift), (refs. 19 and 20). This approach requires the inverse of a larger system matrix than is required for generalized coordinates, and the choice of coordinates is restricted.

Evidently, the dynamical equations for both elastic and inelastic suspensions are of interest. The existing formulations for these two suspension models differ significantly in form and in analytical and computational requirements, and difficulties of derivation or computation associated with existing methods for inelastic cables become significant for dual-lift and multilift systems.

In the present work, slung-load dynamics are treated systematically. For this purpose, many formulations of the equations for dynamical systems can be applied to both elastic and inelastic suspensions. The Newton-Euler equations are suited to slung-load systems and are used herein. Simulation equations are derived by applying the Newton-Euler equations to each rigid body, defining configuration vectors for the n -body system, and introducing generalized velocity coordinates. The result for inelastic cables is obtained by applying d'Alembert's principle. Two formulations are obtained, one for elastic and one for inelastic suspensions. These formulations generalize the previous case-specific results to general slung-load systems and any set of generalized coordinates. The method is similar to that described in references 22-24 for general multibody systems. The result for inelastic cables requires the inverse of a $d \times d$ matrix for which an analytical inverse is unknown, where d is the number of degrees of freedom (DOF). Slung-load systems with inelastic cables have only a few constraints, so d is relatively large, near $6n$ in all cases, where n is the number of rigid bodies. Values of d are listed in figure 1; $d = 20$ for the dual-lift system 10.

A second pair of formulations is obtained by selecting the generalized coordinates to represent the constraints found in slung-load systems. The generalized coordinates for the elastic system are selected to

be partitioned into d coordinates that represent the configuration motion with invariant cable lengths and c coordinates that define the motion caused by cable stretching, where c is the number of constraints imposed by the inelastic suspension. This can usually be done by including appropriate cable velocity coordinates in the generalized coordinates. The result for inelastic cables is obtained by nulling the cable-stretching coordinates to obtain an equation for the resultant constraint forces on the configuration's rigid bodies. The solution for this equation requires the inversion of a relatively small $c \times c$ matrix ($c = 4$ for dual-lift system 10 of fig. 1), and the resultant force appears in the EOMs as an additive force, just as in the elastic-cable equations.

The second formulation has reduced the computational penalty relative to the elastic-cable equations, can be integrated with the elastic-cable equations in one simulation, and can be expanded nearly completely in terms of natural vectors and matrices to obtain compact, tractable formulations. It is readily applied to the multilift systems. Results are given herein for the three dual-lift systems of figure 1 (systems 8-10), and these can be integrated into a single simulation. Additional results are included for some single-helicopter systems to permit comparison with past work, and for the multilift system (system 11) of figure 1 extended to any number of helicopters. The derivation and results are sufficiently brief so that hand analysis and computer programming are practical. In addition, degenerate-body (point masses, rigid rods) approximations are given for general slung-load systems and for two multilift cases. Last, linearized equations of motion are formulated for general slung-load systems, and for dual-lift system 10 of figure 1.

Equations of Motion for Multibody Systems

A large body of literature on the dynamics of multibody systems has accumulated since the early 1960s in response to the increasing importance of multibody dynamics in the design of, for example, spacecraft, machines, robotic arms, and human motion models, and the relevance of the approaches used and of the results obtained to multilift helicopter systems is of interest. The principal aim in the literature has been to develop general-purpose computer programs to provide EOMs from a minimal amount of user input data defining the multibody system. This aim is motivated by the impracticality or excessive labor and unfavorable error probabilities of using hand derivation in most working

circumstances in these applications. Theory and analysis are given, for example, in references 24-26, and surveys of computer programs that encode EOMs for a general system or that generate and compile symbolic case-specific code from user inputs are provided in references 27 and 28.

Slung-load systems differ from the applications discussed above. First, slung-load systems with inelastic cables have only a few constraints relative to the number of DOFs ($c \ll d, 6n$) and can be equally well represented as unconstrained (elastic cables). The applications cited above are all highly constrained, with relatively few DOFs. For example, spacecraft and robotic arms are commonly represented as n rigid bodies with fixed orbit or base connected by $n - 1$ joints which permit one DOF of relative rotational motion; hence, $d = d_b + n - 1$, where d_b is the number of base body DOFs. Consequently, the conventional formulation in which a $d \times d$ matrix is formed and inverted is computationally more efficient for these applications than one containing a $c \times c$ matrix, but the converse is true for slung loads. Moreover, in most references the interbody connections are modeled as joints, and then convenient generalized coordinates are predefined according to the joint model. These have little applicability to slung-load suspensions. Gimbal-type joints can represent one to three DOFs of relative rotational motion, whereas inelastic suspensions allow three to five DOFs of relative motion, and elastic suspensions impose no constraints.

One code-generating program, NEWEUL, and its underlying formulation (given in refs. 22-24), does not specialize the interbody connection and can be applied to slung loads. The equations from this program are in the conventional form which requires the inverse of a $d \times d$ matrix, and the results are obtained with all terms expanded to their scalar elements.

An alternative computer-based approach is to use symbolic computations to carry out routine analytical steps—for example, the energy derivatives in Lagrange's equations. Some general possibilities of applying MACSYMA (ref. 29) for this purpose are discussed in reference 30 and this approach is used in reference 7 to obtain linearized hover equations for dual-lift systems from Lagrange's equations.

Symbolic computation has many practical advantages, especially that of error-free derivations, and it has been applied where possible in the present work.

Its ability to generate useful scalar equations for dual-lift systems from traditional methods has been limited by the explosion in the number of scalar dynamic terms. In the present efforts, it appeared necessary to seek more efficient analytical methods. A new formulation and a new applications technique are presented which improve the computational efficiency of the inelastic-suspension equations over previous forms, and which render hand derivation, analysis, and programming feasible for the previously difficult dual-lift and multilift systems.

2. SYSTEM DESCRIPTION

The systems of interest consist of one or more helicopters that support a load (or more than one load, in some instances) by means of a suspension. For typical slung loads and nominal trajectories, the total load to be supported by the helicopters due to load weight, acceleration, and aerodynamics, is dominated by the load weight. The suspension consists of cables, usually of nylon webbing, and hooks, rings, isolator springs, spreader bars, and other hardware (ref. 31). Suspension designs with controllable geometry obtained by active cable winching and attachment-point movement have been proposed for load-attitude stabilization (refs. 32 and 33), and are included in the present formulation.

These systems can be partitioned into n rigid bodies of non-negligible weight, B_1, \dots, B_n (helicopters, load, spreader bar). The remainder of such systems, referred to as the "suspension" hereinafter, consists of m straight-line links which support force only in the direction of the link (or only tension, in the case of cables) and have negligible mass and aerodynamic force compared to those of interest in trajectory control. The number of suspension links m is listed in figure 1 for the systems shown there. In many cases, short links attached to the load are considered part of the load rigid body, because their elastic stretch is negligible and they are immobile relative to the load. The links can be modeled as inelastic, in which case $c \leq m$ holonomic (position) constraints are imposed on the motion of the rigid bodies, and the system has $d = 6n - c$ DOFs. Values of c and d are listed in figure 1. Alternatively, the links can be modeled as elastic, because of cable or isolator-spring stretching, in which case there are $6n$ DOFs.

An examination of cable and suspension elasticity and its effect on rigid-body motion is reported in reference 34. Cable stretching under tension is usually modeled as that of an undamped spring with damping supplied by the aerodynamic resistance of the attached bodies. Cables tend to be stiff, but the suspension design must avoid an upper bound which is set by resonance with the helicopter rotor frequency (about 4–5 Hz) where a divergent pilot-induced vertical bounce mode has been observed near hover. The net result is that natural frequencies of practical suspensions are about 2–2.5 Hz. This frequency is sufficiently high to be disjoint from the frequency range of interest in trajectory control (about 0.5 Hz). The corresponding mode is one of rapid and significant cable tension variations, but with small stretching excursions so that the rigid-body coordinates are nearly unaffected.

Both elastic- and inelastic-suspension models are of interest in trajectory control. For practical suspensions, simulations can employ the simpler, more general, and more computationally efficient nonlinear equations of the elastic model. If actual suspension stiffness were significantly greater, then difficulties of numerical stability and ill conditioning might arise in real-time digital simulation of the higher-frequency, low-amplitude cable-stretching motion. In control designs, practical suspensions can be approximated as inelastic thereby eliminating feedback of states that have negligible influence on the rigid-body motion. If actual suspension stiffness were significantly lower, then the lower-frequency, higher-amplitude motions caused by cable stretching would be of interest in trajectory control. In the present report, simulation equations for both elastic and inelastic suspensions are considered.

The simulation of cable collapse is an application detail outside the scope of the present paper. If a cable collapses, the resulting system is still a member of the class of interest and can be simulated. Practical suspensions are designed and operated such that cable collapse does not occur except during large unstable excursions from the nominal configuration, or during load pickup and dropoff. System 4 of figure 1 (inverted-V suspension) is a special case in which one or two cables can collapse during small yawing motions if the cables are assumed inelastic, but this does not occur in cables with typical elastic properties.

3. EQUATIONS OF MOTION OF GENERAL SLUNG-LOAD SYSTEMS

Configuration Vectors

Physical vectors are referred to inertial or body-axis reference frames in the following discussion. Translational motion and forces are given in inertial coordinates, and rotational motion and moments are given in body axes. The reference frame is indicated by a subscript, which is N for inertial space and $i \in \{1, 2, \dots, n\}$ for body axes of the i th body. Body-axis components of translational velocity and motion variables relative to a reference body are commonly used in slung-load simulations, and are readily introduced later when generalized coordinates for an application are selected.

It is convenient to use configuration vectors that define the motion and forces of the n rigid bodies whose masses, inertias, c.g. translational motion, Euler attitude-angle triplets, and angular velocities relative to inertial space are denoted by $(m1, J1, \mathbf{R1}^*, \mathbf{V1}^*, \alpha1, \omega1), \dots, (mn, Jn, \mathbf{Rn}^*, \mathbf{Vn}^*, \alpha n, \omega n)$. The configuration vectors of position r and velocity v are defined as lists of the rigid body c.g. positions and Euler attitude angles, and the rigid-body c.g. translational and angular velocities:

$$r = \begin{pmatrix} R1^*_N \\ \vdots \\ Rn^*_N \\ \alpha1 \\ \vdots \\ \alpha n \end{pmatrix} \quad v = \begin{pmatrix} V1^*_N \\ \vdots \\ Vn^*_N \\ \omega1_1 \\ \vdots \\ \omega n_n \end{pmatrix} \quad (1)$$

Let f be a list of the resultant forces and moments applied to each rigid body, and let fg, fa, fc be corresponding lists of the gravitational forces, the aerodynamic and rotor forces, and the cable forces, respectively:

$$f = fg + fa + fc$$

$$\begin{aligned}
fg &= \begin{pmatrix} m1 \dot{g}_N \\ \vdots \\ mn \dot{g}_N \\ 0 \\ \vdots \\ 0 \end{pmatrix} fa = \begin{pmatrix} FA1_N \\ \vdots \\ FAn_N \\ MA1_1 \\ \vdots \\ MA_n \end{pmatrix} \\
fc &= \begin{pmatrix} FC1_N \\ \vdots \\ FCn_N \\ MC1_1 \\ \vdots \\ MCn_n \end{pmatrix} \quad (2)
\end{aligned}$$

where \mathbf{FA}_i , \mathbf{MA}_i are the sum of the aerodynamic and rotor forces applied to the i th body and the sum of their moments about its c.g., respectively; and where \mathbf{FC}_i , \mathbf{MC}_i are similar force and moment sums due to all cables acting on B_i . The applied forces f depend on r, v , and the helicopter controls; any dependence of the aerodynamics on the acceleration \dot{v} is assumed to be negligible.

Last, let f^* be a list of the inertia reactions of the n bodies:

$$\begin{aligned}
f^* &= - \begin{pmatrix} m1 \dot{V}1_N^* \\ \vdots \\ mn \dot{V}n_N^* \\ J1 \dot{\omega}1_1 \\ \vdots \\ Jn \dot{\omega}n_n \end{pmatrix} - \begin{pmatrix} 0 \\ \vdots \\ 0 \\ S(\omega1_1)J1 \omega1_1 \\ \vdots \\ S(\omega n_n)Jn \omega n_n \end{pmatrix} \\
&= -D \dot{v} - X \quad (3)
\end{aligned}$$

The term f^* is abbreviated to the form $-D \dot{v} - X$, where D is block-diagonal with masses and inertia matrices along the diagonal, \dot{v} is the configuration acceleration, and X contains Coriolis terms due to the use of body-axis components of rotational motion.

Kinematics

The systems of interest consist of n rigid bodies connected by m cables which impose c constraints on the motion of the rigid bodies; they have $d = 6n - c$ DOFs, where $c = 0$ for elastic cables. These are holonomic systems; that is, the constraints imposed by an inelastic suspension can be given as functions of position only. These constraints are usually

time-invariant, but in the special case of active cable winching or attachment-point movement they have explicit dependence on time. To accommodate this case, the kinematic model below includes parameters $p = (p_1, \dots, p_\pi)^T$, which can represent the controllable geometric parameters of such a suspension or other known time-varying parameters convenient to the kinematic model in particular applications.

For holonomic systems with d DOFs there exist d generalized position coordinates, $q = (q_1, \dots, q_d)^T$, which suffice to locate all points in the system and also the configuration position

$$r = r(q, p) \quad (4)$$

and d generalized velocity coordinates which suffice to define all inertial velocities of the system:

$$u = U(q, p)\dot{q} \quad (5)$$

The configuration velocity is related to u by a linear expression of the form

$$v = A(q, p)u + B(q, p)\dot{p} \quad (6)$$

Here, U is a nonsingular $d \times d$ matrix; it can be unity, but velocity coordinates different from \dot{q} are commonly useful in applications. Note that v is asserted in equation (6) to be linear in u, \dot{p} . This follows from the usual linear relationship $v(\dot{r})$ from rigid-body kinematics (appendix A),

$$\left. \begin{aligned} Vi_N^* &= \dot{R}i_N^* \\ \omega i_i &= Wi_i(\alpha i) \dot{\alpha} i \end{aligned} \right\} i = 1, \dots, n$$

and equations (4) and (5). The term A is a $6n \times d$ matrix. For inelastic suspensions, A expresses the constraints by confining that part of the configuration velocity due to u to the d -dimensional linear vector subspace defined by the columns of A . If $\dot{p} = 0$, then this subspace is tangent to the configuration trajectory $r(t)$.

Equations of Motion

The Newton-Euler equations for each rigid body are as follows:

$$Fi_N - mi \dot{V}i_N^* = 0$$

$$Mi_i - Ji \dot{\omega}i_i - S(\omega i_i) Ji \omega i_i = 0$$

where $\mathbf{F}_i, \mathbf{M}_i$ are the total applied forces and moments about the c.g. of body B_i . The same equations listed for all n bodies are

$$fc + fg + fa + f^* = 0 \quad (7)$$

To obtain the simulation equations, differentiate equation (6) with respect to time, introduce the result in f^* (eq. (3)), premultiply equation (7) by A^T , and solve for \dot{u} :

$$\dot{u} = [A^T D A]^{-1} A^T [f_o + f_c] \quad (8)$$

where

$$f_o \triangleq f_g + f_a - D \dot{A} u - X - D(B \ddot{p} + \dot{B} \dot{p})$$

The configuration vector f_o denotes the combined external forces, second-order velocity effects resulting from the choice of coordinates u, v , and the inertia reaction of the configuration to $p(t)$.

If the cables are elastic, then A is a nonsingular $6n \times 6n$ matrix and

$$\dot{u} = A^{-1} D^{-1} [f_o + f_c] \quad (9a)$$

In the case that $\dot{p} = 0$ and we choose $u = v$, then $A = I$ and the result is identical to the Newton-Euler equations applied to each body:

$$\dot{v} = D^{-1} [f_g + f_a - X + f_c] \quad (9b)$$

Equation (9b) for the rigid-body velocity coordinates can be applied to any configuration without further analysis except as needed to express f_c . Equation (9a) generalizes this case to allow a choice of generalized velocity coordinates; for example, the use of cable-velocity coordinates in u provides a convenient and well-conditioned calculation of cable lengths and directions for use in the calculation of the cable forces f_c . It should be noted here that the matrix A^{-1} in equation (9a) represents the kinematic relation $u(v)$ and can be given analytically from the kinematics as readily as the matrix A representing the reverse relation $v(u)$. Therefore, it is unnecessary to perform a matrix inversion to obtain A^{-1} .

The constraint force f_c in equations (9) can be given as a sum of forces and moments applied by the suspension at each attachment point:

$$f_c = \sum_{j=1}^M h_j TC_j$$

where j enumerates every attachment of a cable to a rigid body, h_j is a configuration vector defined in the next section, and TC_j is the cable tension, which is given by the spring model of the cable as

$$TC_j = \max\{0, K_j(\ell_j - \ell_{oj}) + c_j \dot{\ell}_j\} \quad j = 1, 2, \dots, M$$

where $\{\ell_{oj}, K_j, c_j\}$ are the unloaded cable length and cable spring and damping constants, respectively. Cable damping, $c_j \neq 0$, is introduced in reference 15,

but otherwise has been neglected in simulations with elastic-cable models. For cables made of nylon webbing, the spring rate K depends on loading and cable length (ref. 34). This dependency is readily included in the calculation of cable tensions from the above equations. If accurate simulation of the small motions that result from suspension stretching is unimportant, then a simplified spring model of the cable elasticity that is consistent with typical natural modes will suffice. The spring constants K, c are related to the cable's natural mode parameters by $\omega_n^2 = Kg/F$, $2\zeta\omega_n = cg/F$, where F is the load supported by the cable. In simulations with elastic cables, initial values of cable tension and stretch can be calculated in cases with nonredundant suspensions from the solution for the constraint forces f_c for inelastic cables given below. Alternatively, the configuration can be allowed to settle from an approximate initial arrangement, possibly with the aid of cable damping as a settling device (ref. 15).

Simulation Equations for Inelastic Suspensions Using d'Alembert's Principle

If the cables are inelastic then the cable forces f_c drop out of equation (8) ($A^T f_c = 0$) in accordance with d'Alembert's principle for constrained holonomic systems; the constraint forces do no virtual work. This result is shown as follows. First, enumerate the cable attachments $1, 2, \dots, M$ at attachment points $\mathbf{R}_1, \mathbf{R}_2, \dots, \mathbf{R}_M$ on their corresponding bodies $B_i, i = i(1), i(2), \dots, i(M)$. One or more cables are attached at an attachment point and every such attachment of a cable to a body is numbered. The constraint force on the configuration is then (see fig. 2(a))

$$f_c = \sum_{j=1}^M h_j TC_j \quad (10)$$

where TC_j is the cable tension. The j th cable attachment at point \mathbf{R}_j on body $i(j)$ applies a force and moment to $B_{i(j)}$ given by

$$\mathbf{F}C_{ij} = \mathbf{k}c_j TC_j$$

$$\mathbf{M}C_{ij} = (\mathbf{R}_i^* \mathbf{j} \times \mathbf{k}c_j) TC_j$$

where $\mathbf{k}c_j$ is the cable direction outward from the body and $\mathbf{R}_i^* \mathbf{j}$ is the moment arm of the attachment point about the c.g. ($\mathbf{R}_j - \mathbf{R}_i^*$). Thus, h_j in equation (10) is a configuration vector whose nonzero elements are $\mathbf{k}c_j$ and $(\mathbf{R}_i^* \mathbf{j} \times \mathbf{k}c_j)$, corresponding to the constraint force and moment on $B_{i(j)}$ due to the j th cable attachment, per unit tension.

Second, enumerate the cables and links which constitute the suspension, C_1, C_2, \dots, C_m . Each end of

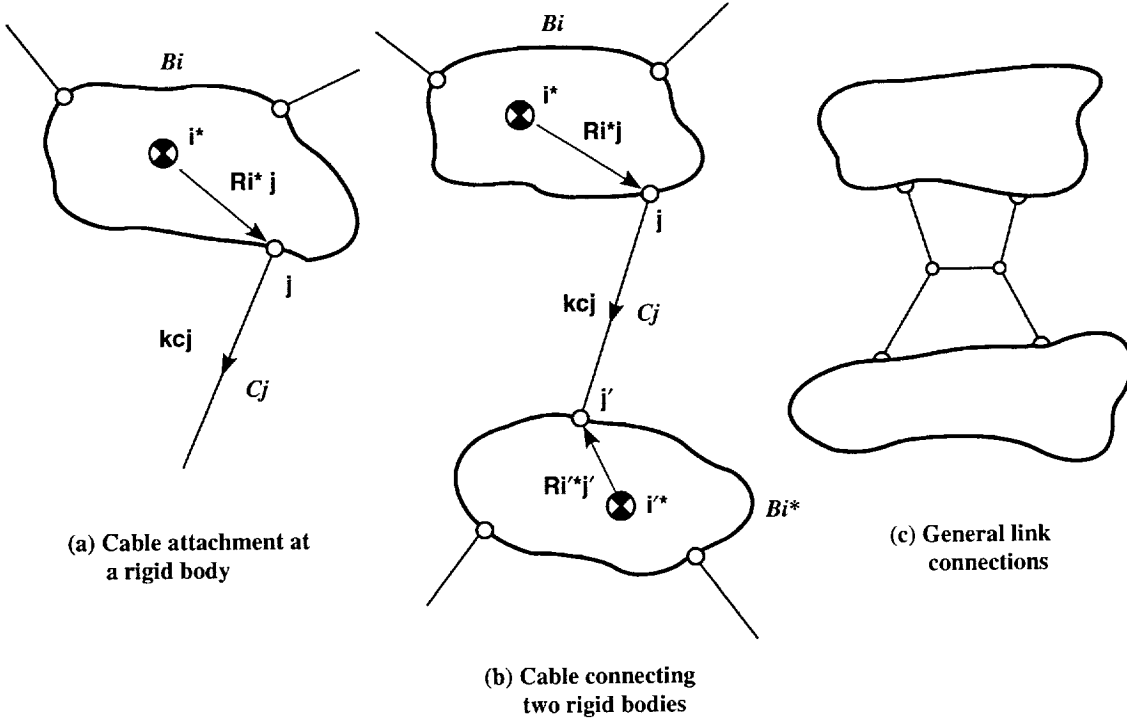


Figure 2. Suspension forces.

a cable or link is attached to either a rigid body or to another link. In the restricted case, in which all cables are attached at both ends to rigid bodies, all terms in equation (10) can be combined in pairs, with each pair corresponding to a single cable:

$$fc = \sum_{j=1}^m H_j TC_j \quad (11)$$

where the nonzero elements of H_j are \mathbf{kc}_j , $-\mathbf{kc}_j$, $(\mathbf{R}_j - \mathbf{R}_{i^*}) \times \mathbf{kc}_j$, $-(\mathbf{R}_{j'} - \mathbf{R}_{i'^*}) \times \mathbf{kc}_j$, corresponding to the forces and moments on bodies B_i , $B_{i'}$ to which the cable C_j is attached at points \mathbf{R}_j , $\mathbf{R}_{j'}$ (see fig. 2(b)). Here, \mathbf{kc}_j is the direction of the line segment $(\mathbf{R}_{j'} - \mathbf{R}_j)$. From the definitions of H_j, v it follows that $v^T H_j$ combines the rigid-body c.g. and angular velocities to give the difference in cable endpoint velocities along the cable direction:

$$\begin{aligned} v^T H_j &= \mathbf{V}_{i^*} \bullet \mathbf{kc}_j - \mathbf{V}_{i'^*} \bullet \mathbf{kc}_j + \omega_i \bullet (\mathbf{R}_{i^*j} \times \mathbf{kc}_j) \\ &\quad - \omega_{i'} \bullet (\mathbf{R}_{i'^*j'} \times \mathbf{kc}_j) \\ &= (\mathbf{V}_j - \mathbf{V}_{j'}) \bullet \mathbf{kc}_j = -\dot{\ell}_j \end{aligned}$$

That is, it is the cable stretch rate. Recalling equation (6), $u^T A^T H_j$ is the cable stretch rate due to u . Since all cable lengths are invariant for arbitrary u in an inelastic system, then

$$A^T H_j = 0 \quad j = 1, 2, \dots, m$$

and

$$A^T fc = 0$$

For inelastic suspensions, all systems in figure 1 except system 6 can be partitioned into rigid bodies such that every cable connects two rigid bodies.

For more general suspensions in which links are connected at both ends to a rigid body or to another link (fig. 2(c)), fc is given by equation (10), and $v^T fc$ is a linear combination of the attachment-point velocities. To this combination, first add and subtract the velocities of the cable interconnection points in the cable directions, and then apply the force-balance condition to the linear combinations of cable forces at these interconnections. The result is

$$\begin{aligned} v^T fc &= \sum_{j=1}^M \mathbf{V}_j \bullet \mathbf{kc}_j TC_j \\ &= \sum_{j=1}^m (\mathbf{V}_j - \mathbf{V}_{j'}) \bullet \mathbf{kc}_j TC_j \\ &= - \sum_{j=1}^m \dot{\ell}_j TC_j \end{aligned} \quad (12)$$

where the second and third sums are taken over all cables and $\{\dot{\ell}_j\}$ are cable lengths. Consequently, if

the suspension is inelastic then all cable lengths are invariant for arbitrary u , and

$$A^T f_c = 0 \quad (13)$$

Equation (13) indicates that the cable force f_c is orthogonal to all the columns of A and therefore to the configuration velocity v , when $\dot{p} = 0$. This result also expresses d'Alembert's principle for constrained holonomic systems (the constraint forces f_c do no virtual work) and Jourdain's principle for nonholonomic systems (the constraint forces have no virtual power):

$$f_c^T \delta r = 0$$

and

$$f_c^T \delta v = 0$$

where the virtual position and velocity in this context are

$$\delta r = [\nabla_q^T v] \delta q = A U \delta q$$

and

$$\delta v = [\nabla_u^T v] \delta u = A \delta u$$

and the constraint forces to which these principles apply in slung-load systems are shown above to be the resultant cable forces if the suspension is inelastic. Equation (8) for inelastic suspensions is now

$$\dot{u} = [A^T D A]^{-1} A^T f_o \quad (14)$$

Here, $[A^T D A]$ is a positive definite $d \times d$ matrix; D contains the system mass-inertia parameters; A contains the system geometry and constraints; and f_o (defined by eq. (8)) contains the term $D \dot{A} u + X$, which is second-order in velocity coordinates, and the inertia reactions to \dot{p} . It is unnecessary to calculate cable tensions in this result.

The principal difficulty in implementing equation (14) is the required inversion of $[A^T D A]$. A general analytical inverse is unknown. For slung loads, d is relatively large (near $6n$) and the inversion is therefore computationally more costly than it is for the elastic-cable case (eq. (9)), which requires no inversion. Some analysis of its numerical conditioning over the flight envelope is needed before inversion can be confidently implemented. In addition, the matrix inversion obstructs further expansion and rationalization in terms of three-dimensional dynamics whereas equation (9) can be fully expanded in applications in terms of natural vectors and matrices to obtain analytically the sensitivities of the elements of \dot{u} to the forces and moments. A Gauss-Jordan elimination procedure to reduce the matrix to a block-diagonal form

was considered in initial efforts to reduce the inversion to the inverses of smaller blocks given in terms of three-dimensional vectors. The procedure was applied in each case after defining the coordinates u and identifying some subdivision of u into natural vectors or groups of coordinates with which to associate the blocks of the diagonalized form. For typical choices of u , these blocks usually represented the rigid-body inertia matrices modified by the constraint moments (effective inertia).

Analytical results were obtained for systems 1, 2, 7, and 8 of figure 1, but the labor required increased rapidly with the number of DOFs, and the procedure appeared impractical to do by hand for dual-lift system 10 of figure 1. No generalization of the effective inertia interpretation of the blocks or of the simplification required at each step of the reduction was found, so the procedure was *ad hoc* and specific to each system and choice of coordinates, and could not be given effectively as a MACSYMA algorithm for analytical reduction.

A second form of the simulation equations, which requires the inverse of a much smaller $c \times c$ matrix, was obtained after restricting the generalized coordinates appropriately for slung-load systems; it is described next. The result can be applied with much less labor and likelihood of error than the procedure considered above.

Equation (14), or equivalent forms obtained by means of Lagrange's equations, is implemented in many of the general multibody programs, where d is relatively small in typical applications in the multibody literature. Numerical inversion of positive definite matrices can be carried out by various algorithms based on the Cholesky (square-root) decomposition (ref. 35) previously applied in the field of estimation. These are computationally efficient and resist numerical instabilities. The conditioning of the coefficient matrix $[A^T D A]$ depends on A in equation (14) or, equivalently, on the choice of coordinates u . In the multibody programs these coordinates are often preselected based on the joint model of interbody connections, and these appropriate coordinates tend to result in well-conditioned coefficient matrices in typical applications. In the present work, the interbody connections are suspensions composed of cables; it is left to the applications phase to determine in each case what constraints are imposed and what choice of coordinates best represents the constrained system motion.

Simulation Equations for Inelastic Suspension: Explicit Constraint Method

The approach in this section is to select the generalized velocity coordinates for the elastic system in equation (9) so as to separate the motion due to cable stretching from the remaining motion by means of invariant cable lengths, and then to study the results when the stretching motion is nulled. A solution for the constraint force and new simulation equations for the inelastic system are obtained.

First, let the generalized velocity coordinates of the elastic system u be composed of $6n - c$ coordinates, $u1$, of the system with invariant cable lengths, and c length rates, $\dot{\lambda}$, which suffice to define the motion resulting from cable stretching. In general, if the c independent position constraints imposed by an inelastic suspension are given by $\{\lambda1(r) = 0, \dots, \lambda c(r) = 0\}$ then λ can be taken as $(\lambda1, \dots, \lambda c)^T$. For slung-load systems, λ can usually be taken as the cable lengths and the complete set of coordinates $(u1, \dot{\lambda})$ can be taken as the c.g. velocity of a reference body, the angular velocities of all rigid bodies, and the cable angular velocities and stretching rates.

Next, substitute the partitioned u in equations (6) and (9):

$$v = A u + B \dot{p} = A1 u1 + L \dot{\lambda} + B \dot{p} \quad (15)$$

$$\dot{u} = \begin{pmatrix} \dot{u}1 \\ \ddot{\lambda} \end{pmatrix} = \begin{pmatrix} A11^T \\ \Lambda^T \end{pmatrix} D^{-1}(f_o + f_c) \quad (16)$$

where f_o is defined in equation (8); $A1$, L are the $6n - c$ and c columns of A which, respectively, define the contributions of $u1$, $\dot{\lambda}$ to v ; and $A11^T$, Λ^T are the $6n - c$ and c rows of A^{-1} which, respectively, define the relations $u1(v)$ and $\dot{\lambda}(v)$. As noted earlier, A^{-1} can be obtained without matrix inversion since it defines the relation $u(v)$ for the elastic system and can be given from the kinematics as readily as A , which defines the relation $v(u)$.

Equation (16) gives the simulation equation for systems with elastic suspensions in terms of the coordinates $(u1, \dot{\lambda})$, where $u1$ leaves the cable lengths invariant. The influence of cable-stretching motion on $u1$ can be viewed by entering the derivative of the partitioned generalized velocity coordinates given by equation (15) in f^* , and rederiving equation (8). The first $6n - c$ equations can be arranged as

$$\dot{u}1 = [A1^T D A1]^{-1} A1^T [f_o - D(L\ddot{\lambda} + \dot{L}\dot{\lambda})]$$

where f_o is as defined with equation (8) except that $A1 u1$ replaces $A u$. As in equation (14), f_c drops out ($A1^T f_c = 0$ in view of eq. (13)) and the result differs from the inelastic system equations (eq. (14)) only in the presence of the configuration acceleration due to elastic stretching. The effect of the stretching motion on $u1$ depends on the cable spring constants: for a fixed disturbance, the extremes of $\dot{\lambda}$ decline with increasing spring stiffness, whereas the extremes of the term in $\ddot{\lambda}$ remain fixed in magnitude, although $\ddot{\lambda}(t)$ increases in frequency (ref. 15).

The constraint force can be given in terms of c independent parameters; that is, it can be given in the form

$$f_c = [H1, \dots, Hc] \begin{pmatrix} s1 \\ s2 \\ \vdots \\ sc \end{pmatrix} = H s$$

where s is arbitrary, $\{Hj\}$ are configuration vectors, and $\text{rank}[H] = c$. From equation (13), $A1^T H = 0$, and from the construction of A^{-1} , $A1^T \Lambda = 0$. Therefore, the columns of H and Λ are both bases of the same linear vector space, and Λ can be used to define the constraint force:

$$f_c = \Lambda s \quad (17)$$

where Λ^T is the Jacobian $[\nabla_v^T \lambda]$, and s has units of force, if the coordinates λ are lengths.

For inelastic suspensions, $\ddot{\lambda} = 0$, and equation (16) gives c equations from which to calculate the constraint forces:

$$0 = \Lambda^T D^{-1}(f_o + f_c) \quad (18)$$

Introduce equation (17) into equation (18) and solve for s :

$$s = -[\Lambda^T D^{-1} \Lambda]^{-1} \Lambda^T D^{-1} f_o \quad (19)$$

Further, Λ can be replaced in equations (17) and (19) by any other convenient basis, H , of the space containing f_c . For example, in the special case that every cable connects two bodies and $c = m$, then s can be taken as the c cable tensions with the basis vectors $H1, \dots, Hc$, as defined by equation (11) above.

The cable tensions are related to s , and can be uniquely determined from s if the suspension is not redundant. However, the constraint force applied to the configuration, f_c , can always be calculated. A suspension can be separated into disjoint sets of interconnected links. Each such set imposes one holonomic

constraint; if the number of sets is c , then all cable tensions can be uniquely determined from s , but if it exceeds c , then the constraints are redundantly imposed. In the special case that all cables connect two rigid bodies, then each cable is a disjoint set and all cable tensions can be found only if $c = m$.

Finally, the simulation equations are

$$\dot{u} = A^{-1}D^{-1}(f_0 + \Lambda s) \quad (20)$$

or, for the inelastic DOFs;

$$\dot{u}_1 = AI_1^T D^{-1}[I - \Lambda[\Lambda^T D^{-1} \Lambda]^{-1} \Lambda^T D^{-1}]f_0 \quad (21)$$

This result has several advantages over equation (14) for the slung-load systems. First, the leading coefficient matrix, A^{-1} or AI_1 , is known analytically. Second, equations (19) and (20) require the inversion of a $c \times c$ matrix, $[\Lambda^T D^{-1} \Lambda]$, where $c = 1$ for system 1 and $c = 4$ for dual-lift system 10 (fig. 1), compared with the required inversion of 11×11 and 20×20 matrices, respectively, for these two systems when equation (14) is used. In many cases, the cable tensions can also be generated by equation (19).

Computational efficiency in calculating the dynamics can be compared among the formulations of the simulation equations defined above by counting the number of multiplications required to generate \dot{u} , given $A, A^{-1}, D, D^{-1}, f_0$. These are shown in table 1 for systems 1 and 10 of figure 1.

In table 1, $g()$ refers to the number of multiplications and divisions required for the Cholesky inversion, which increases with the square of the matrix size (ref. 35). The general formulas (derivations omitted) include savings gained from generic zeros, ones, and matrix symmetries. The number of coordinates u, v that are identical is represented by i in these formulas, and accounts for the generic zeros and ones. In most cases, u can be selected such that $i = 3n+3$. Additions are omitted from the operations count for brevity, but this omission does not affect the conclusions. Equation (14) is representative of previous single-case formulations of the slung load dynamics with inelastic

cables, as well as those in the multibody literature (e.g., refs. 24 and 36). As shown, equations (19) and (20) provide a significant reduction in the computational requirements to represent these dynamics, and a much reduced penalty compared to the elastic cable formulation (eq. (9)). The same conclusion applies to all systems of figure 1.

Computational requirements are of interest in real-time simulation and control. In simulations, the time required to compute the dynamical terms are of interest if these are a significant fraction of the cycle time. In control systems, linear control laws use coefficient matrices that can be calculated off line, and are nearly unaffected by the underlying formulation of the nonlinear EOMs. However, modern control-law design methods for aeronautical systems (inverse model, output linearization) treat systems with significant aerodynamic or dynamic nonlinearities by partially inverting the simulation equations. It is beyond the scope of this report to consider such control laws in detail, but it is expected that the formulation of the dynamics in the EOMs will affect the computational requirements for such control laws significantly for slung-load systems.

Simulation Equations for Inelastic Suspensions from Lagrange's Equations

Lagrange's equations have been the principal analytical approach in slung-load controls studies, where the object is usually to obtain linearized EOMs. The EOMs for general slung-load systems with inelastic suspension are derived here from Lagrange's equations, and it will be shown that they have the same form as equation (14).

Lagrange's equations for general holonomic systems with d DOFs are

$$\frac{d}{dt} \nabla_{\dot{q}} KE - \nabla_q KE = Q \quad (22)$$

where $q = (q_1, \dots, q_d)^T$ are generalized position coordinates; $Q = (Q_1, \dots, Q_d)^T$ are the generalized forces, including conservative forces; and KE is the

Table 1. Multiplications required to calculate \dot{u}

Equation	Multiplies		
	System 1	System 10	General formula
(9)	60	264	$6n(6n - i + 2)$
(14)	$616 + g(11^2)$	$3430 + g(20^2)$	$d((6n - i)\frac{(d+3)}{2} + 12n + d) + g(d^2)$
(19) and (20)	119	$868 + g(4^2)$	$d(6n - i) + 3n(c^2 + 9c + 4) + c^2 + g(c^2)$

kinetic energy. For slung-load systems, KE , Q can be given as

$$KE = (1/2) v^T D v = (1/2) \dot{q}^T A^T D A \dot{q}$$

$$Q = A^T (fg + fa) \quad (23)$$

where A defines $v(\dot{q})$ as

$$v = A\dot{q}$$

and v, fg, fa are defined in equations (1) and (2). The controllable parameters, \dot{p} , in equation (6) have been omitted from the velocity relation and kinetic energy for brevity, but they can be routinely included in KE and its derivatives. The generalized forces are obtained as coefficients of the generalized coordinate displacements in the virtual work, $\delta W = f^T \delta r = f^T A \delta q$. Here, f is the resultant force on the configuration, $f = fg + fa + fc$. For inelastic cables, fc is orthogonal to the columns of A in accordance with d'Alembert's principle, and drops out of Q .

After carrying out the derivatives of the kinetic energy in equation (22), the general slung-load equations are obtained as a second-order ordinary differential equation:

$$M(q)\ddot{q} + k(q, \dot{q}) = Q$$

$$M = A^T D A$$

$$k = A^T D \dot{A} \dot{q} + (\dot{A} - G)^T D A \dot{q} \quad (24)$$

where

$$G = [\nabla_q^T (A(q) \dot{q})]$$

$$\dot{A} = \sum_{i=1}^d \frac{\partial A}{\partial q_i} \dot{q}_i$$

All terms in k are second order in the velocity coordinates of \dot{q} . Equation (14) can be placed in the same form as equation (24) for comparison:

$$M(q)\ddot{q} + k(q, \dot{q}) = A^T (fg + fa)$$

$$M = A^T D A$$

$$k = A^T (D \dot{A} \dot{q} + X) = A^T D \dot{A} \dot{q} + A^T X \quad (25)$$

where u has been taken to be identical to \dot{q} for the comparison.

The equations of motion, (24) and (25), from Lagrange's equations and from equation (14), respectively, have the same form. The inverse of a $d \times d$ matrix, M , to obtain \ddot{q} is required in both cases.

In the slung-load literature, Lagrange's equations (22) have been applied by defining generalized

position coordinates q , forming $KE(q, \dot{q})$, and generating the latter's derivatives routinely (refs. 10, 15, and 7). Contact with the rigid-body velocities is lost in KE , and the terms M , k , Q in equation (24) are obtained as structureless objects in the d -dimensional space of constrained motion. This has sufficed for studies of single helicopters, but appears to be impractical for multilift systems.

Equation (23) introduces the multibody structure of slung-load systems in the Lagrangian formulation, following similar steps found in the multibody literature, to obtain equation (24) in terms of objects A , D , $\dot{A}\dot{q}$, and f in the $6n$ -dimensional space of configuration motion. Equations (24) and (25) are identical except for differences in the analytical statement of the second-order velocity terms, k . In particular, the term $A^T X$ in equation (25) is given easily from the kinematics and from equation (3), but its numerical equivalent in equation (24), $(\dot{A} - G)^T D A \dot{q}$, requires numerous derivatives of A . However, k can be neglected in the derivation of linearized equations for windless hover because its gradients with respect to q, \dot{q} are zero for practical choices of coordinates, q .

Additional differences between equations (14) and (24) occur in all terms when the velocity coordinates u are different from \dot{q} . In the applications work, these terms can be generated more easily from equation (14) than from equation (24) owing to the simpler kinematics A , usually obtained using generalized velocities, and the simpler expression for the nonlinear term, k .

Simulation Equations for Inelastic Suspensions Using Rigid Body Velocity Coordinates

Simulation equations for the rigid-body velocity coordinates v , (eq. (1)) have been derived assuming inelastic suspension for several slung-load systems in reference 16 and for dual lift in reference 20. These specialized derivations are obtained by extracting a subset of the Newton-Euler equations with the suspension forces eliminated and appending derivatives of the constraint equations to obtain $6n$ equations for the rigid-body accelerations \dot{v} . This procedure can be formally extended to general slung-load systems with inelastic suspension by using the partitioned coordinates previously defined in equation (15).

As before, partition the generalized velocity coordinates of the elastic system u into $6n - c$ coordinates $u1$ of the system with invariant cable lengths and c length rates $\dot{\lambda}$ with suffice to define the motion due

to cable stretching. Then the kinematics can again be partitioned as

$$v = Au = A1 u1 + L\dot{\lambda}$$

$$u = \begin{pmatrix} u1 \\ \dot{\lambda} \end{pmatrix} = A^{-1}v = \begin{pmatrix} A11^T \\ \Lambda^T \end{pmatrix} v \quad (26)$$

Controllable parameters p have been omitted from the kinematics for brevity but can be included routinely in the derivation. Here, the columns of A and the rows of A^{-1} are partitioned into $[A1, L]$ and $[A11^T, \Lambda^T]$. The term $A1$ is a basis of the space perpendicular to the suspension forces fc and Λ is a basis of the space containing these forces. The suspension forces can be expressed as in equation (17) in terms of Λ and c independent constraint force parameters s . Introduce this into the Newton-Euler equation (9b) and premultiply the result by A^T to obtain the dynamic equations (note that $A1^T fc = 0$ and $L^T \Lambda = I$):

$$A1^T D\dot{v} = A1^T (fg + fa - X) \quad (27)$$

$$s = L^T (D\dot{v} - fg - fa + X) \quad (28)$$

A derivative of equation (26) provides c additional kinematic constraint equations for inelastic suspensions:

$$\ddot{\lambda} = \Lambda^T \ddot{v} + \dot{\Lambda}^T v = 0 \quad (29)$$

Together, equations (27) and (29) comprise $6N$ scalar equations for the rigid-body accelerations in which the suspension forces have been eliminated. These yield the simulation equations in the form

$$\dot{v} = M(r)^{-1} z$$

where

$$M = \begin{pmatrix} A1^T D \\ \Lambda^T \end{pmatrix} \quad (30)$$

$$z = \begin{pmatrix} A1^T (fg + fa - X) \\ -\dot{\Lambda}^T v \end{pmatrix}$$

Equation (30) requires the inversion of the $6n \times 6n$ matrix, M , composed of $6n - c$ columns from $D A$ and c rows from A^{-1} . General results for its rank or for efficient inversion algorithms are not available. The second-order velocity terms occur in $X, \dot{\Lambda}^T v$. The use of the rigid-body velocity coordinates results in calculation of relative motions from small differences of large numbers in a simulation.

The suspension force parameters, s , can be computed from equation (28) after computing accelerations. Alternatively, equation (19) gives s in terms of the applied forces and the velocity coordinates, but requires more computation than equation (28). In general s suffices to define the resultant suspension forces applied to each rigid body of the configuration. Cable tensions are related to s by $fc = \Lambda s = H\tau$, where τ is a list of cable tensions and H contains appropriate configuration vectors defining the force and moment action of each cable on each rigid body. If the number of cables equals the number of constraints, then the cable tensions are readily obtained from this relation.

4. APPLICATIONS

The object of this section is to demonstrate and apply the methods of this report to slung-load systems of practical interest, particularly the dual-lift systems for which general simulation equations were not previously available. Results are given for systems 1, 2, and 7 and for all three dual-lift systems shown in figure 1, as well as for multilift system 11 extended to any number of helicopters. These results are given as summaries of simulation equations in programmable form in the appendixes.

General Procedure

A general procedure for applying and implementing the present results for slung-load simulation equations is outlined in figure 3. Both elastic suspensions (eq. (9) or (16)) and inelastic suspensions (eqs. (19) and (20)) are included. The first task (fig. 3(a)) is to perform an analysis to (1) determine the constraints of the inelastic suspension; (2) define $6n$ generalized velocity coordinates $(u1, \dot{\lambda})$ such that $u1$ are d coordinates for the inelastic suspension and such that $\dot{\lambda}$ are c coordinates which define system motion caused by cable stretching; and (3) obtain expressions for A, A^{-1}, \dot{A} from the kinematics and for B, \dot{B} from the suspension geometry, if it is controlled. These items are case specific.

The selection of appropriate generalized coordinates u is case specific, but several features were used repeatedly in the applications to maintain simplicity of the kinematics and equations. The coordinates u can be selected to consist largely or entirely of natural vectors. If u contains rigid-body velocities identical to those in v , then the corresponding rows of A, A^{-1}, \dot{A} are from

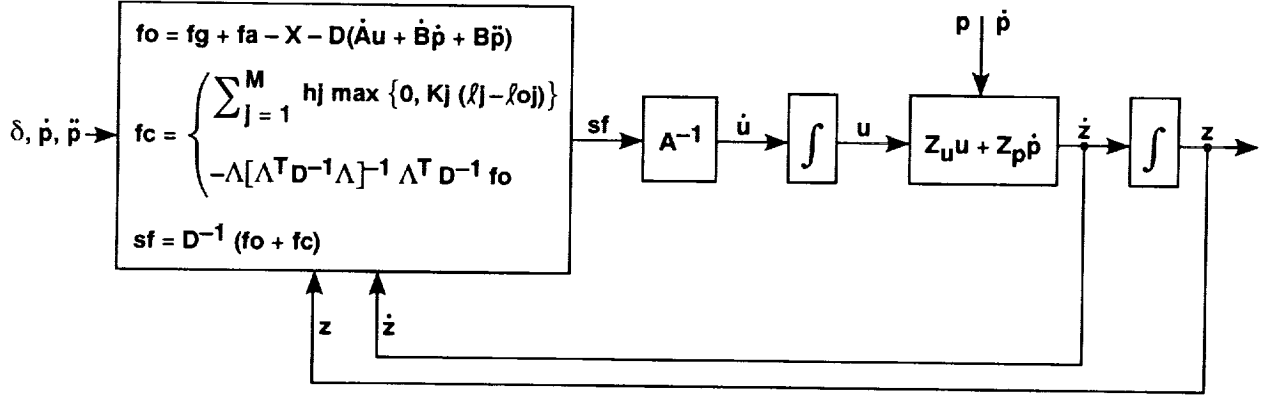
c	number of holonomic constraints on configuration for inelastic suspension
u_1	$6n - c$ generalized velocity coordinates for system with inelastic suspension
$\dot{\lambda}$	c generalized velocity coordinates defining suspension stretching motion
u	$6n$ generalized velocity coordinates for system with elastic suspension $u = (u_1^T, \dot{\lambda}^T)^T$
A	the Jacobian $[\nabla_u^T v]$ obtained from the kinematics
A^{-1}	the Jacobian $[\nabla_v^T u]$ obtained from the kinematics
Λ	the Jacobian $[\nabla_u \dot{\lambda}^T]$ from A^{-1} or any basis of the interaction force space
B	the Jacobian $[\nabla_p^T v]$ (required only if $\dot{p} \neq 0$)

(a) Quantities required a priori.

$$\begin{aligned}
 f_a &= f_a(r, v, \delta) && (\delta = \text{helicopter controls}) \\
 f_o &= f_g + f_a - D \dot{A} u - X - D(B\ddot{p} + \dot{B}\dot{p}) \\
 f_c &= \begin{cases} \sum_{j=1}^M h_j \max\{0, K_j (\ell_j - \ell_{oj})\} & \text{(elastic cables)} \\ -\Lambda[\Lambda^T D^{-1} \Lambda]^{-1} \Lambda^T D^{-1} f_o & \text{(inelastic cables)} \end{cases} \\
 s f &= D^{-1}(f_o + f_c) \\
 \dot{u} &= A^{-1} s f \\
 u &= \int \dot{u} dt \\
 v &= A u + B \dot{p} \quad \text{or} \quad \dot{z} = Z_u u + Z_p \dot{p} \\
 \dot{r} &= \dot{r}(r, p, v, \dot{p}) \\
 r &= \int \dot{r} dt \quad \text{or} \quad z = \int \dot{z} dt
 \end{aligned}$$

(b) Simulation equations.

Figure 3. Procedure for simulation of slung-load systems.



(c) Simulation flow diagram.

Figure 3. Concluded.

the unit matrix or zero. If u contains cable velocities, the corresponding rows of A , A^{-1} , \dot{A} contain only coordinate transformations and skew-symmetric matrices representing Coriolis velocities and Coriolis and centrifugal accelerations. In most of the applications discussed in this paper, u consists of the c.g. velocity of a reference body, the angular velocities of all bodies, and various cable velocities or their equivalents. A consideration in choosing u is that the relation $v(u)$ should be nonsingular and well-conditioned over the domain of motions (v, r) of interest; that is, all configuration motion should be readily detected from a knowledge of u . Among the examples given, this was a factor only for system 7 (fig. 1).

The second task is to implement the simulation equations (16) or (19) and (20) as given in the equation summary (fig. 3(b)) and the information flow diagram for the general n -body system (fig. 3(c)). The applied forces and moments due to weight, aerodynamics, and rotor are combined in f_o with the inertia coupling associated with the choice of coordinates u, v and the controllable geometry, if any. The configuration vectors fg , fa , X , and D were previously defined in terms of physical vectors and matrices of the three-dimensional rigid-body mechanics of the system's constituent bodies, in equations (2) and (3). The aerodynamic term fa need not be considered in detail here, except to note that it can be assumed to be a function of the configuration kinematics and the aerodynamic controls, δ . These dependencies are considered in more detail later in deriving the linearized EOMs.

The forces and moments applied by the suspension to the configuration fc are calculated from equations (10) or (11) (elastic cables) or equations (18)

and (19) (inelastic cables). Both elastic and inelastic cable models can be accommodated by switching formulas for the interaction force. Expressions are given for both cases in all examples. For elastic cables, fc is calculated from cable tensions and from configuration vectors defining the force and moment action of each cable on the n rigid bodies. For inelastic cables, fc is calculated from any basis of the constraint force space Λ , and the corresponding independent constraint force parameters s . The Jacobian, $[\nabla_v \lambda^T]$, from A^{-1} is always a basis. When every cable connects two bodies and when $m = c$, as in the dual-lift systems, then the constraint force parameters s can be taken as the cable tensions, and the coefficient matrix defined in equation (11) can be used for both models:

$$fc = Hs$$

$$s = \begin{cases} (\max\{0, K_j(\ell_j - \ell_{0j})\}, & j = 1, \dots, c)^T \\ \text{(elastic cables)} \\ -[H^T D^{-1} H]^{-1} H^T D^{-1} f_o \\ \text{(inelastic cables)} \end{cases}$$

Subsequently, the configuration-specific forces and moments sf , and, finally, \dot{u} are calculated. The remaining steps generate the kinematics u, v, \dot{r}, r routinely or, more generally, these kinematic variables can be expanded to any set of velocity and position coordinates \dot{z}, z of interest after defining $\dot{z}(z, p, u, \dot{p})$ from the kinematics and geometry. For inelastic cables, the coordinates $\dot{\lambda}$ and their equations can be eliminated since $\ddot{\lambda}$ is theoretically zero. Alternatively, all $6n$ equations can be retained to permit simulation of both cable models; for inelastic cables, the computed $\dot{\lambda}$ indicates numerical accuracy.

The general simulation equations shown in figure 3 are given in terms of vectors in the $6n$ -dimensional configuration space. These are expressed in all results in terms of the natural vectors and matrices of the underlying three-dimensional rigid-body mechanics and geometry. General formulas used to obtain this form are given in appendix A. The required equations are relations from the classic vector theory of rigid-body dynamics in a programmable form. First, the skew-symmetric matrix is introduced to represent the cross products which occur in the Coriolis velocities, Coriolis and centrifugal accelerations, and cable moments that pervade A , A^{-1} , $\dot{A}u$, and fc . Second, reference frames are defined for all rigid bodies, and standard expressions are given for the coordinate transformations, angular velocities, and transformation rates that occur in the results. All transformations are given in terms of the customary Euler-angle sequence of aeronautics. Third, the treatment of cable direction angles, cable axes, and cable velocities is outlined; Euler angles are again used, but only two angles are needed.

Examples

The literature describes a variety of existing and proposed slung-load systems (fig. 1). These are grouped, for this discussion, into (1) single helicopters with a single attachment point on the helicopter, (2) single helicopters with multiple attachment points, (3) dual-lift systems, and (4) multilift systems. Several suspensions are of interest in each category, including controllable geometry in systems 5 and 6 of figure 1. Results are given for systems 1, 2, and 7 and for all three dual-lift systems, as well as for a simple multilift system. Systems with controllable suspension geometry are not included in the present examples.

The single-helicopter systems 1, 2, and 3 of figure 1, with a single attachment point on the helicopter, are considered in appendix B. Results are obtained for systems 1 and 2 by using the above procedure. The suspensions for systems 1 and 2 impose three constraints and one constraint, respectively, on the load relative motion when inelastic. Appropriate partitioning coordinates were readily obtained by including the load relative velocity (system 1) or cable-axis components of the cable velocity (system 2) in the generalized coordinates. Differences from the earlier formulations of simulation equations include the use of relative-acceleration coordinates for the elastic suspension case, the nonlinear EOMs for the inelastic suspension with explicit calculation of cable tensions, and

the integration of both elastic and inelastic suspension models into one equation set.

Partitioning coordinates for single-cable-and-sling system 3 of figure 1 were not found. If the suspension is inelastic, this system is identical to system 2 and can be represented by the same equations. For the elastic suspension, the principal elastic elements are the sling legs, in which case no cable connects two rigid bodies. Here, the suspension geometry and cable tensions are determined from the force balance at the sling vertex. Coordinates are given in appendix B that simplify this calculation relative to the method found in the earlier literature. Kinematic relations needed to obtain the EOMs from equation (9a) are given, but these depend on suspension elasticity parameters, as well as on ordinary kinematics. A complete set of EOMs is omitted because the coordinates given are not of the type that is of interest in the present applications work. In this case the EOMs for an inelastic suspension are simpler than those for an elastic suspension because of the complexity in calculating interaction forces when each elastic link is not connected to two rigid bodies.

The single-helicopter systems, 4–7 of figure 1, with multiple attachment points on the helicopter, are considered in appendix C. These suspensions were developed in the 1965–1975 period to stabilize difficult loads such as the standard cargo container (MILVAN). They provide yaw restraint to stabilize elongated loads in a minimum-drag heading, and pitch attitude is restricted. The addition of active cable-length and attachment-point control to increase load-motion damping was also considered.

Results are given in appendix C for the bifilar suspension (system 7, fig. 1), which imposes two constraints on load relative-motion when inelastic. This system also approximates the inverted-Y suspension (system 6, fig. 1) when the bar is sufficiently close to the load. For inelastic suspension, several sets of load-suspension coordinates have been used in the earlier literature. The load-suspension geometry is examined in detail in appendix C, and several choices of coordinates, some of which are ill-conditioned and some well-conditioned, are identified. One set is selected and expanded to a set of partitioning coordinates, and a complete set of nonlinear EOMs for both elastic and inelastic-suspension is given. Differences from the earlier literature include the use of relative accelerations for the elastic suspension case, and the formulation of efficient equations for the inelastic suspension with cable tensions explicitly calculated.

The remaining suspensions in this group are analytically difficult to represent as inelastic. In the inverted-Y suspension (with or without the spreader bar) no cable connects two rigid bodies, and the force balance at the suspension interconnections must be considered as in system 3, discussed above. Further, if the bar or interconnections are close to the helicopter, the suspension can be represented as an inverted V, and if close to the load, as bifilar. For inelastic cables, there can be one, two, or three constraints, depending on these details of suspension geometry. Finally, it appears that representation of the inverted-V suspension as inelastic is both unrealistic and intractable. Simulation equations for the elastic inverted-V suspension are given in the literature, along with approximate equations in which cable stretching motion is neglected. Although the existing analytical difficulties in simulating the multipoint suspensions of practical interest are not relieved by the methods presented in this report, recall that the principal object here is to treat the difficult multilift systems discussed next.

Simulation equations for the three- and four-body dual-lift systems (8–10, fig. 1) are given in appendix D. Appropriate partitioning coordinates for applying equation (16) were readily found by using cable-axis components of the cable velocities or their equivalents. The results integrate elastic and inelastic suspension models; since $c = m$ for these systems, the suspension forces $fc = Hs$ can be calculated by using the identical matrix of configuration vectors H for the two models. Further, all three systems can be simulated by a single equation set. System 8 is a three-body subsystem of system 10 obtained by deleting the load and bridle cables, and can be represented by a subset of the coordinates and equations for system 10, and system 9 is a simple specialization of system 8 with coincident attachment points on the load. General nonlinear equations for these systems with inelastic suspensions were not previously available owing to the complexity of representing the dynamics by the traditional methods found in the slung-load literature. The methods of this report render these dynamics accessible and tractable, and provide a new formulation of the EOMs for inelastic suspensions that is efficient and that provides explicit calculation of the suspension forces.

Simulation equations for the multilift system 11 of figure 1 extended to any number of helicopters are given in appendix E. Each helicopter is connected to the load by a single cable, which, if inelastic, imposes one constraint on the motion of a helicopter relative

to the load. Equations for this system are readily obtained by extending the single-helicopter/single-cable system formulation in appendix B. The generalized coordinates include cable velocities for every cable, and the results represent either elastic or inelastic cables.

The EOMs in the above applications work have been systematically formulated in terms of the natural vectors and matrices of rigid-body mechanics. This departs from the earlier formulations which were given in terms of the scalar components of all vectors. One consequence is that repeated matrix and vector products are visible in the equation summaries, and their repeated calculation can be eliminated in efficient coding. Another is that programming in a language that admits operators for such products would result in simpler, briefer code with associated savings in the programming task. These have not been significant issues for single-helicopter simulations, but they are of greater consequence for the dual-lift and multilift systems.

5. APPROXIMATE NONLINEAR MODELS

Approximations that reduce the number of DOFs and thereby simplify the system are always of interest in control analysis and design. These include the assumption of inelastic cables considered in the previous sections. Approximations of the rigid bodies as point masses or as rigid rods have also appeared in the literature (e.g., ref. 10), particularly for dual-lift systems. In references 6 and 7, the dual-lift system with spreader bar is approximated by using a point-mass load and a rigid-rod spreader bar. In references 17 and 18 all bodies, including the helicopters, are approximated as point masses. Modification of the nonlinear EOMs to include these degenerate-body approximations is considered in this section.

The nature of these approximations in representing real systems is of interest. The rigid rod can approximate elongated bodies with negligible inertia about one axis. The point-mass assumption implies negligible inertia about all axes. This is never realistic in slung loads, but it does approximate possible practical situations in which the attitude dynamics of a rigid body do not affect the remaining DOFs (reduced system). First, if the suspension is attached at the c.g. of a body and the applied forces are negligibly dependent on attitude, then the reduced system motion is independent of its attitude dynamics and is governed by EOMs identical to those obtained assuming a point

mass. Second, if a helicopter can be assumed to control the slung-load system solely through its applied force, then its attitude dynamics are dependent DOFs as required to generate that force, and can be removed from the system DOFs to leave a reduced system in which the helicopter's applied force is the control. Simulation and control analysis of the reduced system can then proceed without the details of the helicopter model being considered, and separately from implementation of the applied-force controller in the helicopter. A corresponding separation of the EOMs is examined below and it is shown to result in equations for the load-suspension subsystem that are identical to those obtained when point-mass helicopters are assumed. This separation of the slung-load control and the related point-mass approximations in references 17 and 18 are of interest for control synthesis based on inversion of the nonlinear model.

Degenerate Body Approximations

Point-mass bodies– If any bodies in the system are approximated as point masses, then all formulations of the EOMs (eqs. (8), (9), (14), (16)-(20)) can be applied by removing the attitude coordinates, angular velocities, applied and suspension moments, and inertias of the point-mass bodies from the configuration vectors and matrices r , v , X , fa , fc , and D .

Rigid rods– A rigid rod has a singular inertia matrix so that equations (9) and (16) for the unconstrained system, in which D^{-1} occurs, are invalid. Repairs can be made by defining a reduced configuration velocity that contains only as many coordinates as there are DOFs of the unconstrained system and retracing the derivations of section 3, beginning with the Newton-Euler equations.

A rigid rod is a line segment in space with only two attitude DOFs. Attach body axes $\mathcal{F}_b = \{\mathbf{ib}, \mathbf{jb}, \mathbf{kb}\}$ to the rod with \mathbf{ib} along the rod and located in inertial space by its heading and pitch angles:

$$\begin{aligned} Jb &= \text{diag}\{0, Jb', Jb'\} \\ T_{b,N} &= E_2(\theta_b) E_3(\psi_b) \\ \omega b_b &= \begin{pmatrix} 0 & -\sin \theta_b \\ 1 & 0 \\ 0 & \cos \theta_b \end{pmatrix} \begin{pmatrix} \dot{\theta}_b \\ \dot{\psi}_b \end{pmatrix} = \overline{W}b_b \dot{\alpha}b \end{aligned} \quad (31)$$

The overbar ($\overline{}$) is introduced to indicate objects from the three-DOF rigid-body attitude dynamics, such as Wb_b , αb , which are reduced to represent rigid rods. The direction angles are taken as heading and pitch here, with the assumption that the rod is never vertical. The columns of $\overline{W}b_b$ are the axes of rotation for pitch and heading. Also, $\overline{\alpha}b = \overline{W}b_b^T \omega b_b$, since $\overline{W}b_b^T \overline{W}b_b = I$.

Next, consider a system of n bodies containing rigid rods, where \mathcal{R} are the indices indicating the rigid rods, and ωr , $\overline{\alpha}r$ are lists of their angular velocities and rates; $\omega r = (\omega j_j, j \in \mathcal{R})$, $\overline{\alpha}r = (\overline{\alpha}j_j, j \in \mathcal{R})$. To avoid the difficulties in deriving the EOMs from equation (7) that result from the singular D , define the reduced configuration velocity \overline{v} to contain the Euler-angle rates of the rigid rods. The relation $v(\overline{v})$ is

$$v = \begin{pmatrix} v1 \\ \omega r \end{pmatrix} = \overline{W} \overline{v} = \begin{pmatrix} I & 0 \\ 0 & \overline{W}r \end{pmatrix} \begin{pmatrix} v1 \\ \overline{\alpha}r \end{pmatrix} \quad (32)$$

where

$$\overline{W}r = \text{diag}\{\overline{W}j_j, j \in \mathcal{R}\}$$

Here, v has been partitioned into the angular velocities of the rigid rods ωr and the remaining configuration velocities $v1$, and \overline{v} contains $6n - r$ coordinates corresponding to the DOFs of the unconstrained system. Also, $\overline{v} = \overline{W}^T v$ since $\overline{W}^T \overline{W} = I$.

Next, let u be the generalized velocity coordinates for the system and denote the relations $v(u)$, $\overline{v}(u)$ as

$$v = A u \quad \text{and} \quad \overline{v} = \overline{A} u$$

where, from equation (32), A, \overline{A} are related by

$$A = \overline{W} \overline{A} \quad \text{and} \quad \overline{A} = \overline{W}^T A$$

Since $v = \overline{W} \overline{A} u$, replacing A in equation (8) by $\overline{W} \overline{A}$ gives the following convenient form for the EOMs:

$$\dot{u} = [\overline{A}^T \overline{D} \overline{A}]^{-1} \overline{A}^T \overline{W}^T (fo + fc)$$

where

$$\overline{D} = \overline{W}^T D \overline{W} \quad (33)$$

The \overline{D} term is a nonsingular $(6n - r) \times (6n - r)$ reduced mass-inertia matrix, where the rigid-rod inertias are now 2×2 matrices:

$$\overline{J}j = \overline{W}j_j^T Jj \overline{W}j_j = Jj' \text{diag}\{1, \cos^2 \theta_j\}, \quad j \in \mathcal{R}$$

The configuration forces f_o, f_c are the usual objects in $6n$ -dimensional space previously defined, with forces and moments listed in the same order as the rigid-body linear and angular velocities in v above (eq. (32)).

For the constrained system with inelastic cables, equation (13) expressing d'Alembert's principle still applies ($A^T f_c = \bar{A}^T \bar{W}^T f_c = 0$), and then equation (33) can be rewritten in a form analogous to equation (14):

$$\dot{u} = [\bar{A}^T \bar{D} \bar{A}]^{-1} \bar{A}^T \bar{W}^T f_o \quad (34)$$

For the system with elastic cables, \bar{A} is a nonsingular square matrix so that equation (34) can be expanded in a form analogous to that of equation (9a):

$$\dot{u} = \bar{A}^{-1} \bar{D}^{-1} \bar{W}^T (f_o + f_c) \quad (35)$$

The coordinates u can be selected as in equation (16) to contain $6n - r - c$ coordinates u_1 , representing the configuration motion with inelastic suspension, and c coordinates λ , which define the motion induced by cable stretching. Equation (35) then becomes

$$\dot{u} = \begin{pmatrix} \dot{u}_1 \\ \dot{\lambda} \end{pmatrix} = \begin{pmatrix} \bar{A} \bar{1}^T \\ \bar{\Lambda}^T \end{pmatrix} \bar{D}^{-1} \bar{W}^T (f_o + f_c) \quad (36)$$

For inelastic cables, the condition $\ddot{\lambda} = 0$ yields c scalar equations in the constraint force. This force may be expressed as

$$\bar{f}_c = \bar{W}^T f_c = \bar{H} s$$

where s is c independent parameters and \bar{H} is a basis of the $6n - r$ dimensional constraint force space for \bar{f}_c . As in section 3, it can be shown that $\bar{\Lambda}$ and \bar{H} are bases of the same space, and then the equations obtained above yield the solution for s as

$$s = -[\bar{H}^T \bar{D}^{-1} \bar{H}]^{-1} \bar{H}^T \bar{D}^{-1} \bar{W}^T f_o \quad (37)$$

where $\bar{H} = \bar{W}^T H$, and where H is some known basis in $6n$ -dimensional space, or $\bar{\Lambda}$ from the kinematics $u(\bar{v})$ in $(6n - r)$ -dimensional space. Equations (36) and (37) are analogous to equations (16) and (19), respectively.

Applications— Example applications are given in appendixes D and E. In appendix D, the dual-lift system with spreader bar is approximated as three point masses, representing the two helicopters and load, and a rigid-rod spreader bar. This system has 14 and 10 DOFs for elastic and inelastic cables, respectively. The result completes the work begun in reference 17 to obtain a degenerate-body approximation for this

system. In appendix E, equations are given for the multilift system with m helicopters and a pendant suspension with all bodies approximated as point masses. These extend the equations given in reference 18 for a two-helicopter, two-dimensional point-mass system.

Center-of-Gravity Attachments

To examine coupling between the attitude DOFs of body B_n in an n -body system with the remaining DOFs, partition the configuration vectors and matrices to separate its attitude coordinates, inertia, and moments:

$$r = \begin{pmatrix} r_1 \\ \alpha_n \end{pmatrix}$$

$$v = \begin{pmatrix} v_1 \\ \omega_{n_n} \end{pmatrix}$$

$$\dot{r} = \begin{pmatrix} \dot{r}_1 \\ \dot{\alpha}_n \end{pmatrix} = \begin{pmatrix} W^{-1} & 0 \\ 0 & W_{n_n}^{-1} \end{pmatrix} \begin{pmatrix} v_1 \\ \omega_{n_n} \end{pmatrix}$$

$$D = \begin{pmatrix} D_1 & 0 \\ 0 & J_n \end{pmatrix}$$

$$f_a = \begin{pmatrix} f_{a1} \\ M A n_n \end{pmatrix}$$

$$f_c = \begin{pmatrix} f_{c1} \\ M C n_n \end{pmatrix}$$

The Newton-Euler equations (9b) for the configuration with elastic suspension are then similarly partitioned as

$$\dot{v}_1 = D_1^{-1} (f_{o1} + f_{c1})$$

$$= D_1^{-1} (f_{g1} + f_{a1} - X_1 + f_{c1})$$

$$\dot{\omega}_{n_n} = J_n^{-1} (M A n_n - S(\omega_{n_n}) J_n \omega_{n_n} + M C n_n)$$

Coupling of the reduced system (r_1, v_1, \dot{v}_1) with the attitude dynamics $(\alpha_n, \omega_{n_n}, \dot{\omega}_{n_n})$ can occur in the aerodynamics, f_{a1} , and the suspension forces, f_{c1} . Aerodynamic coupling is principally coupling of the body's attitude and c.g. dynamics, plus secondary interbody interferences. This coupling can be neglected

if the aerodynamic force is negligible (e.g., load aerodynamics at hover and low speeds) or nearly independent of attitude (e.g., load aerodynamics when these are dominated by attitude-independent drag, or when the attitude is assumed to be constant).

The bodies interact principally through fc . For an elastic suspension, fc can be given by equations (10) or (11) from the inertial cable directions and lengths, and the attitude angles of all bodies, and these are functions of the configuration position r . It can be shown that

$$\text{If } \mathbf{Rn}^*j = 0, \quad j \in Cn$$

$$\text{then } MCn_n = 0, \quad fc1 = fc1(r1)$$

where $Cn =$ indices of the cables attached to Bn at attachment points $\{\mathbf{Rn}^*j, \quad j \in Cn\}$ on Bn

Thus, if the suspension is attached at the c.g. of Bn , and the dependence of $fa1$ on its attitude is neglected, then the subsystem $(r1, v1, \dot{v}1)$ is independent of $(\alpha n, \omega n, \dot{\omega} n)$. Further, generalized coordinates for the reduced system can be selected according to the procedure of section 4 to represent both elastic and inelastic suspensions. The coordinates $(r1, v1)$ are also those of a configuration in which Bn is assumed to be a point mass, and the Newton-Euler equations for this reduced system are identical to those obtained when Bn is assumed to be point mass.

If Bn is a helicopter, then its aerodynamic force is attitude dependent. However, system control is simplified by a c.g. attachment at the helicopter. The helicopter controls $\dot{v}1$ solely through its applied force, $F0n_N$, and attitude is selected to generate the required control force. For c.g. attachment, the helicopter's attitude dynamics are those of a free rigid body and are unaffected by the suspension or the motion of any other body. The extension of this separation of the control to more general single-point attachments is considered next.

Simplified Helicopter Model

Helicopter aerodynamics are a significant source of complexity in the simulation of multilift systems and of their control analysis and design. It is desirable to separate the design of the helicopter control from that of the slung-load system control to allow a similar separation of the simulation and analysis work. The general approach is to view the helicopters as force generators that control the slung-load system by means of

their controllable applied forces, and then to consider the slung-load control independently of the details of controlling the helicopters' applied forces. The helicopters' applied forces are controlled through the helicopter attitude DOFs; that is, given the instantaneous helicopter state and the desired force, the helicopter's force and moment balance equations can be solved for the corresponding helicopter attitude angles and control settings, and then the controls can be used to drive to its desired value. If the attitude control bandwidth is much faster than the bandwidth of the applied forces required to control the slung-load motion, then it can be assumed that the attitude is always approximately at the required value; that is, the attitude control is instantaneous and the attitude DOFs are in steady state ($\dot{\omega} = 0$) relative to the applied force variations needed to control the remaining DOFs of the system. The condition $\dot{\omega} = 0$ characterizes the "controlled helicopter approximation" considered next.

Partitioned EOMs— Let \mathcal{H} be the indices identifying the helicopter rigid bodies $\{Bj, \quad j \in \mathcal{H}\}$ in an n -body slung-load system. Denote the helicopters' angle coordinates, inertias, moments, and forces as $\alpha h, \omega h, Jh, fc2, fo2, foh$, as defined in part a of table 2. Assume that $6n$ generalized velocity coordinates u have been selected for use with equations (16)-(20); that these include the helicopter angular velocities ωh ; and that the remaining coordinates $u1$ suffice to define the velocity of any point in the system outside the helicopters. A review of the generalized coordinates selected for the examples in the appendixes shows that these are "reference-point coordinates"; that is, they contain the velocity of a reference point and additional coordinates that define the motion of all points relative to the reference point. As such, ωh is present in u for all examples, but the use of a helicopter c.g. as the reference point in most examples violates the above requirement for $u1$. This can be repaired by moving the reference point to the load, as in appendix E, or to a suspension attachment point on a helicopter. Next, partition the kinematics, the mass-inertia matrix, and the configuration forces $u, v, v(u), u(v), D, fo, fc$, as shown in part b of table 2, to separate the EOMs into equations for $\dot{\omega} h$ and for the remaining (reduced system) DOFs, $\dot{u}1$:

$$\begin{aligned} \dot{u}1 &= [AI_{11} \quad AI_{12}]D^{-1} (fo + fc) \\ &= AI_{11} D1^{-1} (fo1 + fc1)t + AI_{12} \dot{\omega} h \\ \dot{\omega} h &= Jh^{-1} (fo2 + fc2) \end{aligned}$$

In general, $\dot{u}1$ is coupled with the helicopter attitude dynamics $(\alpha h, \omega h, \dot{\omega} h)$ through the term $AI_{12} \dot{\omega} h$ and the possible dependence of $fc1, fo1$, and AI_{11} on $(\alpha h, \omega h)$.

Table 2. Equations of motion for controlled helicopter approximation

(a) Helicopter attitude variables, inertias, moments, and forces:

\mathcal{H} = indices of helicopters in an n -body system:

$$\alpha h = (\alpha_j, \quad j \in \mathcal{H})$$

$$\omega h = (\omega_j, \quad j \in \mathcal{H})$$

$$Jh = \text{diag}\{J_j, \quad j \in \mathcal{H}\}$$

$$fc2 = (MCj_j, \quad j \in \mathcal{H})$$

$$fo2 = (M0j_j, \quad j \in \mathcal{H})$$

$$foh = (F0j_N, \quad j \in \mathcal{H})$$

(b) Partitioned equations:

$$v = \begin{pmatrix} v1 \\ \omega h \end{pmatrix} = A u = \begin{pmatrix} A_{11} & A_{12} \\ 0 & I \end{pmatrix} \begin{pmatrix} u1 \\ \omega h \end{pmatrix}$$

$$u = \begin{pmatrix} u1 \\ \omega h \end{pmatrix} = A^{-1} v = \begin{pmatrix} AI_{11} & AI_{12} \\ 0 & I \end{pmatrix} \begin{pmatrix} v1 \\ \omega h \end{pmatrix}, \quad (AI_{11} = A_{11}^{-1}; \quad AI_{12} = -A_{11}^{-1} A_{12})$$

$$D = \begin{pmatrix} D1 & 0 \\ 0 & Jh \end{pmatrix}$$

$$fo = \begin{pmatrix} fo1 \\ fo2 \end{pmatrix}, \quad fo = fg + fa - X - D \dot{A} u$$

For inelastic suspension:

$$fc = \begin{pmatrix} fc1 \\ fc2 \end{pmatrix} = \begin{pmatrix} \Lambda1 \\ \Lambda2 \end{pmatrix} s$$

$$s = -[\Lambda1^T D1^{-1} \Lambda1 + \Lambda2^T Jh^{-1} \Lambda2]^{-1} (\Lambda1^T D1^{-1} fo1 + \Lambda2^T Jh^{-1} fo2)$$

$$\dot{u}1 = AI_{11} D1^{-1} (fo1 + fc1) + AI_{12} \dot{\omega} h$$

$$\dot{\omega} h = Jh^{-1} (fo2 + fc2)$$

Table 2. Concluded

(c) Controlled helicopter approximation:

If: $\dot{\omega}h = 0$

Then: $\dot{u}1 = A_{11}^{-1} D1^{-1} (fo1 + fc1)$

$$fo2 = -fc2$$

$$s = -[\Lambda1^T D1^{-1} \Lambda1]^{-1} \Lambda1^T D1^{-1} fo1$$

If also: $fc1 = fc1(r1)$, $A_{11} = A_{11}(r1)$, $fo1 = fo1(r1, u1, foh)$

where: $\dot{r}1 = \dot{r}1(r1, u1)$ and foh are the helicopter applied forces

Then: (1) The reduced system EOMs are independent of the helicopter

attitude DOFs: $\dot{u}1 = \dot{u}1(r1, u1, foh)$

And: (2) The steady-state controls and attitude of conventional helicopters

satisfy the following quasi-static trim equations:

For $j \in \mathcal{H}$:

Given: $F0j_N$, $\dot{\alpha}j$, Vj_N^* , ψj

Find: $(\delta j, \phi j, \theta j)$ such that

$$VAj_j^* = T_{j,N} (Vj_N^* - W0_N)$$

$$\omega j_j = Wj_j(\alpha_j) \dot{\alpha}j$$

$$T_{N,j} FAj_j (VAj_j^*, \omega j_j, \delta j) + mj g_N = F0j_N + mj \dot{A}j u$$

$$MAj_j(VAj_j^*, \omega j_j, \delta j) = S(\omega j_j) Jj \omega j_j - MCj_j$$

where

$F0j_N$ is an element from foh

Aj are rows of A which give $Vj_N^* = Aj u$

MCj_j is an element of $fc2 = \Lambda2(r) s(r1)$

$W0_N$ is the mean wind velocity

Wj_j defines angular velocity from Euler-angle rates of Bj

(appendix A, eq. (72))

Controlled helicopter approximation– If the condition $\dot{\omega}h = 0$ is imposed, then the coupling of $\dot{u}1$ with $\dot{\omega}h$ drops out, and the helicopter applied-moments satisfy $f_{o2} = -f_{c2} = -\Lambda 2 s$. Substitute this expression for f_{o2} in the equation for the interaction force parameters s to obtain the result shown in part c of table 2: $s = -[\Lambda 1^T D 1^{-1} \Lambda 1]^{-1} \Lambda 1^T D 1^{-1} f_{o1}$. These parameters are independent of the helicopter moments and inertias, f_{o2}, Jh . In general, Λ depends only on position variables. If $\Lambda 1$ depends only on position variables $r1$, which can be determined from $u1$, then $f_{c1} = \Lambda 1 s$ is independent of the helicopter attitudes, except for possible dependence of f_{o1} on $(\alpha h, \omega h)$. This condition is met in all the applications examples presented in the appendixes for the coordinates u selected there. In these examples, $\Lambda 1$ depends on the cable directions and the attitude angles of the bodies other than the helicopters, and $u1$ contains the cable velocities and the angular velocities of these bodies.

To examine f_{o1} , partition it into the helicopter applied forces and inertia reactions, $f_{oh} = F O j_N, j \in \mathcal{H}$, and the forces and moments on the remaining bodies of the system (load, spreader bar, ...):

$$f_{o1}' = \begin{pmatrix} F O j_N, & j \notin \mathcal{H} \\ M O j_j, & j \notin \mathcal{H} \end{pmatrix} \\ = \begin{pmatrix} m_j g_N + F A j_N - m_j \dot{A} j u & j \notin \mathcal{H} \\ M A j_j - S(\omega j_j) J j \omega j_j & j \notin \mathcal{H} \end{pmatrix}$$

The helicopter forces f_{oh} are considered to be the controls of the reduced system. The remaining forces, f_{o1}' , contain the aerodynamics and the inertia reactions of the remaining bodies. Coupling of these aerodynamics with $(\alpha h, \omega h)$ can be neglected. In the inertia reactions, $A j$ are the rows of A that define $V j^*_N(u)$ and that can introduce coupling with $(\alpha h, \omega h)$. In the examples in the appendixes this occurs as centrifugal accelerations in the helicopter attachment-point moment arms, but these terms are zero for straight-line flight ($\omega h \approx 0$) and are expected to be negligible otherwise.

Last, the submatrix $A I_{11} = [\nabla_{v_1}^T u 1]$ is independent of αh in the examples in the appendixes for the coordinates u selected there.

Reduced system EOMs– For the examples in the appendixes, the reduced slung-load system $(r1, u1, \dot{u}1)$ can be approximated as being independent of the helicopter attitude variables by using the controlled helicopter condition and neglecting secondary coupling in f_{o1}' . The helicopter applied forces f_{oh} are the controls for the reduced system.

Examples are omitted since the reduced system equations are identical to the equations obtained by assuming point-mass helicopters. For point-mass helicopters, $\omega h, f_{c2}$, and f_{o2} are undefined, and for c.g. attachments at the helicopters, $A I_{12} = 0$ and $f_{c2} = 0$, so that the resulting equations for $\dot{u}1$ and s are identical, in both cases, to those of the reduced system given above.

Quasi-static equations for helicopter attitude and controls– If the reduced system is known, then the helicopter attitude angles and controls are dependent variables that can be determined by solving the quasi-static trim equations given in part c of table 2. The helicopters are assumed to be conventional, with four controls, and $F O j_N, V j^*_N, \dot{\alpha} j$ are known for each helicopter, $B j, j \in \mathcal{H}$, along with a specified value of the redundant attitude angle ψ_j . Then the four helicopter controls and remaining two attitude angles can be determined from the kinematic equations and the force-and-moment balance equations listed in part c of table 2. The quasi-static trim equations are related to the usual static trim algorithm found in conventional helicopter simulations. The helicopter model $(F A j_j, M A j_j)$ has the usual independent variables as noted in the table. For isolated helicopters in static equilibrium, the angular velocity, linear acceleration, and suspension forces and moments are zero. Here, the equations account (1) for nonzero angular motion, $\dot{\alpha} j$, which is presumed to be known from the attitude history; (2) for linear acceleration and suspension forces in $F O j_N$, which are known from the reduced system; and (3) for the suspension moments, $M C j_j$, in the moment equation. The body axis components of the suspension moments and rigid-body velocities depend on attitude, and these relations are included in the iterative solution procedure.

6. LINEARIZED EQUATIONS OF MOTION FOR GENERAL SLUNG-LOAD SYSTEMS WITH INELASTIC SUSPENSIONS

Linear analysis is the most commonly used technique in stability studies and control system design, hence

trim-solution algorithm. References 15 and 16 describe trim algorithms for single helicopters with one- and two-point suspensions. No complete algorithm has been given yet for any dual-lift system, but a study of equilibrium configurations along general reference trajectories for the dual-lift system with spreader bar obtained by solving a simplified trim problem is described in reference 5. Results are given for configuration geometry, cable forces, and thrust requirements.

The reference trajectory generalized coordinates $q_o(t)$, $u_o(t)$, $\dot{u}_o(t)$ are needed for the linearization, and are obtained from the reference configuration motion using the following geometry and kinematics:

$$\begin{aligned} r &= r(q) \\ v &= A(q) u + w \\ \dot{v} &= \dot{A} u + A \dot{u} \end{aligned} \quad (42)$$

Here, the kinematic model assumes that the coordinates u are chosen to generate configuration velocities relative to the mean wind, $v - w$, as is usual for linear analysis. If $\dot{v} = 0$, then $\dot{A}u = -A\dot{u}$, and it does not follow that u is fixed in static equilibrium without further assumptions about the generalized coordinates. If u is selected such that $A(q)$ depends only on variables that are fixed in static equilibrium, then $A(q_o)$, u_o are fixed and \dot{A}_o , \dot{u}_o are zero in static equilibrium. Such variables can be the coordinates of any line segment connecting points in the configuration, such as the rigid-body attitude angles and cable angles relative to inertial or body axes. The coordinates selected for the nonlinear EOMs in all the applications cases presented in appendixes B-E are *reference point coordinates* of this type. That is, (q, u) contain the position and velocity of a reference point $(R1^*_N, V1^*_N)$ and additional coordinates (\bar{q}, \bar{u}) , which suffice to define the positions and velocities of all points in the system relative to the position and velocity of the reference point

$$q = \begin{pmatrix} R1^*_N \\ \bar{q} \end{pmatrix}, \quad u = \begin{pmatrix} V1^*_N \\ \bar{u} \end{pmatrix}, \quad v = A(\bar{q}) u$$

where \bar{q} is constant and $\bar{u} = 0$ if the configuration is fixed and nonrotating. For linear analysis, the reference-point coordinates are usually given relative to the mean wind in body axes:

$$q = \begin{pmatrix} \int VA1^*_1 dt \\ \bar{q} \end{pmatrix}, \quad u = \begin{pmatrix} VA1^*_1 \\ \bar{u} \end{pmatrix}, \quad v = A(\bar{q}) u + w$$

where, as above, \bar{q} is constant and $\bar{u} = 0$ for fixed, non-rotating configurations. Then, for static equilibrium,

$$\begin{aligned} \bar{q}_o(t) &= \bar{q}(r_o(t)) \\ u_o &= \begin{pmatrix} VA0_N \\ 0 \end{pmatrix} \\ \dot{u}_o &= 0 \end{aligned} \quad (43)$$

and

$$\dot{A}_o = \sum_{q_i \in \bar{q}} \left(\frac{\partial A}{\partial q_i} \dot{q}_i \right)_o = 0$$

Linearized Equations from Lagrange's Equation

The nonlinear EOMs are obtained from Lagrange's equations in terms of the generalized position coordinates q . Equations for general slung-load systems are given by equations (23) and (24) and these are repeated in table 3. The terms M, k are obtained from derivatives of the kinetic energy. In the generalized forces, A defines $v(q, \dot{q})$, and T, fba, va are defined in equation (39). All dependencies on the independent variables $\{q, \dot{q}, \ddot{q}, \delta\}$ are indicated.

The reference trajectory $\{q_o(t), \dot{q}_o(t), \ddot{q}_o(t), \delta_o(t)\}$ satisfies the EOMs. The LEOMs are obtained by expanding these to first order in variations about the reference trajectory:

$$\begin{aligned} q &= q_o + \delta q \\ \dot{q} &= \dot{q}_o + \delta \dot{q} \\ \ddot{q} &= \ddot{q}_o + \delta \ddot{q} \\ \delta &= \delta_o + \Delta \end{aligned}$$

and then subtracting the EOMs evaluated on the reference trajectory to get

$$M_o \delta \ddot{q} + \delta M \ddot{q}_o + [\nabla_{\dot{q}}^T k]_o \delta \dot{q} + [\nabla_q^T k]_o \delta q = \delta Q$$

The variations $\delta M, \delta Q$ are further expanded by using their general dependencies on the independent variables of the problem. Complete results are given in the equation summary, table 3. Products and variations are interchanged where useful, for example, $\delta M(q) \ddot{q}_o = \delta(M(q) \ddot{q}_o) = [\nabla_q^T (M(q) \ddot{q}_o)]_{q_o} \delta q$.

The terms in the perturbation equations that are due to the dynamics $M(q) \ddot{q}$ and $k(q, \dot{q})$ are M_o, \bar{M}_o , and $k_q, k_{\dot{q}}$. The term \bar{M}_o is zero whenever $\ddot{q}_o = 0$; the coordinates q are usually selected such that this

Table 3. Linearized EOMs for slung-load systems from Lagrange's equations

Nonlinear EOMs:

$$M(q) \ddot{q} + k(q, \dot{q}) = Q(q, \dot{q}, \delta)$$

$$v = A(q) \dot{q} + w, \quad \dot{w} = 0$$

$$KE = \frac{1}{2} v^T D v$$

$$M = \nabla_q^T \nabla_{\dot{q}} KE = A^T D A$$

$$k = [\nabla_q^T \nabla_{\dot{q}} KE] \dot{q} - \nabla_q KE = A^T D \dot{A} \dot{q} + (\dot{A} - G)^T D v$$

$$G = [\nabla_q^T (A(q) \dot{q})]$$

$$Q = A(q^T) (fg + fa)$$

$$fa = T(q) fba(va, \delta)$$

$$va = T(q)^T (v - w)$$

LEOMs:

Reference trajectory: $\{q_o(t), \dot{q}_o(t), \ddot{q}_o(t), \delta_o(t)\}$

Perturbations: $\{\delta q, \delta \dot{q}, \delta \ddot{q}, \Delta\}$

Equations: $M_o \delta \ddot{q} + C_o \delta \dot{q} + K_o \delta q = Q_\delta \Delta$

where $C_o = k_{\dot{q}} - Q_{\dot{q}}$

$$K_o = \overline{M}_o + k_q - Q_q$$

$$Q_\delta = A_o^T T_o Fb_\delta$$

and $Q_{\dot{q}} = A_o^T F_{vaN} A_o$

$$\overline{M}_o = [\nabla_q^T (M(q) \ddot{q}_o)]_{q_o}$$

$$Q_q = Q1_q + Q2_q$$

$$k_q = [\nabla_q^T k]_{q_o, \dot{q}_o}$$

$$Q1_q = [\nabla_q^T (A(q)^T (fg + T(q) fba_o))]_{q_o}, \quad k_{\dot{q}} = [\nabla_{\dot{q}}^T k]_{q_o, \dot{q}_o}$$

$$Q2_q = A_o^T T_o \nabla_q^T fba = A_o^T F_{vaN} [\nabla_q^T (T_o T(q)^T (v_o - w) + A(q) \dot{q}_o)]_{q_o}$$

where $F_{vaN} = T_o Fb_{va} T_o^T$; $Fb_\delta, F_{va}, T, fba$ are defined in eqs. (39) and (40)

occurs in static equilibrium. All terms in $k_q, k_{\dot{q}}$ contain a velocity coordinate from \dot{q}_o and are zero whenever $\dot{q}_o = 0$; the coordinates q are usually selected such that this occurs in hover, and then $k(q, \dot{q})$ need not be formed, and

$$\delta\ddot{q} = M_o^{-1}(Q_{\dot{q}} \delta\dot{q} + Q_q \delta q + Q_\delta \Delta) \quad (44)$$

The terms that are due to k also drop out or simplify in static equilibrium for special choices of the generalized coordinates as established in the next subsection.

The terms in the LEOMs that are due to the applied forces are $Q_\delta, Q_{\dot{q}}, Q_q$. To obtain these expressions, the extended chain of dependencies

$$Q(q, \dot{q}, \delta) = Q(A(q), fa(T(q), fba(\delta, va(v(q, \dot{q}))))$$

should be noted. It can be seen in table 3 that Q_δ contains the control derivatives and that $Q_{\dot{q}}$ contains the stability derivatives. Furthermore, Q_q has been separated into $Q1_q$, which contains the equilibrium forces, and $Q2_q$, which contains a combination of stability derivatives with the reference velocity. The term $Q2_q$ is zero in windless hover where $\dot{q}_o, v_o - w$ are zero. The gradients of T, A in Q_q expand principally to gradients of coordinate transformations in the applications work; useful general formulas for this are given in appendix A (table 7).

Linearized Equations from d'Alembert's Principle

The nonlinear equation (14) can be arranged in a form that parallels the result from Lagrange's equations, and this form is given in the equation summary, table 4. All dependencies on the independent variables $\{q, u, \dot{u}, \delta\}$ are noted. These EOMs differ from the Lagrangian equations in the formulation of the second-order velocity terms $k(q, u)$ and in the use of generalized velocity coordinates, u different from \dot{q} . The second-order velocity term X is formulated in equation (3) in terms of the system's angular velocities, which are coordinates of v , whereas \dot{A} is formulated in the applications work (appendixes B-E) in terms of $\{q, u\}$ in all cases; these dependencies are assumed in table 4. The notation $\xi = \dot{A}u$, introduced for convenience, represents a configuration acceleration. Equation (14) is applied by formally defining the generalized velocity coordinates u , and position variables are introduced as needed to define $v(q, u)$ and $T(q)$. In general, fewer than d such variables may suffice for this purpose, and these are assumed to be given by a linear relation $\dot{q} = Y(q) u$ in table 4, where Y has full rank. If q is expanded to a set of d coordinates sufficient to define $r(t)$, then Y is nonsingular.

A reference trajectory is any $\{q_o(t), u_o(t), \dot{u}_o(t), \delta_o(t), t_o \leq t \leq t_f\}$ which satisfies the EOMs. The LEOMs are obtained by expanding the EOMs to first order in the independent variations, $\{\delta q, \delta u, \delta \dot{u}, \Delta\}$, and then subtracting the EOMs evaluated on the reference trajectory:

$$M_o \delta \ddot{u} + \delta M \dot{u}_o + \delta A^T (X_o + D\xi_o) + A_o^T (\delta X + D\delta\xi) = \delta Q$$

The variations $\delta M, \delta A, \delta X, \delta\xi, \delta Q$ can be expanded further; the results are given in the equation summary, table 4. In the coefficient matrices of the linearized equations, M_o, \bar{M}_o are from the term $M(q) \dot{u}$; k_u, k_q are from $k(q, u)$; and Q_u, Q_q, Q_δ are from the generalized forces.

In static equilibrium, the rigid-body angular velocities are zero, so that X_o, X_v, X_u, X_q are all zero regardless of the choice of generalized coordinates. Furthermore, the generalized coordinates used in all application examples given in appendixes B-E are reference-point coordinates. If inertial coordinates of the reference-point velocity, $V1^*_{N}$, are used as in these appendixes, then it is readily shown that the terms k_u and k_q due to k , and \bar{M}_o , are zero in static equilibrium. However, for linear analysis it is customary to use body axis coordinates of the velocity relative to the mean wind, $VA1^*_1$. In this case, A has the partitioned form

$$v = \begin{pmatrix} T_{N,1} & \vdots \\ \vdots & \vdots \\ T_{N,1} & \vdots \\ 0 & \vdots \\ \vdots & \vdots \\ 0 & \vdots \end{pmatrix} \bar{A}(\bar{q}) \begin{pmatrix} VA1^*_1 \\ \bar{u} \end{pmatrix} + \begin{pmatrix} I \\ \vdots \\ I \\ 0 \\ \vdots \\ 0 \end{pmatrix} W0_N \quad (45)$$

where \bar{q} is fixed and $\bar{u} = 0$ is in static equilibrium, and where A depends only on coordinates $(\bar{q}, \alpha 1)$, which are fixed in static equilibrium. Then

$$\begin{aligned} \bar{M}_o &= 0 \\ \xi_o &= 0 \\ \xi_q &= 0 \\ \xi_u &= \nabla_u^T \dot{A}u_o = -\nabla_u^T \begin{pmatrix} I \\ \vdots \\ I \\ 0 \\ \vdots \\ 0 \end{pmatrix} T_{N,1} S(VA0_1) \omega 1_1 \end{aligned}$$

Table 4. Linearized slung-load EOMs from equation (14)

Nonlinear EOMs:

$$M(q) \dot{u} + k(q, u) = Q(q, u, \delta)$$

$$\dot{q} = Y(q) u$$

$$v = A(q) u + w, \quad \dot{w} = 0$$

$$M = A(q)^T D A(q)$$

$$k = A(q)^T (X(v) + D \xi(q, u))$$

$$\xi = \dot{A}(q, u) u$$

$$Q = A(q)^T (fg + fa)$$

$$fa = T(q) fba(va, \delta)$$

$$va = T(q)^T (v - w)$$

LEOMs:

Reference trajectory: $\{q_o(t), u_o(t), \dot{u}_o(t), \delta_o(t)\}$

Perturbations: $\{\delta q, \delta u, \delta \dot{u}, \Delta\}$

Equations: $M_o \delta \dot{u} + C_o \delta u + K_o \delta q = Q_\delta \Delta$

$$\delta \dot{q} - \bar{Y}_o \delta q = Y_o \delta u$$

where

$$\bar{Y}_o = [\nabla_q^T Y(q) u_o]_{q_o}$$

$$C_o = k_u - Q_u$$

$$K_o = \bar{M}_o + k_q - Q_q$$

$$Q_\delta = A_o^T T_o F b_\delta$$

and

$$\bar{M}_o = [\nabla_q^T (M(q) \dot{u}_o)]_{q_o}$$

$$k_u = A_o^T [X_u + D \xi_u]$$

$$k_q = A_o^T [X_q + D \xi_q] + [\nabla_q^T A(q)^T (X_o + D \xi_o)]_{q_o}$$

where

$$X_v = [\nabla_v^T X]_{v_o}$$

$$X_u = X_v A_o$$

Table 4. Concluded.

$$X_q = X_v [\nabla_q^T A(q) u_o]_{q_o}$$

$$\xi_u = \dot{A}_o + [\nabla_u^T \dot{A}(q_o, u) u_o]$$

$$\xi_q = [\nabla_q^T \dot{A}(q, u_o) u_o]_{q_o}$$

and

$$Q_u = A_o^T F_{vaN} A_o$$

$$Q_q = Q1_q + Q2_q$$

$$Q1_q = [\nabla_q^T (A(q)^T (fg + T(q) fba_o))]_{q_o}$$

$$Q2_q = A_o^T F_{vaN} [\nabla_q^T (T_o T(q)^T (v_o - w) + A(q) u_o)]_{q_o}$$

where $F_{vaN} = T_o Fb_{va} T_o^T$; Fb_δ, Fva, T, fba are defined in eqs. (39) and (40)

Second-order ODE for δq :

$$M'_o \delta \ddot{q} + C'_o \delta \dot{q} + K'_o \delta q = Q_\delta \Delta$$

$$u = U(q) \dot{q}$$

$$M'_o = M_o U_o$$

$$C'_o = C_o U_o + M_o [\dot{U}_o + \nabla_{\dot{q}}^T (\dot{U}(q_o, \dot{q}) \dot{q}_o)]$$

$$K'_o = K_o + C_o [\nabla_q^T U(q) \dot{q}_o]_{q_o} + M_o [\nabla_q^T (\dot{U}(q, \dot{q}_o) \dot{q}_o + U(q) \ddot{q}_o)]_{q_o}$$

where $\mathbf{VA0} = \mathbf{V0} - \mathbf{W0}$. Assuming that ω_{11} is included in the generalized coordinates u , then the only nonzero column of ξ_u is the gradient with respect to ω_{11} :

$$\xi_u \delta u = \xi_{\omega_{11}} \delta \omega_{11} = - \begin{pmatrix} I \\ \vdots \\ I \\ 0 \\ \vdots \\ 0 \end{pmatrix} T_{N,1} S(\mathbf{VA0}_1) \delta \omega_{11} \quad (46a)$$

For this case, the LEOMs for static equilibrium simplify to

$$\delta \dot{u} = M_o^{-1} ((Q_u - A_o^T D \xi_u) \delta u + Q_q \delta q + Q_\delta \Delta) \quad (46b)$$

Here, ξ_u is the only contribution from the second-order velocity terms k . It is given from $\xi_{\omega_{11}}$ above; it is zero in hover, and otherwise adds terms in $\mathbf{VA0} \times \delta \omega_{11}$ to the velocity coefficient matrix in the LEOMs. The equations for static equilibrium and hover differ in form only by the terms ξ_u and Q_{2q} from Q_q ; these terms are proportional to the reference airspeed.

The LEOMs can also be given as a second-order ordinary differential equation (ODE) in the generalized position coordinates. This equation is obtained by forming the variations $\delta u(\delta q, \delta \dot{q})$, $\delta \dot{u}(\delta q, \delta \dot{q}, \delta \ddot{q})$ from the kinematic relation $u = U(q) \dot{q}$ and substituting these in the state equation. Here, q contains d coordinates, which suffice to define $r(t)$, and U is nonsingular. Results for general reference conditions and coordinates are included in table 4. For static equilibrium and reference-point coordinates such that

$$u = \begin{pmatrix} V A 1^* \\ \bar{u} \\ 1 \end{pmatrix} = \begin{pmatrix} I & \vdots & 0 \\ \dots & \vdots & \dots \\ 0 & \vdots & \bar{U}(\bar{q}) \end{pmatrix} \begin{pmatrix} V A 1^* \\ \bar{q} \\ 1 \end{pmatrix}$$

where \bar{u}, \bar{q} have the same meaning as above and are zero in static equilibrium, the second-order ODE form simplifies to

$$M_o U_o \delta \ddot{q} - (Q_u - A_o^T D \xi_u) U_o \delta \dot{q} - Q_q \delta q = Q_\delta \Delta \quad (47)$$

In applications, U is usually block diagonal and the modifications of the coefficient matrices in equation (46b) that are required to obtain the coefficient matrices in equation (47) are simple.

Linearized Equations from Explicit Constraint Method

The nonlinear equations (19) and (20) for the inelastic system are repeated in the equation summary, table 5. This form assumes that $6n$ coordinates u have been selected for the elastic system, which contain $6n - c$ coordinates, u_1 , of the system with inelastic suspension, and c coordinates, λ , which suffice to define the motion resulting from cable stretching. The matrices A, A^{-1} define the relations $v(q, u)$, $u(q, v)$, respectively, and the matrices A_1, A_1^{-1}, Λ , which appear in the EOMs for the inelastic subsystem u_1 , are submatrices of A, A^{-1} . Equations (19) and (20) differ from equation (14) in the formulation of the coefficient matrix of f_o , which is known analytically in equations (19) and (20) up to the inverse of the $c \times c$ matrix, S . The EOMs are linearized by expanding to first order in the variations $\{\delta q, \delta u, \delta \dot{u}, \Delta\}$ and then subtracting equations (19) and (20) evaluated on the reference trajectory $\{q_o(t), u_o(t), \dot{u}_o(t), \delta_o(t)\}$:

$$\delta \dot{u}_1 = \delta A_1^{-1} A_1^{-1} \dot{u}_1 + A_1^{-1} D^{-1} [\delta f_o + \delta f_c] \quad (48a)$$

In the first term, $D^{-1}(f_{o_o} + f_{c_o})$ has been replaced with its equivalent, $A_1^{-1} \dot{u}_1$. The variation of f_o is assembled from the variations of its terms, all of which were previously treated in tables 3 and 4. The constraint force perturbation is obtained from variations of

$$\begin{aligned} f_c &= \Sigma f_o = \Lambda s \\ s &= -S^{-1} \Lambda^T D^{-1} f_o \\ S &= \Lambda^T D^{-1} \Lambda \end{aligned}$$

which yield

$$\delta s = -S_o^{-1} [\delta S s_o + \delta \Lambda^T D^{-1} f_{o_o} + \Lambda_o^T D^{-1} \delta f_o]$$

where

$$\delta S s_o = \delta \Lambda^T D^{-1} f_{c_o} + \Lambda_o^T D^{-1} \delta \Lambda s_o$$

and then

$$\delta s = -S_o^{-1} [\delta \Lambda^T A_1^{-1} \dot{u}_1 + \Lambda_o^T D^{-1} \delta \Lambda s_o \Lambda_o^T D^{-1} \delta f_o] \quad (48b)$$

and also

$$\begin{aligned} \delta f_c &= \delta \Lambda s_o + \Lambda_o \delta s = \Sigma_o \delta f_o \\ &+ (I + \Sigma_o) \delta \Lambda s_o - \Lambda_o S_o^{-1} \delta \Lambda^T A_1^{-1} \dot{u}_1 \end{aligned} \quad (48c)$$

In equation (48b), $A_1^{-1} \dot{u}_1$ replaces its equivalent as above. The completed expansions of the constraint-force perturbations $\delta s, \delta f_c$ are included in table 5. Finally, the results for $\delta \dot{u}_1$ in table 5 can be obtained by

Table 5. Linearized slung-load EOMs from equations (19) and (20)

Nonlinear EOMs:

$$v = A(q) u + w = A1 u1 + L \dot{\lambda} + w, \quad \dot{w} = 0$$

$$\begin{pmatrix} u1 \\ \dot{\lambda} \end{pmatrix} = A^{-1}(q) (v - w) = \begin{pmatrix} A11^T \\ \Lambda^T \end{pmatrix} (v - w)$$

For $\dot{\lambda} = 0$:

$$\dot{q} = Y(q) u1$$

$$\dot{u}1 = A11(q)^T D^{-1} (fo + fc)$$

$$fc = \Sigma(q) fo = \Lambda(q) s$$

$$\Sigma = -\Lambda(q) S(q)^{-1} \Lambda(q)^T D^{-1}$$

$$s = -S(q)^{-1} \Lambda(q) D^{-1} fo$$

$$S = \Lambda(q)^T D^{-1} \Lambda(q)$$

$$fo = fg + T(q) fba(va, \delta) - X(v) - D \xi(q, u1)$$

$$va = T(q)^T (v - w)$$

$$\xi = \dot{A}1(q, u1) u1$$

Linearized suspension forces ($\dot{\lambda} = 0, \dot{w} = 0$):

$$\delta s = s_q \delta q + s_u \delta u1 + s_\delta \Delta$$

$$\delta fc = \Lambda_o \delta s + [\nabla_q^T \Lambda(q) s_o]_{q_o} \delta q$$

$$s_q = \bar{s}_q + \bar{S}_o [F_q - D \xi_q - X_q]$$

$$s_u = \bar{S}_o [F_{vaN} A1_o - D \xi_u - X_u]$$

$$s_\delta = \bar{S}_o T_o Fb_\delta$$

and

$$\bar{S}_o = -S_o^{-1} \Lambda_o^T D^{-1}$$

$$\bar{s}_q = -S_o^{-1} [\nabla_q^T \Lambda(q)^T A1_o \dot{u}1_o]_{q_o}$$

Table 5. Concluded.

LEOMs:

$$\delta \dot{u}1 = \Gamma_q \delta q + \Gamma_u \delta u1 + \Gamma_\delta \Delta$$

$$\delta \dot{q} = \bar{Y}_o \delta q + Y_o \delta u1$$

where

$$\bar{Y}_o = [\nabla_q^T Y(q) u1_o]_{q_o}$$

$$\Gamma_q = \bar{\Gamma}_q + G_o [F_q - D \xi_q - X_q]$$

$$\Gamma_u = G_o [F_{vaN} A1_o - D \xi_u - X_u]$$

$$\Gamma_\delta = G_o T_o Fb_\delta$$

and

$$G_o = A1_o^T D^{-1} [I + \Sigma_o]$$

$$X_u = X_v A1_o$$

$$X_q = X_v [\nabla_q^T A1(q) u1_o]_{q_o}$$

$$X_v = [\nabla_v^T X]_{v_o}$$

$$\xi_u = \dot{A}1_o + [\nabla_{u1}^T \dot{A}1(q_o, u1) u1_o]_{u1_o}$$

$$\xi_q = [\nabla_q^T \dot{A}1(q, u1_o) u1_o]_{q_o}$$

and

$$\bar{\Gamma}_q = \nabla_q^T [A1(q)^T - A1_o^T D^{-1} \Lambda_o S_o^{-1} \Lambda(q)^T]_{q_o} A1_o \dot{u}1_o$$

$$F_q = F1_q + F2_q$$

$$F1_q = [\nabla_q^T (T(q) fba_o + \Lambda(q) s_o)]_{q_o}$$

$$F2_q = F_{vaN} [\nabla_q^T (T_o T(q)^T (v_o - w) + A1(q) u1_o)]_{q_o}$$

where

$$s_o = -S_o^{-1} \Lambda_o^T D^{-1} f_o_o$$

$$F_{vaN} = T_o Fb_{va} T_o^T$$

Fb_δ , Fb_{va} , T , fba are defined in equations (39) and (40)

combining equations (48a) and (48c) and expanding the remaining variations. The gradients of the second-order velocity dynamics X, ξ and the stability and control derivatives F_{vaN}, F_δ occur in the coefficients of $\delta u, \delta q, \Delta$ as previously seen in table 4. The matrix \bar{T}_q is linear in the acceleration coordinates $\dot{u}1_o$, and is zero whenever $\dot{u}1_o = 0$. The reference trajectory forces occur in $F1_q$, and differ from their occurrence in the analogous $Q1_q$ of table 4 in that a term in the cable-tension parameters s replaces a term in the external forces.

Finally, if the coordinates, q, u , are reference-point coordinates with body axis coordinates of the reference-point velocity (eq. (45)) then for static equilibrium $X_o, X_u, X_q, \xi_q, \bar{T}_q$ are zero, ξ_u is given by equation (46), and the LEOMs simplify to

$$\delta \dot{u}1 = G_o [(F_{vaN} A1_o - D \xi_u) \delta u1 + F_q \delta q + T_o Fb_\delta \Delta] \quad (49)$$

The matrices G_o, F_q are defined in table 5.

Linearized Equations for Dual-Lift Systems

Linearized equations of motion for the dual-lift system with spreader bar are derived in appendix F for static equilibrium by using the formulation from equation (14). Reference-point coordinates are used with body axis components of the reference-point velocity, and equation (46) is applied. These results extend the hover equations given in references 6 and 7 to general static-equilibrium flight conditions, and include load and spreader-bar inertias and aerodynamics, and dissimilar helicopters.

The coefficient matrices are expanded to a working form in terms of the natural vectors and matrices of three-dimensional rigid-body mechanics. The number of such terms is much greater for the linearized equations for $\delta \dot{u}$ than for the nonlinear EOMs for \dot{u} , but the derivation is feasible with the methods of this report. MACSYMA was used to expand matrix products in order to reduce error probabilities in the analytical expressions.

7. CONCLUSIONS

Nonlinear simulation equations for general slung-load systems have been derived. These account for any suspension geometry, including controllable geometry and both elastic and inelastic suspensions, for

any number of helicopters, and for any choice of generalized velocity coordinates. Two formulations are given that generalize the previous case-specific conventional formulations for elastic and inelastic suspensions that are given in the slung-load literature. These formulations differ significantly in form and computational requirements. A third, new formulation is given by selecting the generalized coordinates of the unconstrained system to represent the constraints of the inelastic suspension. The internal suspension forces are calculated explicitly for both elastic and inelastic suspensions. The new formulation improves computational efficiency significantly for inelastic suspensions, enables integration of elastic and inelastic suspension models in a single equation set, by using a single set of generalized coordinates, and is readily applied to the complex dual-lift and multilift systems.

An inelastic suspension imposes constraints on the system motion, but their number is small compared with the number of DOFs. This fact, along with the cable interbody connections, distinguishes the slung-load systems from typical applications considered in the literature on multibody systems, and accounts for the efficiency of the new formulation for inelastic suspensions compared with the conventional ones in the slung-load and multibody literatures, the latter being efficient for highly constrained systems.

In past work, simulations have usually utilized elastic suspension models and rigid-body velocity coordinates, whereas control analyses have been based on the inelastic suspension model. These methods are selected because of the analytical simplicity and computational efficiency of the former, and the elimination of DOFs characterized by small motions in the latter. For simulation, the present results allow the use of any generalized velocity coordinates with the elastic suspension model, and the use of inelastic suspension models with reduced computational penalties. For control, the formulation of efficient nonlinear EOMs for inelastic suspensions makes it possible to apply the recent global inverse-model methods to slung-load systems, and facilitates the derivation of linearized EOMs for single-flight-condition designs.

Application of the general equations to the derivation of simulation equations for specific systems is demonstrated for a series of single-, dual-, and multiple-helicopter systems. Results are given in programmable form, with the dynamics formulated in terms of the natural vectors and matrices of three-dimensional rigid-body mechanics. This formulation

allows the devices of efficient coding to be applied to the vector-mechanical structure of the equations.

The single-helicopter systems with single attachment points at the helicopter are readily treated, and the results provide alternative formulations of the EOMs to those already given in the literature. Results for single-helicopter systems with multiple attachment points at the helicopter are more difficult to derive and were given solely for the bifilar suspension, which has also been treated in the literature. Nonlinear equations for the inelastic inverted-V and inverted-Y suspensions are not found in the open literature. The methods of this report do not address the analytical difficulties of these cases, which are omitted from the present work.

The principal new results are those for dual-lift and multilift systems. Equations for three dual-lift configurations are given and it is shown that these can be integrated in a single simulation. The multilift system extended to any number of helicopters was also treated. These previously difficult problems are seen to be tractable for derivation, analysis, and programming by hand with the methods of this report.

Equations for degenerate-body approximations (point masses, rigid rods) are given to accommodate various simplifications useful in control analysis, and results for dual-lift and multilift systems are given. A reduced-order load-suspension system is obtained by assuming that the helicopters control the system solely through their applied forces with the helicopter attitudes in steady state relative to the reduced system motion. The reduced system equations are those obtained assuming point-mass helicopters. The reduced system can be studied and a control law formulated for the applied forces independently of any helicopter details and of the problem of implementing the applied force controller in the helicopters. This simplification is expected to be realistic for helicopters with single-point attachments, including the dual-lift and multilift systems.

Linearized equations of motion for general slung-load systems with inelastic suspensions are derived from the nonlinear equations of motion, and results for the dual-lift system with spreader bar are given for general static-equilibrium flight conditions.

APPENDIX A SUMMARY OF USEFUL KINEMATIC RELATIONS

INTRODUCTION

This appendix collects the general kinematic formulas used in applying the methods of this report to derive the simulation equations given in appendixes B-E and the linearized equations for dual-lift systems. These formulas are mostly counterparts of relations from the classic physical vector theory of rigid-body dynamics given here in a form appropriate for digital computations by introducing coordinate-frame transformations. They facilitate derivation of the simulation equations in the preferred form of this work, in which all terms appear as operations on the underlying physical vectors.

The notation for this work is stated in the list of symbols. Occasionally, the general notational rules for vector kinematics advocated by Kane (ref. 40), are used; these are as follows:

${}^1\mathbf{v}_a$	Velocity of point \mathbf{R}_a relative to reference frame \mathcal{F}_1
${}^2\omega_1$	Angular velocity of reference frame \mathcal{F}_1 or of rigid body \mathcal{B}_1 relative to frame \mathcal{F}_2
$\frac{{}^1d\mathbf{V}}{dt}$	Time-derivative of physical vector \mathbf{V} relative to reference frame, \mathcal{F}_1

To work with the scalar equations used in digital computations a subscript can be added to indicate the reference frame in which the coordinates of the vector are given:

${}^1V_2^a$	Velocity of point \mathbf{R}_a relative to frame \mathcal{F}_1 given by its coordinates in frame \mathcal{F}_2
${}^2\omega_3^1$	Angular velocity of frame \mathcal{F}_1 relative to frame \mathcal{F}_2 given by its coordinates in frame \mathcal{F}_3

Time-derivatives of these objects are necessarily with respect to the reference frame in which they are given:

\dot{V}_1 $\frac{dV_1}{dt}$ or $\left(\frac{{}^1d\mathbf{V}}{dt}\right)_1$; time-derivative of physical vector \mathbf{V} relative to \mathcal{F}_1 and given by the coordinates in \mathcal{F}_1

The notational specializations stated in the list of symbols are continued in this appendix (e.g., \mathbf{V}_a , ω_b are reserved for the inertial velocity of \mathbf{R}_a , \mathcal{F}_b , respectively), but there is no conflict with the notation shown above, in which superscripts are used. Definitions and specializations reflect aeronautical usage and are generally consistent with those in reference 41.

Skew-Symmetric Matrix

First, the general skew-symmetric matrix $S(x, y, z)$ is defined from the scalar triplet (x, y, z) as shown in table 6. This allows scalar representation of the vector cross products, which occur frequently in this work, as shown in equation (51) for vectors $\mathbf{V}_1, \mathbf{V}_2$ referenced to frame \mathcal{F}_a . The algebra of skew-symmetric matrices is consistent with corresponding relations in vector algebra such as product reversals (eq. (51)) and triple products. Geometrically, $S(V_{1a})$ maps any vector \mathbf{V} given in \mathcal{F}_a to the vector $\mathbf{V}_1 \times \mathbf{V}$ referenced to \mathcal{F}_a and perpendicular to the plane of $(\mathbf{V}_1, \mathbf{V})$. The reference frames of vectors occurring in expressions based on equation (51) can be selected in any convenient and consistent way using transformations (eq. (52)). When viewed as an isolated matrix, the columns of $S(V_a)$ physically represent cross products of \mathbf{V} with the axes of \mathcal{F}_a and referred to \mathcal{F}_a (eq. (53)). Identities in the matrix $S(V_a)$ represent vector operations on an arbitrary vector, such as product reversal and the cross product with a sum of vectors (eqs. (54) and (55)).

Cross products representing Coriolis velocities and accelerations and centrifugal accelerations (eqs. (56)-(58)) are the basis from three-dimensional kinematics of virtually all terms in Au , $A^{-1}v$, $\dot{A}u$, in the applications of this report. Cross products also represent the applied moments due to cables in the term fc . In general, the force \mathbf{F} applied to body B at point \mathbf{R}_a imposes a moment on B about the point \mathbf{R}_c , which is given by $\mathbf{M}^{(c)} = \mathbf{R}_{ca} \times \mathbf{F}$. In the present work, this

can be specialized to cables in tension and to moments about the rigid body c.g.'s (eq. (59) and accompanying sketch). If cable Cj applies tension TCj in the direction kcj at point Rj on body Bi , then its moment about the c.g. of Bi is given by

$$M_{ij} = R_i^* j \times kcj \quad TCj = \xi_{ij} TCj$$

where the symbol ξ_{ij} is reserved for the moment of Cj on Bi per unit tension.

Coordinate Transformations, Angular Velocities, and Transformation Rates

Formulas defining the transformation of a vector from its coordinates in inertial space, \mathcal{F}_N , to its coordinates in body axes, \mathcal{F}_b , are given in table 7 along with relations governing its occurrence in kinematic equations with time-derivatives and its gradient.

The primitive transformations for rotations about a single axis i, j, k of a right-handed orthogonal reference frame, \mathcal{F} are denoted $E_1(\sigma), E_2(\sigma), E_3(\sigma)$, respectively (eqs. (60)-(62)). Then the usual Euler-angle transformations of aeronautics is given by the yaw, pitch, and roll sequence of rotations $T_{b,N}$ as illustrated and defined in table 7 (eq. (63)). It is often useful to note that the rows of $T_{b,N}$ are the \mathcal{F}_N -components of the axis vectors of \mathcal{F}_b and its columns are the \mathcal{F}_b -components of the axis vectors of \mathcal{F}_N (eq. (64)). The notation (ϕ, θ, ψ) is reserved in this work for inertial angles, and a subscript is attached to indicate the body axes. Euler-angle transformations from other axes \mathcal{F}_a are sometimes needed and an ad hoc notation is defined in text (e.g., $\Delta\phi_b, \Delta\theta_b, \Delta\psi_b$).

In general, if frame \mathcal{F}_b is obtained from \mathcal{F}_N by any arbitrary sequence of independent rotation angles $\beta_1, \beta_2, \dots, \beta_n$ about the axes $\mathbf{u}_1, \mathbf{u}_2, \dots, \mathbf{u}_n$, respectively, then its inertial angular velocity is given by the superposition

$$\mathbf{N}_{\omega} \mathbf{b} = \dot{\beta}_1 \mathbf{u}_1 + \dots + \dot{\beta}_n \mathbf{u}_n \quad (78)$$

Equation (66) specializes this rule to the Euler-angle sequence defined above, and the familiar linear relation from aeronautics for $\omega_b(\dot{a}b)$ and its inverse are noted in the table, along with expressions for Euler-angle rates in terms of dot products with ω_b . The notation \mathbf{Wb} is introduced to indicate the row list of the axes of roll, pitch, and yaw rotations for body axes \mathcal{F}_b , and a subscript indicates the coordinate frame in which these are given.

Transformation rates arise in the inertial coupling term \dot{A} or $\dot{A} u$ in the equations of motion, and useful expressions are noted in equations (69) and (70). In general, if $T_{a,b}$ is a transformation from \mathcal{F}_b to \mathcal{F}_a , then

$$\dot{T}_{a,b} = T_{a,b} S(\omega_b^b) \quad (79)$$

This relation follows as a counterpart of the Coriolis equation relating the time-derivative of a vector, \mathbf{V} , relative to two different frames, $\mathcal{F}_a, \mathcal{F}_b$; that is, using Kane's notation,

$${}^a d\mathbf{V} = \frac{b d\mathbf{V}}{dt} + {}^a \omega^b \times \mathbf{V}$$

but the time-derivative of

$$V_a = T_{a,b} V_b$$

is

$$\dot{V}_a = T_{a,b} \dot{V}_b + \dot{T}_{a,b} V_b$$

whence $\dot{T}_{a,b} V_b$ is identified as the scalar counterpart of ${}^a \omega^b \times \mathbf{V}$ for arbitrary V_b ; this establishes equation (79). In all cases, $\dot{A} u$ is composed of terms that are Coriolis and centrifugal accelerations that arise from the Coriolis equation and utilize equation (79).

Derivatives of transformations with respect to Euler angles occur in the linearized EOMs, especially in the position-perturbation term. These derivatives can be obtained from equation (79) by identifying the terms in the expansion

$$\dot{T}_{b,N} = \frac{\partial T_{b,N}}{\partial \phi_b} \dot{\phi}_b + \frac{\partial T_{b,N}}{\partial \theta_b} \dot{\theta}_b + \frac{\partial T_{b,N}}{\partial \psi_b} \dot{\psi}_b$$

with corresponding terms in the expansion of $T_{b,N} S(\omega_b^b)$, using $\omega_b = \dot{\phi}_b \mathbf{ib} + \dot{\theta}_b \mathbf{jb}' + \dot{\psi}_b \mathbf{kb}$ and the distributive property (eq. (55)). The results are listed in table 7 (eqs. (71)-(73)) and here as

$$\frac{\partial T_{b,N}}{\partial \phi_b} = -T_{b,N} S(ib_N) = -S(ib_b) T_{b,N}$$

$$\frac{\partial T_{b,N}}{\partial \theta_b} = -T_{b,N} S(jb'_N) = -S(jb'_b) T_{b,N} \quad (80)$$

$$\frac{\partial T_{b,N}}{\partial \psi_b} = -T_{b,N} S(kb_N) = -S(kb_b) T_{b,N}$$

These derivatives are cross products with the axes of roll, pitch, and yaw rotations, which are illustrated in table 7. They are also maps from \mathcal{F}_N to \mathcal{F}_b , and the rotation axes can be given in any convenient reference frame by using transformations as required for consistency with the input and output reference frames.

Derivatives of transformations arise commonly in the linearized EOMs from gradients of vectors,

$$v_b = T_{b,N} v_N, \quad v_N = T_{N,b} v_b$$

relative to Euler angles, where the vectors on the right-hand side are independent of $(\phi_b, \theta_b, \psi_b)$. It follows from equation (80) that

$$\begin{aligned} \frac{\partial T_{b,N} v_N}{\partial \phi_b} &= -(\mathbf{i}b \times \mathbf{v})_b = (\mathbf{v} \times \mathbf{i}b)_b \\ \frac{\partial T_{b,N} v_N}{\partial \theta_b} &= -(\mathbf{j}b' \times \mathbf{v})_b = (\mathbf{v} \times \mathbf{j}b')_b \\ \frac{\partial T_{b,N} v_N}{\partial \psi_b} &= -(\mathbf{k}N \times \mathbf{v})_b = (\mathbf{v} \times \mathbf{k}N)_b \end{aligned} \quad (81)$$

The vector-mechanical meaning and output reference frame is apparent in equation (81). Reference frames for the vectors and the order of the cross product can be selected in any convenient way consistent with these characteristics. By using equation (81), the gradient with respect to the Euler-angle triplet is

$$\begin{aligned} \nabla_{\alpha b}^T(T_{b,N} v_N) &= T_{b,N} S(v_N) [ib_N, jb'_N, kN_N] \\ &= T_{b,N} S(v_N) Wb_N \end{aligned} \quad (82)$$

and also

$$\nabla_{\alpha b}^T(T_{N,b} v_b) = -T_{N,b} S(v_b) Wb_b = -S(v_N) Wb_N$$

Again, the notation Wb_N, Wb_b indicates the matrix of Euler-angle rotation axes given by inertial or body-axis components, respectively. These results are included in table 7 and are valid for any arbitrary vector, \mathbf{v} .

Cables Axes

The general treatment of cable angles and cable axes in this report is summarized in table 8. The cable direction $\mathbf{k}c$ is located by inertial roll and pitch angles (ϕ_c, θ_c) taken in the usual Euler sequence, as illustrated in the table and in equation (83).

Cable axes $\mathcal{F}_c = \{\mathbf{i}c, \mathbf{j}c, \mathbf{k}c\}$ are constructed from these two angles with $\mathbf{k}c$ along the cable and $\mathbf{i}c$ in the inertial vertical plane of $(\mathbf{i}N, \mathbf{k}N)$. The transformation $T_{c,N}$ (eqs. (84) and (85)) is a specialization of the usual Euler-angle transformation with $\psi_c = 0$, and its rows and columns are the axes of \mathcal{F}_c expressed by its coordinates in \mathcal{F}_N and, conversely, as before.

Useful formulas are given for the inertial angular velocity of \mathcal{F}_c in terms of cable-angle rates (eqs. (86)-(88)), and for the cable velocity expressed in terms of cable length and angle rates (eqs. (89)-(92)). The \mathcal{F}_c coordinates of the cable velocity (eq. (92)) separate the cable-stretching motion ($\dot{\ell}_c$) from the orthogonal motion caused by cable rotation; this fact is frequently used in selecting the generalized coordinates u in the applications.

Cable angles relative to some noninertial axes \mathcal{F}_1 (e.g., helicopter body axes or level-heading axes) may be more useful coordinates in some problems. For these cases, Euler pitch and roll angles relative to \mathcal{F}_1 are used with special notation (e.g., $\Delta\phi_c, \Delta\theta_c$) to distinguish them from inertial angles. The previous coordinate transformations and illustration apply by analogy with a change of notation (eq. (93)). The longitudinal cable axis $\mathbf{i}c$ is now in the \mathcal{F}_1 vertical plane of $(\mathbf{i}1, \mathbf{k}1)$. The velocities of $\mathbf{R}c, \mathcal{F}_c$ relative to \mathcal{F}_1 (eqs. (95) and (96)) are given by analogy to equations (88) and (92). The relative cable velocity in cable axes ${}^1V_c^c$ separates the cable-stretching motion and motion due to cable rotations relative to \mathcal{F}_1 into orthogonal components. The inertial transformation and velocities (eqs. (97)-(99)) are obtained from elementary rules. Cable-stretching motion is again isolated in $\mathbf{V}c$ and its rotational motion is represented as a superposition of orthogonal rotation relative to \mathcal{F}_1 plus the effect of \mathcal{F}_1 's inertial angular velocity.

Gradients of the cable-axis transformations $T_{c,N}$ occur in the linearized EOMs. The required general formulas are specializations of the previous results obtained by dropping the yaw derivative and the axis of yaw rotation $\mathbf{k}N$ from table 7 (eqs. (71)-(75)).

Table 6. Skew-symmetric matrices and cross products

$$S(x, y, z) = \begin{pmatrix} 0 & -z & y \\ z & 0 & -x \\ -y & x & 0 \end{pmatrix} \quad (50)$$

$$(\mathbf{V1} \times \mathbf{V2})_a = S(V1_a) V2_a = -(\mathbf{V2} \times \mathbf{V1})_a = -S(V2_a) V1_a \quad (51)$$

$$(\mathbf{V1} \times \mathbf{V2})_a = S(V1_a) T_{a,b} V2_b = T_{a,b} S(V1_b) V2_b \quad (52)$$

$$S(V_a) = [(\mathbf{V} \times \mathbf{ia})_a, (\mathbf{V} \times \mathbf{ja})_a, (\mathbf{V} \times \mathbf{ka})_a] \quad (53)$$

$$S^T(V_a) = -S(V_a) \quad (54)$$

$$S(V1_a + V2_a) = S(V1_a) + S(V2_a) \quad (55)$$

Coriolis and centrifugal terms:

$$(\omega \times \mathbf{R})_a = S(\omega_a) R_a = -S(R_a) \omega_a \quad (56)$$

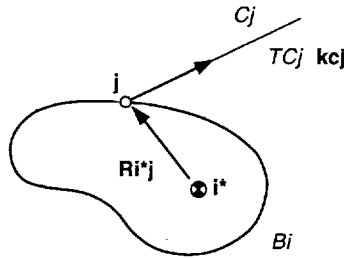
$$(\omega \times \mathbf{V})_a = S(\omega_a) V_a = -S(V_a) \omega_a \quad (57)$$

$$(\omega \times \omega \times \mathbf{R})_a = S^2(\omega_a) R_a = -S(\omega_a) S(R_a) \omega_a = \omega \bullet \mathbf{R} \omega_a - \omega^2 R_a \quad (58)$$

Moment of cable C_j on body B_i about \mathbf{Ri}^* :

$\mathcal{F}_i = \{\mathbf{ii}, \mathbf{ji}, \mathbf{ki}\} =$ body axes for B_i

$$M_{ij_i} = (\mathbf{Ri}^* \mathbf{j} \times TC_j \mathbf{kcj})_i = S(Ri^* j_i) kc_{j_i} TC_j = \xi_{ij_i} TC_j \quad (59)$$



Cable moment.

Table 7. Coordinate transformations, angular velocities, and transformation rates

Single-axis transformations:

$$E_1(\sigma) = \begin{pmatrix} 1 & 0 & 0 \\ 0 & \cos \sigma & \sin \sigma \\ 0 & -\sin \sigma & \cos \sigma \end{pmatrix} \quad (60)$$

$$E_2(\sigma) = \begin{pmatrix} \cos \sigma & 0 & -\sin \sigma \\ 0 & 1 & 0 \\ \sin \sigma & 0 & \cos \sigma \end{pmatrix} \quad (61)$$

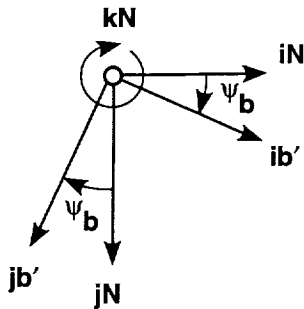
$$E_3(\sigma) = \begin{pmatrix} \cos \sigma & \sin \sigma & 0 \\ -\sin \sigma & \cos \sigma & 0 \\ 0 & 0 & 1 \end{pmatrix} \quad (62)$$

Euler-angle transformation, $T_{b,N}$:

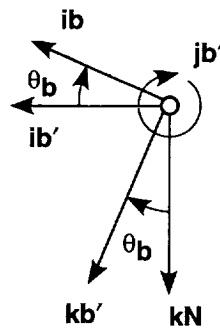
$\mathcal{F}_N = \{\mathbf{i}_N, \mathbf{j}_N, \mathbf{k}_N\}$ = inertial axes

$\mathcal{F}_b = \{\mathbf{i}_b, \mathbf{j}_b, \mathbf{k}_b\}$ = body axes

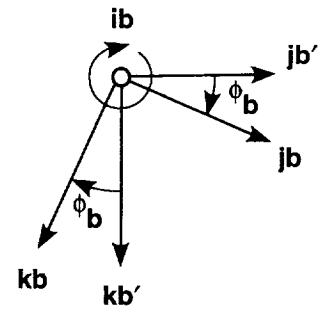
$\alpha_b = (\phi_b, \theta_b, \psi_b)^T$ = Euler-angle triplet



(a) ψ_b = heading rotation
(about \mathbf{k}_N)



(b) θ_b = pitch rotation
(about \mathbf{j}_b')



(c) ϕ_b = roll rotation
(about \mathbf{i}_b)

Euler angles.

Table 7. Continued.

$$T_{b,N}(\alpha b) = E_1(\phi_b) E_2(\theta_b) E_3(\psi_b)$$

$$= \begin{pmatrix} \cos \psi_b \cos \theta_b & \sin \psi_b \cos \theta_b & -\sin \theta_b \\ \sin \phi_b \cos \psi_b \sin \theta_b - \cos \phi_b \sin \psi_b & \sin \phi_b \sin \psi_b \sin \theta_b + \cos \phi_b \cos \psi_b & \sin \phi_b \cos \theta_b \\ \cos \phi_b \cos \psi_b \sin \theta_b + \sin \phi_b \sin \psi_b & \cos \phi_b \sin \psi_b \sin \theta_b - \sin \phi_b \cos \psi_b & \cos \phi_b \cos \theta_b \end{pmatrix} \quad (63)$$

$$T_{b,N} = \begin{pmatrix} ib_N^T \\ jb_N^T \\ kb_N^T \end{pmatrix} = (iN_b, jN_b, kN_b) \quad (64)$$

$$T_{N,b} = T_{b,N}^T \quad (65)$$

Angular velocity of \mathcal{F}_b relative to \mathcal{F}_N :

$$\mathbf{N}_\omega \mathbf{b} = \dot{\psi}_b \mathbf{k}_N + \dot{\theta}_b \mathbf{j}_b' + \dot{\phi}_b \mathbf{i}_b \quad (66)$$

$$\omega b_b = W b_b \dot{\alpha} b = \begin{pmatrix} 1 & 0 & -\sin \theta_b \\ 0 & \cos \phi_b & \sin \phi_b \cos \theta_b \\ 0 & -\sin \phi_b & \cos \phi_b \cos \theta_b \end{pmatrix} \begin{pmatrix} \dot{\phi}_b \\ \dot{\theta}_b \\ \dot{\psi}_b \end{pmatrix} = (ib_b, jb_b', kN_b) \begin{pmatrix} \dot{\phi}_b \\ \dot{\theta}_b \\ \dot{\psi}_b \end{pmatrix} \quad (67)$$

$$\dot{\alpha} b = W b_b^{-1} \omega b_b = \begin{pmatrix} 1 & \sin \phi_b \tan \theta_b & \cos \phi_b \tan \theta_b \\ 0 & \cos \phi_b & -\sin \phi_b \\ 0 & \sin \phi_b / \cos \theta_b & \cos \phi_b / \cos \theta_b \end{pmatrix} \omega b_b = \begin{pmatrix} \mathbf{i}_b' \bullet \omega \mathbf{b} / \cos \theta_b \\ \mathbf{j}_b' \bullet \omega \mathbf{b} \\ \mathbf{k}_b' \bullet \omega \mathbf{b} / \cos \theta_b \end{pmatrix} \quad (68)$$

where $\{\mathbf{i}_b', \mathbf{j}_b', \mathbf{k}_b'\}$ are unit vectors related to $\mathcal{F}_b, \mathcal{F}_N$ as illustrated above.

Transformation rates:

$$\dot{T}_{a,b} = T_{a,b} S({}^a \omega_b^b) = S({}^a \omega_a^b) T_{a,b} \quad (69)$$

$$\dot{T}_{N,b} = T_{N,b} S(\omega b_b) = S(\omega b_N) T_{N,b}$$

$$\dot{T}_{b,N} = -S(\omega b_b) T_{b,N} = -T_{b,N} S(\omega b_N) \quad (70)$$

Table 7. Concluded.

Transformation gradients:

$$\frac{\partial T_{b,N}}{\partial \phi_b} = \left(\frac{\partial T_{N,b}}{\partial \phi_b} \right)^T = -T_{b,N} S(ib_N) = -S(ib_b) T_{b,N} \quad (71)$$

$$\frac{\partial T_{b,N}}{\partial \theta_b} = \left(\frac{\partial T_{N,b}}{\partial \theta_b} \right)^T = -T_{b,N} S(jb'_N) = -S(jb'_b) T_{b,N} \quad (72)$$

$$\frac{\partial T_{b,N}}{\partial \psi_b} = \left(\frac{\partial T_{N,b}}{\partial \psi_b} \right)^T = -T_{b,N} S(kN_N) = -S(kN_b) T_{b,N} \quad (73)$$

$$\nabla_{\alpha b}^T T_{b,N}(\alpha b) v_N = T_{b,N} S(v_N) Wb_N = S(v_b) Wb_b \quad (74)$$

$$\nabla_{\alpha b}^T T_{N,b}(\alpha b) v_b = -T_{N,b} S(v_b) Wb_b = -S(v_N) Wb_N \quad (75)$$

$Wb = [\mathbf{ib}, \mathbf{jb}', \mathbf{kN}] = \text{roll, pitch, yaw axes of rotation}$

$$Wb_N = \begin{pmatrix} \cos \theta_b \cos \psi_b & -\sin \psi_b & 0 \\ \cos \theta_b \sin \psi_b & \cos \psi_b & 0 \\ -\sin \theta_b & 0 & 1 \end{pmatrix} \quad (76)$$

$$Wb_b = \begin{pmatrix} 1 & 0 & -\sin \theta_b \\ 0 & \cos \phi_b & \sin \phi_b \cos \theta_b \\ 0 & -\sin \phi_b & \cos \phi_b \cos \theta_b \end{pmatrix} \quad (77)$$

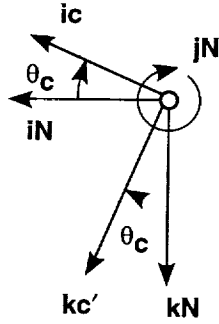
Table 8. Inertial cable angles and cable axes

Cable direction:

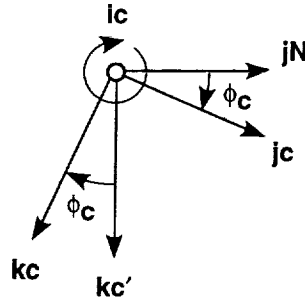
$\mathcal{F}_N = \{iN, jN, kN\}$ = inertial axes

(θ_c, ϕ_c) = cable pitch and roll angles

$$kc = \cos \phi_c \sin \theta_c iN - \sin \phi_c jN + \cos \phi_c \cos \theta_c kN \quad (83)$$



(a) Pitch rotation (about jN)



(b) Roll rotation (about ic)

Cable angles.

Cable axes, \mathcal{F}_c :

$\mathcal{F}_c = \{ic, jc, kc\}$

$$T_{c,N} = E_1(\phi_c) E_2(\theta_c) = \begin{pmatrix} \cos \theta_c & 0 & -\sin \theta_c \\ \sin \phi_c \sin \theta_c & \cos \phi_c & \sin \phi_c \cos \theta_c \\ \cos \phi_c \sin \theta_c & -\sin \phi_c & \cos \phi_c \cos \theta_c \end{pmatrix} \quad (84)$$

$$T_{c,N} = \begin{pmatrix} ic_N^T \\ jc_N^T \\ kc_N^T \end{pmatrix} = (iN_c \quad jN_c \quad kN_c) \quad (85)$$

Table 8. Concluded.

Inertial angular velocity of \mathcal{F}_c :

$$\omega^c = \dot{\theta}_c \mathbf{jN} + \dot{\phi}_c \mathbf{ic} \quad (86)$$

$$\omega^c = \dot{\phi}_c \mathbf{ic} + \dot{\theta}_c (\cos \phi_c \mathbf{jc} - \sin \phi_c \mathbf{kc}) \quad (87)$$

$$\omega^c = \dot{\phi}_c (\cos \theta_c \mathbf{iN} - \sin \theta_c \mathbf{kN}) + \dot{\theta}_c \mathbf{jN} \quad (88)$$

Inertial velocity of cable line segment, \mathbf{Rc} :

$$\mathbf{Rc} = \ell_c \mathbf{kc} \quad (89)$$

$$\mathbf{Vc} = \dot{\ell}_c \mathbf{kc} + \ell_c \dot{\mathbf{k}}c \quad (90)$$

$$\dot{\mathbf{k}}c = \omega^c \times \mathbf{kc} = \dot{\theta}_c \cos \phi_c \mathbf{ic} - \dot{\phi}_c \mathbf{jc} \quad (91)$$

$$\mathbf{Vc} = \ell_c \dot{\theta}_c \cos \phi_c \mathbf{ic} - \dot{\phi}_c \ell_c \mathbf{jc} + \dot{\ell}_c \mathbf{kc} \quad (92)$$

Cable angles relative to non-inertial axes, \mathcal{F}_1 :

$$\mathcal{F}_1 = \{\mathbf{i1}, \mathbf{j1}, \mathbf{k1}\}$$

$(\Delta\theta_c, \Delta\phi_c)$ = cable pitch and roll angle relative to \mathcal{F}_1

$$T_{c,1} = E_1(\Delta\phi_c) E_2(\Delta\theta_c) = \begin{pmatrix} \cos \Delta\theta_c & 0 & -\sin \Delta\theta_c \\ \sin \Delta\theta_c \sin \Delta\phi_c & \cos \Delta\phi_c & \cos \Delta\theta_c \sin \Delta\phi_c \\ \sin \Delta\theta_c \cos \Delta\phi_c & -\sin \Delta\phi_c & \cos \Delta\theta_c \cos \Delta\phi_c \end{pmatrix} \quad (93)$$

$$\mathbf{ic} = \cos \Delta\theta_c \mathbf{i1} - \sin \Delta\theta_c \mathbf{k1} \quad (94)$$

$$\mathbf{1}\omega^c = \Delta\dot{\theta}_c \mathbf{j1} + \Delta\dot{\phi}_c \mathbf{ic} = \Delta\dot{\phi}_c \mathbf{ic} + \Delta\dot{\theta}_c (\cos \Delta\phi_c \mathbf{jc} - \sin \Delta\phi_c \mathbf{kc}) \quad (95)$$

$$= \Delta\dot{\theta}_c \mathbf{j1} + \Delta\dot{\phi}_c (\cos \Delta\theta_c \mathbf{i1} - \sin \Delta\theta_c \mathbf{k1})$$

$$\mathbf{1Vc} = \dot{\ell}_c \mathbf{kc} + \ell_c \mathbf{1}\omega^c \times \mathbf{kc} = (\ell_c \Delta\dot{\theta}_c \cos \Delta\phi_c \mathbf{ic} - \ell_c \Delta\dot{\phi}_c \mathbf{jc} + \dot{\ell}_c \mathbf{kc}) \quad (96)$$

$$T_{c,N} = T_{c,1} T_{1,N} \quad (97)$$

$$\omega^c = \mathbf{1}\omega^c + \omega^1 \quad (98)$$

$$\mathbf{Vc} = \mathbf{1Vc} + \ell_c \omega^1 \times \mathbf{kc} \quad (99)$$



APPENDIX B

SIMULATION EQUATIONS FOR SINGLE-POINT SUSPENSIONS

INTRODUCTION

Figure 4 shows three suspensions of interest with a single attachment point on the helicopter. If the cables are modeled as inelastic, then the multicable suspension with three or more cables (fig. 4(a)) imposes three constraints on the load motion whereas the other two suspensions impose only one. If cable elasticity is modeled, then the suspension in figure 4(b) is considered to have only one elastic cable; the sling legs that connect the load to the ring are assumed to be sufficiently short and stiff that their elastic stretching is negligible. Figure 4(c) represents suspensions with long sling legs whose elastic stretching must be considered.

Previous simulations of such systems are described in references 13, 14, and 16. Reference 14 documents a Langley Research Center simulation of the CH-54 helicopter with a MILVAN cargo container suspended from a single elastic cable as in figure 4(b). Reference 13 uses a general formulation for elastic suspensions with multiple attachment points in which every cable connects the two bodies; this is readily specialized to systems *a* and *b* in figure 4, and an approximate adaptation to system *c*, in which no cable connects two bodies, is given. Reference 15 considers a system like *a* with elastic suspension and one like system *b* with elastic or inelastic suspension. These formulations all begin with the rigid-body accelerations, either inertial or relative to body axes, and relative load velocity is calculated in some cases.

This appendix contains simulation equations for systems *a* and *b* obtained by the methods presented in this report. Generalized velocity coordinates are selected specific to each case in order to separate the system motion caused by cable stretching from motion with invariant cable lengths. These are rigid-body velocities and cable velocity or relative motion coordinates in an appropriate coordinate frame. The results account for both elastic and inelastic suspensions. Interaction forces are explicitly calculated in both cases. Appropriate partitioning coordinates for system *c* were not

obtained, but coordinates that simplify the determination of the suspension forces for elastic cables are indicated without elaboration to EOMs.

Nomenclature and enumeration of the attachment points, cables, rigid bodies, and system parameters used in this appendix are defined in figure 4. The cable-length parameters $\{\ell_{oj}\}$ refer to the fixed cable lengths in the case of inelastic cables and to the unloaded cable lengths in the case of elastic cables. Controllable parameters are not considered ($\dot{p} = 0$).

Multicable Suspension

System and constraints— Referring to figure (4a), *m* cables, C_1, C_2, \dots, C_m attach the load, *B2* to the point **Ra** on the helicopter, *B1*. Usually, three or four cables are used. In any case, it is assumed that the cable geometry is such that if the cables are inelastic then the suspension fixes the distances from **Ra** to three noncolinear points on *B2*. This suffices to impose three holonomic constraints on the configuration

$$c = 3, \quad d = 9 \quad (100)$$

by fixing the line segment between the load c.g. and the helicopter attachment point in load-body axes; that is, for inelastic cables,

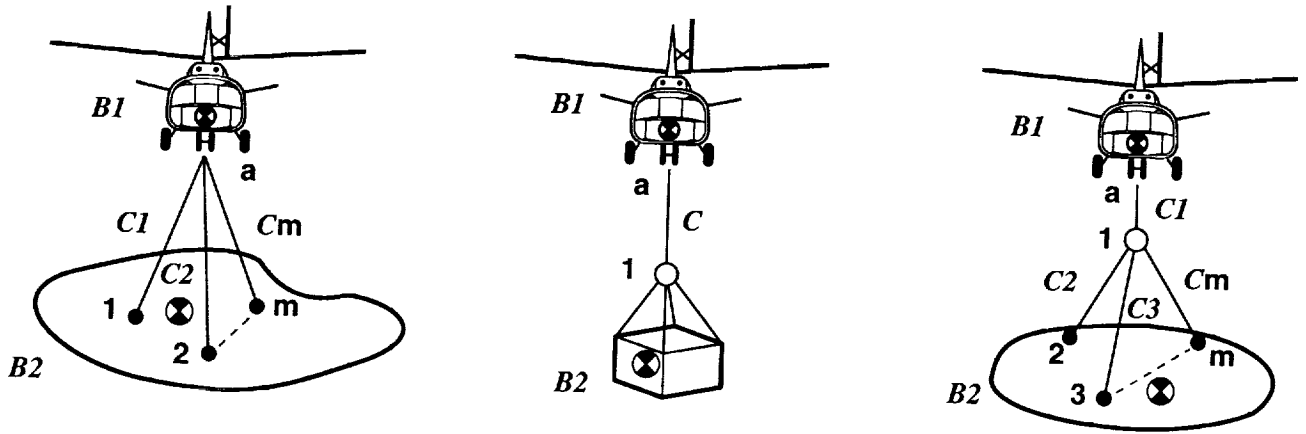
$$\dot{R}a_2^* = 0$$

where

$$Ra_2^*(r) = T_{2,N} (R2^*_N - R1^*_N - T_{N,1} R1^*_a_1)$$

For some arrangements of three cables, collapse of a cable is possible, thus leaving the load free to rotate about a line joining the remaining two attachment points, in which event the number of constraints is reduced to two. However, this is prevented by adding a cable ($m = 4$), and then $c = 3$ even if one cable collapses. With four or more inelastic cables the constraints are imposed redundantly, and the individual cable forces cannot be calculated; however, their resultant can always be calculated, and this calculation is independent of the number of cables used to maintain $c = 3$.

46

Parameters:

$m_1, J_1, R_1^*a_1$
 $m_2, J_2, R_2^*1_2, \dots, R_2^*m_2$
 $\lambda_{oj}, j=1, \dots, m \text{ for } m > 2$

(a) Multi-cable suspension

$m_1, J_1, R_1^*a_1$
 $m_2, J_2, R_2^*1_2$
 λ_o

(b) Single-cable suspension

$m_1, J_1, R_1^*a_1$
 $m_2, J_2, R_2^*2_2, \dots, R_2^*m_2$
 $\lambda_{oj}, j=1, \dots, m \text{ for } m > 2$

(c) Single-cable sling suspension

Figure 4. Single point suspensions.

Generalized velocity coordinates and configuration kinematics— The first task is to find generalized velocity coordinates for the elastic system

$$u = \begin{pmatrix} u_1 \\ \dot{\lambda} \end{pmatrix} \quad (101)$$

such that, if the cables are inelastic, then $\dot{\lambda} = 0$ and u_1 are the generalized coordinates. In the present case, $(V_1^*, \omega_1, \omega_2)$ comprise nine generalized velocity coordinates which suffice to define the configuration velocity of the inelastic cable system and can be taken as u_1 . The remaining element of the configuration velocity, V_2^* , is given from the inertial derivative of

$$R_2^*N = R_1^*N + T_{N,1} R_1^*a_1 + T_{N,2} R_2^*a_2 \quad (102)$$

as

$$V_2^*N = \begin{cases} V_1^*N - T_{N,1} S(R_1^*a_1) \omega_1 \\ -T_{N,2} S(R_2^*a_2) \omega_2 \\ \text{(inelastic cables)} \\ V_1^*N - T_{N,1} S(R_1^*a_1) \omega_1 \\ +T_{N,2} [\dot{R}a_2^* - S(R_2^*a_2) \omega_2] \\ \text{(elastic cables)} \end{cases} \quad (103)$$

Thus, the configuration velocity caused by cable stretch can be given by augmenting the coordinates u_1 for the inelastic cable system given above with the velocity of $R_2^*a_2$ relative to load-body axes, \mathcal{F}_2 :

$$u = \begin{pmatrix} V1^*_{N} \\ \omega 1_1 \\ \omega 2_2 \\ \dot{R}a2^*_2 \end{pmatrix} \quad (104)$$

The inverse relation for $\dot{R}a2^*_2(v)$ is obtained from equation (103) as

$$\dot{R}a2^*_2 = T_{2,N} (-V1^*_N + V2^*_N + T_{N,1} S(R1^*a_1) \omega 1_1) + S(Ra2^*_2) \omega 2_2 \quad (105)$$

The complete kinematic relations $v(u)$, $u(v)$ are assembled in the equation summary, table 9, using equations (103) and (105). The submatrices $AI1$, Λ of A^{-1} required below are identified in the table. Only coordinate transformations and skew-symmetric matrices representing Coriolis terms occur in A , A^{-1} . Otherwise, these matrices each contain nine rows from the unit matrix corresponding to the nine coordinates of u , which are also configuration velocity coordinates.

External forces and inertia coupling terms- The external forces and inertia coupling terms f_o are assembled in part b of table 9. The notation **F01**, ..., **M02** for the vector elements of f_o is introduced for brevity in later equations; f_o contains the sum of the applied forces and moments due to weight ($m1 \mathbf{g}$, $m2 \mathbf{g}$), aerodynamics and rotor output (**FA1**, ..., **MA2**), and the inertia coupling terms, $X + D \dot{A} u$. The time-derivative of A requires only time-derivatives of transformations, for which a general formula is given in appendix A. The three terms in $F02_N$ due to $\dot{A} u$ are recognized as centrifugal and Coriolis acceleration terms of the form $\omega \times \omega \times \mathbf{R}$ and $\omega \times \mathbf{V}$.

Suspension forces- The forces applied to the configuration of rigid bodies by the suspension are denoted for this system by

$$fc = \begin{pmatrix} FC1_N \\ FC2_N \\ MC1_1 \\ MC2_2 \end{pmatrix} \quad (106)$$

where **FC1**, ..., **MC2** are the resultants of cable forces acting on each rigid body and their moments about its c.g.

For inelastic cables, fc is given by equation (17) as

$$fc = \Lambda s = \begin{pmatrix} -T_{N,2} \\ T_{N,2} \\ -A_{22}^T T_{N,2} \\ -S(Ra2^*_2) \end{pmatrix} \begin{pmatrix} s_1 \\ s_2 \\ s_3 \end{pmatrix} \quad (107)$$

where Λ^T are the last three rows of A^{-1} and s are suspension force parameters. Since $FC1_N = -T_{N,2} s$, s is identified as the \mathcal{F}_2 - components of the resultant suspension force applied to the helicopter at \mathbf{Ra} ; that is, $s = -FC1_2$. In that case, s can be conveniently replaced by $-T_{2,N} FC1_N$ in equation (107), and $T_{2,N}$ can be combined with Λ to obtain the simple, alternative expression,

$$fc = \Lambda' FC1_N = \begin{pmatrix} I \\ -I \\ A_{22}^T \\ A_{23}^T \end{pmatrix} FC1_N \quad (108)$$

Finally, for inelastic cables, $FC1_N$ is given in terms of Λ' and f_o from equation (19). The results are listed in the equation summary, part c of table 9.

For elastic cables, fc can be given by equation (11), which applies generally whenever each cable connects two rigid bodies. However, it is simpler to use the form in equation (108), which is valid in this example whether or not the cables are inelastic. It only remains to calculate the resultant suspension force, $FC1_N$, from the cable tensions:

$$\begin{aligned} FC1_N &= \sum_{j=1}^m kc_{jN} TCj \\ &= \sum_{j=1}^m \max\{0, K_j (1 - \frac{\ell_{oj}}{\ell_j}) + c_j \frac{\dot{\ell}_j}{\ell_j}\} Raj_N \end{aligned} \quad (109)$$

Cable damping, c_j , is usually absent from slung-load simulation models. The cable line segments required in equation (109) can be calculated from

$$Raj_N = T_{N,2} (Ra2^*_2 + R2^*j_2) \quad j = 1, \dots, m$$

and each cable length rate can be obtained as the component of cable velocity along the cable, and can be shown to be

$$\dot{\ell}_j = Raj_N^T \dot{R}a2^*_2 / \ell_j \quad j = 1, \dots, m$$

where $\{R2^*j_2, j = 1, \dots, m\}$ are given system parameters and where $Ra2^*_2, \dot{R}a2^*_2, T_{N,2}$ are obtained directly

from the generalized position and velocity coordinates. These results are included in the simulation equation summary (table 9).

Simulation equations— Finally, the simulation equations are listed in part d of table 9. The total specific force, sf , due to $fo + fc$, is assembled and its vector elements are denoted $\mathbf{SF1}, \dots, \mathbf{SM2}$ for convenience. Last, the elements of \dot{u} are obtained by expanding $A^{-1} sf$. If the cables are inelastic it is unnecessary to calculate $\dot{R}a2^*_2$ or the term due to $\dot{R}a2^*_2$ in $\dot{A} u$, but they can be evaluated to monitor computational accuracy.

Single-Cable Suspension

System and constraints— The suspension shown in figure 4(b) has a single main cable, C , attached to the helicopter at \mathbf{Ra} . Additional cables or hardware attach the load to $\mathbf{R1}$, but these are assumed inelastic here, being either short cables with negligible stretch, or inelastic links of any length. In these cases, they can be regarded as part of the load rigid body, $B2$, since the point $\mathbf{R1}$ is fixed relative to the load.

If $C1$ is inelastic then it imposes a single holonomic constraint on the configuration motion by fixing the distance between \mathbf{Ra} on $B1$ and $\mathbf{R1}$ on $B2$, in which case

$$c = 1, \quad d = 11 \quad (110)$$

and the constraint equation can be given as

$$\begin{aligned} \ell(r) &= |Ra1_N| \\ &= |R2^*_N + T_{N,2} R2^*_{12} - R1^*_N - T_{N,1} R1^*_{a1}| \\ &= \ell_0 \end{aligned}$$

Generalized coordinates— The first task is to select appropriate generalized coordinates $(u1, \dot{\lambda})$ with the properties previously stated with equation (101). Assume that the nine rigid-body coordinates, $(V1^*_N, \omega1_1, \omega2_2)$ can again be included in $u1$. Then the remaining rigid-body velocity, $V2^*_N$, can be given from the derivative of

$$R2^*_N = R1^*_N + T_{N,1} R1^*_{a1} + Ra1_N - T_{N,2} R2^*_{12}$$

as (111)

$$\begin{aligned} V2^*_N &= V1^*_N - T_{N,1} S(R1^*_{a1}) \omega1_1 + Va1_N \\ &\quad + T_{N,2} S(R2^*_{12}) \omega2_2 \end{aligned}$$

It remains to express $Va1_N$ in terms of coordinates that separate the cable rotational motion from the cable stretching motion, $\dot{\ell}$. The rotational coordinates can be defined in several ways that represent rotations relative to either inertial space \mathcal{F}_N , or to helicopter body axes \mathcal{F}_1 , or to level heading axes based on the helicopter heading \mathcal{F}_h . The kinematics are given for all three cases, and the simulation equations are given for coordinates defining cable rotations relative to \mathcal{F}_h .

First, inertial cable pitch and roll angles θ_c, ϕ_c are defined in table 10, and then cable axes $\mathcal{F}_c = \{\mathbf{ic}, \mathbf{jc}, \mathbf{kc}\}$ can be constructed with \mathbf{kc} along the cable and \mathbf{ic} in the inertial vertical plane of $(\mathbf{iN}, \mathbf{kN})$. The angular velocity of \mathcal{F}_c relative to \mathcal{F}_N is, from appendix A:

$$\omega c = \dot{\phi}_c \mathbf{ic} + \dot{\theta}_c (\cos \phi_c \mathbf{jc} - \sin \phi_c \mathbf{kc})$$

and the velocity $Va1$ is given from

$$Va1 = \dot{\ell} \mathbf{kc} + \ell \omega c \times \mathbf{kc}$$

or

$$Va1_N = T_{N,c} Va1_c = T_{N,c} (\ell \dot{\theta}_c \cos \phi_c, -\ell \dot{\phi}_c, \dot{\ell})^T \quad (112)$$

The coordinates $Va1_c$ are seen to separate the cable rotational and stretching motion and, together with $(V1^*_N, \omega1_1, \omega2_2)$, they are suitable generalized coordinates for the elastic cable system. The cable rotation is represented by linear velocity components perpendicular to the cable direction. This results in a simpler kinematic relation, $v(u)$, than is obtained by using the cable angular rates θ_c, ϕ_c as coordinates. The kinematic relations $v(u)$, $u(v)$ are readily given from equations (111) and (112), and the results are listed in part a of table 10.

Most loads suspended by a single cable will stabilize at a steady-state position relative to the helicopter on each steady segment of a reference flight path. For such loads, in a steady turn, the cable will trail the vertical at a steady angle in the vertical plane of $(\mathbf{i1}, \mathbf{kN})$ because of load drag, and the load will swing out to a steady cable angle that is about equal to the helicopter roll angle, ϕ_1 , from this vertical plane as a result of centrifugal force. These steady angles are represented by sinusoidal variations of the inertial cable angles θ_c, ϕ_c with helicopter heading, ψ_1 . For example, θ_c alternately represents the trailing angle or the swing angle at different headings. To avoid this complexity in representing ordinary steady motion, other choices of the generalized coordinates are considered next.

Second, cable pitch and roll angles relative to helicopter body axes $\Delta\theta_c, \Delta\phi_c$, are defined in part b of table 10. The following derivation uses general formulas for cable kinematics relative to noninertial axes given in appendix A, table 8. Cable axes, $\mathcal{F}_c = \{\mathbf{ic}, \mathbf{jc}, \mathbf{kc}\}$ are again constructed with \mathbf{kc} along the cable, but \mathbf{ic} is now a direction in the helicopter vertical plane of $(\mathbf{i1}, \mathbf{k1})$. In this case, a steady load-trail angle is represented by a steady relative pitch $\Delta\theta_c$, and a steady load-swing angle is represented by a relative roll angle that is approximately zero. For these coordinates, the angular velocity of \mathcal{F}_c relative to \mathcal{F}_1 is (table 8, eq. (95))

$$\Delta\omega_c = \Delta\dot{\phi}_c \mathbf{ic} + \Delta\dot{\theta}_c(\cos \Delta\phi_c \mathbf{jc} - \sin \Delta\phi_c \mathbf{kc})$$

and then the inertial velocity $\mathbf{Va1}$ is (table 8, eq. (96))

$$\mathbf{Va1} = \dot{\ell} \mathbf{kc} + \ell(\omega_1 + \Delta\omega_c) \times \mathbf{kc}$$

or

$$Va1_N = -T_{N,1} S(Ra1_1) \omega_{1_1} + T_{N,c} \Delta Va1_c$$

where

$$\Delta Va1_c = (\ell \Delta\dot{\theta}_c \cos \Delta\phi_c, -\ell \Delta\dot{\phi}_c, \dot{\ell})^T \quad (113)$$

Here, $\Delta\mathbf{Va1}$ is the velocity of $\mathbf{Ra1}$ relative to \mathcal{F}_1 , and its components in \mathcal{F}_c are seen to separate the cable rotational and stretching motions; then $(V1^*_N, \omega_{1_1}, \omega_{2_2}, \Delta Va1_c)$ are suitable generalized velocity coordinates for the elastic system. The kinematic relations $v(u), u(v)$ are given by using equations (111) and (113), and the results are listed in part b of table 10.

Third, level heading axes, $\mathcal{F}_h = \{\mathbf{ih}, \mathbf{jh}, \mathbf{kN}\}$, are a local vertical frame defined from the helicopter heading ψ_1 , as shown in part c of table 10. Cable pitch and roll angles relative to \mathcal{F}_h , are denoted θ_{ch}, ϕ_{ch} , and then cable axes $\mathcal{F}_c = \{\mathbf{ic}, \mathbf{jc}, \mathbf{kc}\}$ are constructed (part c of table 10) with \mathbf{ic} in the inertial vertical plane of $(\mathbf{ih}, \mathbf{kN})$. In this case, θ_{ch}, ϕ_{ch} have steady values in a steady turn that are approximately the load-trail and load-swing angles, respectively. The angular velocities of \mathcal{F}_h relative to \mathcal{F}_N , and of \mathcal{F}_c relative to \mathcal{F}_h are

$$\begin{aligned} \omega_h &= \dot{\psi}_1 \mathbf{kN} \\ \omega_{ch} &= \dot{\phi}_{ch} \mathbf{ic} + \dot{\theta}_{ch}(\cos \theta_{ch} \mathbf{jc} - \sin \theta_{ch} \mathbf{kc}) \end{aligned}$$

where $\dot{\psi}_1$ is given in terms of ω_{1_1} by the usual kinematic relation for Euler-angle rates (eq. (68) in appendix A):

$$\dot{\psi}_1 = \frac{1}{\cos \theta_1} (0, \sin \phi_1, \cos \phi_1) \omega_{1_1} = \frac{1}{\cos \theta_1} (k1'_1)^T \omega_{1_1}$$

where $\mathbf{k1}'$ can be shown to be a direction in the vertical plane containing $(\mathbf{i1}, \mathbf{ih}, \mathbf{kN})$ at an angle θ_1 from \mathbf{kN} . Then the inertial cable velocity is

$$\mathbf{Va1} = \dot{\ell} \mathbf{kc} + \ell (\omega_h + \omega_{ch}) \times \mathbf{kc}$$

or

$$Va1_N = T_{N,c} \left(\frac{\ell}{\cos \theta_1} (\mathbf{kN} \times \mathbf{kc})_c (k1'_1)^T \omega_{1_1} + Va1h_c \right) \quad (114)$$

where

$$Va1h_c = (\ell \dot{\theta}_{ch} \cos \phi_{ch}, -\ell \dot{\phi}_{ch}, \dot{\ell})^T$$

Here, $\mathbf{Va1h}$ is the velocity of $\mathbf{Ra1}$ relative to \mathcal{F}_h , and its components in \mathcal{F}_c are seen to separate the cable rotational and stretching motion. The coordinates $(V1^*_N, \omega_{1_1}, \omega_{2_2}, Va1h_c)$ are suitable generalized coordinates for the system with elastic cables. The kinematic relations $v(u), u(v)$ are readily given by using equations (111) and (114), and the results are listed in part c of table 10.

The remaining equations for simulating the system with these coordinates are given in parts d-f of table 10. The suspension force is obtained from equation (11) using the last row of A^{-1} which corresponds to $\dot{\ell}(v)$.

Remarks

1. In the event of extraordinary motion in which all the cables collapse ($fc = 0$), the equations for elastic cables still correctly represent the motion of the two independent rigid bodies. However, the equations for inelastic cables assumed c constraints. If the number of constraints is reduced as a result of collapsed cables, the d equations no longer suffice, but the simulation can accommodate this regime by carrying along the complete set of 12 equations. However, additional equations are needed to detect the onset of such collapse, but these are not given here. Since such extreme divergent load motion is unacceptable it may be unnecessary to simulate it.

2. The suspension of figure 4(c) has not yet been specifically discussed. This suspension consists of a three- or four-cable sling which attaches the load to the single cable C1, and the elasticity of the sling is to be simulated. If the sling cables are inelastic, then the treatment and equations of table 10 apply, since the load and sling still form a rigid body. If the sling cables are elastic, then all cables must be considered

in order to determine fc . In this latter case, each cable is connected to only one of the rigid bodies. The principal analytical problem is to locate the interconnection point, $\mathbf{R1}$, from the force-balance equation at $\mathbf{R1}$ and from the sling geometry in order to obtain cable lengths and tensions:

$$\begin{aligned} FC1_2 &= TC1 \, kc1_2 = K_1 \left(1 - \frac{\ell o1}{\ell_1}\right) Ra1_2 \\ &= - \sum_{j=2}^m \max\{0, K_j \left(1 - \frac{\ell o_j}{\ell_j}\right)\} Rj1_2 \\ Ra1_2 &= Ra2^*_2 + R2^*1_2 = \ell_1 \, kc1_2 \quad (115) \\ Rj1_2 &= R2^*1_2 - R2^*j_2 = \ell_j \, kcj_2 \quad j = 2, \dots, m \end{aligned}$$

Cable C1 can be taken as elastic or inelastic in the force-balance equation, and cable damping is omitted. If $Ra2^*_2$ is known as a result of using the coordinates v or including $\dot{Ra2}^*_2$ in the generalized velocity coordinates, then equations (115) is a nonlinear vector equation in $R2^*1_2$ and the (dependent) cable force, $FC1_2$. Reference 13 provides an approximate solution for $R2^*1_2$.

Alternatively, if the generalized coordinates u are selected as $(V1^*_N, \omega_{11}, \omega_{21}, \dot{R2}^*1_2)$, then $R2^*1_2$ and all sling-leg lengths and tensions are known, and $FC1_2$, $Ra1_2$ are readily given from equations (115). This use of specially selected generalized coordinates for the elastic-sling case circumvents the problem of solving equation (115) for $\dot{R2}^*1_2$. Moderate complexity reappears in the velocity relations $V2^*_N(u)$ and $\dot{R2}^*1_2(v)$, which now depend partly on the sling geometry and elasticity parameters:

$$\begin{aligned} V2^*_N &= V1^*_N - T_{N,1} S(R1^*a_1) \omega_{11} \\ &\quad - T_{N,2} S(Ra2^*_2) \omega_{22} - T_{N,2} [I + M] \dot{R2}^*1_2 \end{aligned}$$

or, solving for $\dot{R2}^*1_2$,

$$\begin{aligned} \dot{R2}^*1_2 &= -[I + M]^{-1} T_{2,N} [V2^*_N - V1^*_N \\ &\quad + T_{N,1} S(R1^*a_1) \omega_{11} + T_{N,2} S(Ra2^*_2) \omega_{22}] \quad (116) \end{aligned}$$

where

$$Ra2^*_2 = Ra1_2 - R2^*1_2$$

and M gives $\dot{Ra1}_2$ from $\dot{R2}^*1_2$. Noting in equation (115) that $Ra1_2$ can be given from $FC1_2$ which, in turn, can be given from $R2^*1_2$, then

$$\begin{aligned} \dot{Ra1}_2 &= [\nabla_{FC1_2}^T Ra1_2] \dot{FC1}_2 \\ &= [\nabla_{FC1_2}^T Ra1_2] [\nabla_{R2^*1_2}^T FC1_2] \dot{R2}^*1_2 \\ &= -M \dot{R2}^*1_2 \end{aligned}$$

and (algebra omitted):

$$\begin{aligned} M &= M1 \, M2 \\ M1 &= [\nabla_{FC1_2}^T Ra1_2] = \frac{\ell_1}{TC1} [I - (1 - \frac{\Delta \ell_1}{\ell_1}) KC1] \\ M2 &= -[\nabla_{R2^*1_2}^T FC1_2] \\ &= \sum_{j=2}^m \delta_j K_j [KCj + \frac{\Delta \ell_j}{\ell_j} [I - KCj]] \end{aligned}$$

where for $j = 1, 2, \dots, m$

$$\begin{aligned} KCj &= kcj_2 \, kcj_2^T \\ \Delta \ell_j &= \ell_j - \ell o_j \\ \delta_j &= \begin{cases} 0 & \ell_j \leq \ell o_j \\ 1 & \ell_j > \ell o_j \end{cases} \end{aligned}$$

Here, KCj , $I - KCj$ are projections on and perpendicular to the cable directions, \mathbf{kcj} . If cable C1 is inelastic, then $\Delta \ell_1 = 0$ in $M1$.

The kinematic relations $u(v)$, $v(u)$ can be assembled by using equation (116) and then the simulation equations can be given by applying equation (9a). Further description of the resulting simulation equations is omitted because the treatment here is outside the pattern of interest for the applications work; that is, there is no subset of the coordinates u that represents the inelastic suspension.

3. The EOMs for \dot{v} given in reference 16 for the two systems (a) and (b) of figure 4 with inelastic suspensions can be obtained by the procedure outlined in section 3, equations (26)-(30), by using generalized coordinates which are reference point coordinates like those in part a of tables 9 and, part a of table 10, except that the reference point is moved to the load attachment point for system (a), and to the cable midpoint for system (b).

Table 9. Simulation equation summary: multicable suspension

(a) Configuration kinematics:

$$v = \begin{pmatrix} V1^*_N \\ V2^*_N \\ \omega_{1_1} \\ \omega_{2_2} \end{pmatrix} = A u = \begin{pmatrix} I & 0 & 0 & | & 0 \\ I & A_{22} & A_{23} & | & T_{N,2} \\ 0 & I & 0 & | & 0 \\ 0 & 0 & I & | & 0 \end{pmatrix} \begin{pmatrix} V1^*_N \\ \omega_{1_1} \\ \omega_{2_2} \\ \dot{R}a2^*_2 \end{pmatrix}$$

$$A_{22} = -T_{N,1} S(R1^*a_1)$$

$$A_{23} = -T_{N,2} S(Ra2^*_2)$$

$$u = \begin{pmatrix} V1^*_N \\ \omega_{1_1} \\ \omega_{2_2} \\ \dot{R}a2^*_2 \end{pmatrix} = \begin{pmatrix} AI1^T \\ \text{---} \\ \Lambda^T \end{pmatrix} v = \begin{pmatrix} I & 0 & 0 & 0 \\ 0 & 0 & I & 0 \\ 0 & 0 & 0 & I \\ \text{---} & \text{---} & \text{---} & \text{---} \\ -T_{2,N} & T_{2,N} & -T_{2,N} & A_{22} & S(Ra2^*_2) \end{pmatrix} \begin{pmatrix} V1^*_N \\ V2^*_N \\ \omega_{1_1} \\ \omega_{2_2} \end{pmatrix}$$

(b) External forces and inertia coupling terms:

$$f_o = fg + fa - X - D \dot{A} u$$

$$f_o = \begin{pmatrix} F01_N \\ F02_N \\ M01_1 \\ M02_2 \end{pmatrix} = \begin{pmatrix} m1 g_N + FA1_N \\ m2 g_N + FA2_N - m2 (\dot{A}_{22} \omega_{1_1} + \dot{A}_{23} \omega_{2_2} + \dot{T}_{N,2} \dot{R}a2^*_2) \\ MA1_1 - S(\omega_{1_1}) J1 \omega_{1_1} \\ MA2_2 - S(\omega_{2_2}) J2 \omega_{2_2} \end{pmatrix}$$

$$\dot{A}_{22} \omega_{1_1} = -T_{N,1} S(\omega_{1_1}) S(R1^*a_1) \omega_{1_1} = T_{N,1} S^2(\omega_{1_1}) R1^*a_1$$

$$\dot{A}_{23} \omega_{2_2} = -T_{N,2} [S(\omega_{2_2}) S(Ra2^*_2) + S(\dot{R}a2^*_2)] \omega_{2_2} = T_{N,2} S(\omega_{2_2}) (S(\omega_{2_2}) Ra2^*_2 + \dot{R}a2^*_2)$$

$$\dot{T}_{N,2} \dot{R}a2^*_2 = T_{N,2} S(\omega_{2_2}) \dot{R}a2^*_2$$

Table 9. Concluded.

(c) Suspension forces:

$$fc = \begin{pmatrix} FC1_N \\ FC2_N \\ MC1_1 \\ MC2_2 \end{pmatrix} = \Lambda' FC1_N = \begin{pmatrix} I \\ -I \\ A_{22}^T \\ A_{23}^T \end{pmatrix} FC1_N$$

Inelastic cables:

$$FC1_N = -[\Lambda'^T D^{-1} \Lambda']^{-1} \Lambda'^T D^{-1} fo$$

$$\Lambda'^T D^{-1} fo = \frac{1}{m1} F01_N - \frac{1}{m2} F02_N + A_{22} J1^{-1} M01_1 + A_{23} J2^{-1} M02_2$$

$$\Lambda'^T D^{-1} \Lambda' = \frac{m1+m2}{m1 m2} I + A_{22} J1^{-1} A_{22}^T + A_{23} J2^{-1} A_{23}^T$$

Elastic cables:

$$FC1_N = T_{N,2} \sum_{j=1}^m \max\{0, K_j (1 - \ell_{oj}/\ell_j) + c_j \frac{\dot{\ell}_j}{\ell_j}\} Raj_2$$

$$Raj_2 = R2^* j_2 + Ra2^*_2$$

$$\dot{\ell}_j = Raj_2^T \dot{Ra}2^*_2 / \ell_j$$

(d) Simulation equations:

$$sf = \begin{pmatrix} SF1_N \\ SF2_N \\ SM1_1 \\ SM2_2 \end{pmatrix} = D^{-1} (fo + fc) = \begin{pmatrix} (F01_N + FC1_N)/m1 \\ (F02_N + FC2_N)/m2 \\ J1^{-1} (M01_1 + MC1_1) \\ J2^{-1} (M02_2 + MC2_2) \end{pmatrix}$$

$$\dot{u} = A^{-1} sf$$

$$\dot{V}1^*_N = SF1_N$$

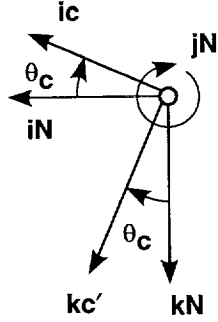
$$\dot{\omega}1_1 = SM1_1$$

$$\dot{\omega}2_2 = SM2_2$$

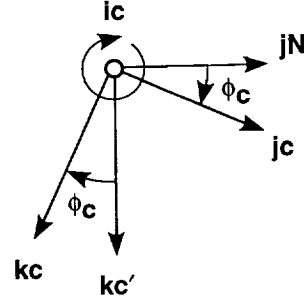
$$\ddot{Ra}2^*_2 = T_{2,N} [SF2_N - SF1_N - A_{22} SM1_1 - A_{23} SM2_2]$$

Table 10. Simulation equation summary: single-cable suspension

(a) Configuration kinematics for inertial cable angles:



(a) q_c = pitch rotation (about j_N)



(b) f_c = roll rotation (about ic)

Inertial cable angles.

$$T_{c,N} = E_1(\phi_c) E_1(\theta_c)$$

$$V a_{1c} = (\ell \dot{\theta}_c \cos \phi_c, -\ell \dot{\phi}_c, \dot{\ell})^T$$

$$v = \begin{pmatrix} V1^*_N \\ V2^*_N \\ \omega_{11} \\ \omega_{22} \end{pmatrix} = A u = \begin{pmatrix} I & 0 & 0 & 0 \\ I & A_{22} & A_{23} & T_{N,c} \\ 0 & I & 0 & 0 \\ 0 & 0 & I & 0 \end{pmatrix} \begin{pmatrix} V1^*_N \\ \omega_{11} \\ \omega_{22} \\ V a_{1c} \end{pmatrix}$$

$$A_{22} = -T_{N,1} S(R1^* a_1)$$

$$A_{23} = T_{N,2} S(R2^* 1_2)$$

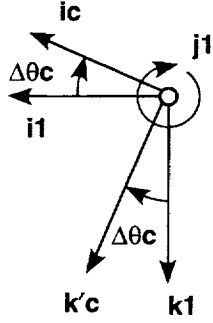
$$u = \begin{pmatrix} V1^*_N \\ \omega_{11} \\ \omega_{22} \\ V a_{1c} \end{pmatrix} = A^{-1} v = \begin{pmatrix} I & 0 & 0 & 0 \\ 0 & 0 & I & 0 \\ 0 & 0 & 0 & I \\ -T_{c,N} & T_{c,N} & B_{43} & B_{44} \end{pmatrix} \begin{pmatrix} V1^*_N \\ V2^*_N \\ \omega_{11} \\ \omega_{22} \end{pmatrix}$$

$$B_{43} = -T_{c,N} A_{22}$$

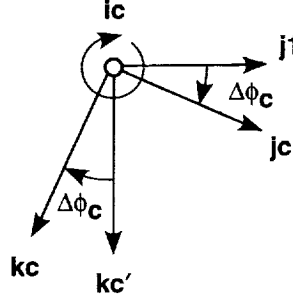
$$B_{44} = -T_{c,N} A_{23}$$

Table 10. Continued.

(b) Configuration kinematics for cable angles relative to \mathcal{F}_1 :



(a) Pitch rotation (about j_1)



(b) Roll rotation (about ic)

Cable angles relative to \mathcal{F}_1 .

$$T_{c,1} = E_1(\Delta\phi_c) E_2(\Delta\theta_c)$$

$$\Delta Va1_c = (\ell \Delta\dot{\theta}_c \cos \Delta\phi_c, -\ell \Delta\dot{\phi}_c, \dot{\ell})^T$$

$$v = \begin{pmatrix} V1^*_N \\ V2^*_N \\ \omega_{11} \\ \omega_{21} \end{pmatrix} = \begin{pmatrix} I & 0 & 0 & 0 \\ I & A_{22} & A_{23} & T_{N,c} \\ 0 & I & 0 & 0 \\ 0 & 0 & I & 0 \end{pmatrix} \begin{pmatrix} V1^*_N \\ \omega_{11} \\ \omega_{22} \\ \Delta Va1_c \end{pmatrix}$$

$$R1^*1_1 = R1^*a_1 + Ra1_1 = R1^*a_1 + \ell kc_1$$

$$A_{22} = -T_{N,1} S(R1^*1_1)$$

$$A_{23} = T_{N,2} S(R2^*1_2)$$

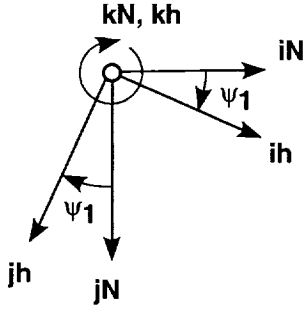
$$u = \begin{pmatrix} V1^*_N \\ \omega_{11} \\ \omega_{22} \\ \Delta Va1_c \end{pmatrix} = \begin{pmatrix} I & 0 & 0 & 0 \\ 0 & 0 & I & 0 \\ 0 & 0 & 0 & I \\ -T_{c,N} & T_{c,N} & B_{43} & B_{44} \end{pmatrix} \begin{pmatrix} V1^*_N \\ V2^*_N \\ \omega_{11} \\ \omega_{22} \end{pmatrix}$$

$$B_{43} = -T_{c,N} A_{22}$$

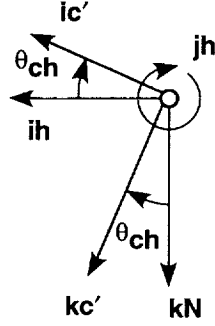
$$B_{44} = -T_{c,N} A_{23}$$

Table 10. Continued.

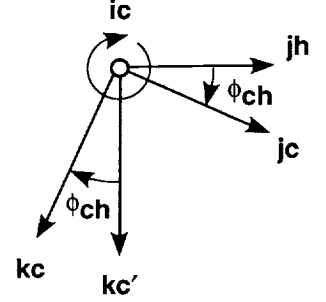
(c) Configuration kinematics for cable angles relative to \mathcal{F}_h :



(a) Heading axes



(b) Pitch rotation (about j_h)



(c) Roll rotation (about i_c)

Cable angles relative to \mathcal{F}_h .

$$T_{h,N} = E_3(\psi_1)$$

$$T_{c,h} = E_1(\phi_{ch}) E_2(\theta_{ch})$$

$$T_{c,N} = T_{c,h} T_{h,N}$$

$$Valh_c = (\ell \dot{\theta}_{ch} \cos \phi_{ch}, -\ell \dot{\phi}_{ch}, \dot{\ell})^T$$

$$v = \begin{pmatrix} V1^*_N \\ V2^*_N \\ \omega_{1_1} \\ \omega_{2_1} \end{pmatrix} = A u = \begin{pmatrix} I & 0 & 0 & 0 \\ I & A_{22} & A_{23} & T_{N,c} \\ 0 & I & 0 & 0 \\ 0 & 0 & I & 0 \end{pmatrix} \begin{pmatrix} V1^*_N \\ \omega_{1_1} \\ \omega_{2_2} \\ Valh_c \end{pmatrix}$$

$$z\omega_N = \frac{\ell}{\cos \theta_1} S(kc_N) kN_N = \frac{\ell}{\cos \theta_1} T_{N,h} (-\sin \phi_{ch}, -\cos \phi_{ch} \sin \theta_{ch}, 0)^T$$

$$k1'_1 = (0, \sin \phi_1, \cos \phi_1)^T$$

$$A_{22} = -T_{N,1} S(R1^*a_1) - z\omega_N(k1'_1)^T$$

$$A_{23} = T_{N,2} S(R2^*1_2)$$

$$u = \begin{pmatrix} V1^*_N \\ \omega_{1_1} \\ \omega_{2_2} \\ Valh_c \end{pmatrix} = A^{-1} v = \begin{pmatrix} I & 0 & 0 & 0 \\ 0 & 0 & I & 0 \\ 0 & 0 & 0 & I \\ -T_{c,N} & T_{c,N} & B_{43} & B_{44} \end{pmatrix} \begin{pmatrix} V1^*_N \\ V2^*_N \\ \omega_{1_1} \\ \omega_{2_2} \end{pmatrix}$$

$$B_{43} = -T_{c,N} A_{22}$$

$$B_{44} = -T_{c,N} A_{23}$$

Table 10. Continued.

(d) External forces and inertia coupling for cable angles relative to \mathcal{F}_h :

$$f_o = fg + fa - X - D \dot{A} u$$

$$f_o = \begin{pmatrix} F01_N \\ F02_N \\ M01_1 \\ M02_2 \end{pmatrix} = \begin{pmatrix} m1 g_N + FA1_N \\ m2 g_N + FA2_N - m2 (\dot{A}_{22} \omega_{11} + \dot{A}_{23} \omega_{22} + \dot{T}_{N,c} Valh_c) \\ MA1_1 - S(\omega_{11}) J1 \omega_{11} \\ MA2_2 - S(\omega_{22}) J2 \omega_{22} \end{pmatrix}$$

Auxiliary expressions for \dot{A} :

$$\begin{pmatrix} \dot{\theta}_{ch} \\ \dot{\phi}_{ch} \\ \dot{\ell} \end{pmatrix} = [diag(\ell \cos \phi_{ch}, -\ell, 1)]^{-1} Valh_c$$

$$\omega_{ch_c} = (\dot{\phi}_{ch}, \dot{\theta}_{ch} \cos \phi_{ch}, -\dot{\theta}_{ch} \sin \phi_{ch})^T$$

$$\begin{pmatrix} \dot{\phi}_1 \\ \dot{\theta}_1 \\ \dot{\psi}_1 \end{pmatrix} = \begin{pmatrix} 1 & \tan \theta_1 \sin \phi_1 & \tan \theta_1 \cos \phi_1 \\ 0 & \cos \phi_1 & -\sin \phi_1 \\ 0 & \sin \phi_1 / \cos \theta_1 & \cos \phi_1 / \cos \theta_1 \end{pmatrix} \omega_{11}$$

$$\omega_{c_c} = \dot{\psi}_1 kN_c + \omega_{ch_c}$$

$$z\dot{\omega}_N = (\dot{\ell}/\ell + \dot{\theta}_1 \tan \theta_1) z\omega_N + \frac{\ell}{\cos \theta_1} \left[kc_N(\omega_c \bullet kN) - T_{N,c} \omega_{c_c} (kc \bullet kN) \right]$$

Terms from $\dot{A} u$:

$$\dot{A}_{22} \omega_{11} = T_{N,1} S^2(\omega_{11}) R1^* a_1 - z\omega_N \cos \theta_1 \dot{\psi}_1 - z\omega_N \dot{\phi}_1 \dot{\theta}_1$$

$$\dot{A}_{23} \omega_{22} = -T_{N,2} S^2(\omega_{22}) R2^* 1_2$$

$$\dot{T}_{N,c} Valh_c = T_{N,c} S(\omega_{c_c}) Valh_c$$

Table 10. Concluded.

(e) Suspension forces: cable angles relative to \mathcal{F}_h :

$$f_c = \begin{pmatrix} FC1_N \\ FC2_N \\ MC1_1 \\ MC2_2 \end{pmatrix} = H TC = \begin{pmatrix} kc_N \\ -kc_N \\ \xi_{1_1} \\ -\xi_{2_2} \end{pmatrix} TC$$

$$\xi_{1_1} = S(R1^* a_1) T_{1,N} kc_N$$

$$\xi_{2_2} = S(R2^* 1_2) T_{2,N} kc_N$$

$$TC = \begin{cases} \max\{0, K(\ell - \ell_0) + c \dot{\ell}\} & \text{(elastic cables)} \\ -(H^T D^{-1} H)^{-1} H^T D^{-1} f_o & \text{(inelastic cables)} \end{cases}$$

$$H^T D^{-1} f_o = kc_N^T (F01_N/m1 - F02_N/m2) + \xi_{1_1}^T J1^{-1} M01_1 - \xi_{2_2}^T J2^{-1} M02_2$$

$$H^T D^{-1} H = \frac{m1+m2}{m1 m2} + \xi_{1_1}^T J1^{-1} \xi_{1_1} + \xi_{2_2}^T J2^{-1} \xi_{2_2}$$

(f) Simulation equations for cable angles relative to \mathcal{F}_H :

$$sf = \begin{pmatrix} SF1_N \\ SF2_N \\ SM1_1 \\ SM2_2 \end{pmatrix} = D^{-1} (f_o + f_c)$$

$$\dot{u} = A^{-1} sf$$

$$\dot{V}1^*_N = SF1_N$$

$$\dot{\omega}1_1 = SM1_1$$

$$\dot{\omega}2_2 = SM2_2$$

$$\dot{V}a1h_c = T_{c,N} [SF2_N - SF1_N - A_{22} SM1_1 - A_{23} SM2_2]$$



APPENDIX C

SIMULATION EQUATIONS FOR BIFILAR SUSPENSIONS

INTRODUCTION

Several multipoint suspensions were developed or considered in the 1965-1975 period of research for the Heavy Lift Helicopter, including the inverted-Y suspensions (fig. 5(a)) with or without spreader bar (ref. 42), or with active longitudinal and lateral control of the attachment points by means of control arms (ref. 32); the inverted-V suspension (fig. 5(b)) (refs. 15 and 43), and the three-point suspension (fig. 5(c)) with active vertical winching of all three cables and active lateral movement of the forward attachment point (ref. 33). The bifilar suspension (fig. 5(d)) is of analytical interest as a tractable approximation of some practical suspensions, and is the case treated in this appendix. These suspension designs, along with wind-tunnel and flight-test results and additional bibliography, are discussed in the references cited above.

The object of these multipoint suspensions was to stabilize difficult loads developing significant aerodynamic specific forces and moments, such as the 8- by 8- by 20-ft standard cargo container (MILVAN). In a single-point suspension, such elongated loads orient themselves broadside to the flight path in a maximum drag attitude and become unstable at speeds (40-60 knots) that are well below the power-limited speed of the helicopter. In addition, the light natural damping factor of the load pendulum motion (less than 0.1) interferes with rapid, precision load placement and can result in pilot-induced oscillations at cruise speeds, especially in IFR operations. The two-point suspensions (figs. 5(a) and 5(b)) provide yaw restraint and restrict pitch attitude to achieve stable flight at higher speeds in a minimum drag orientation, and the addition of active control of appropriate suspension parameters increases pendulum damping sufficiently to achieve precision load placement and stable flight over the helicopter's power-limited speed range under IFR conditions (refs. 32 and 43).

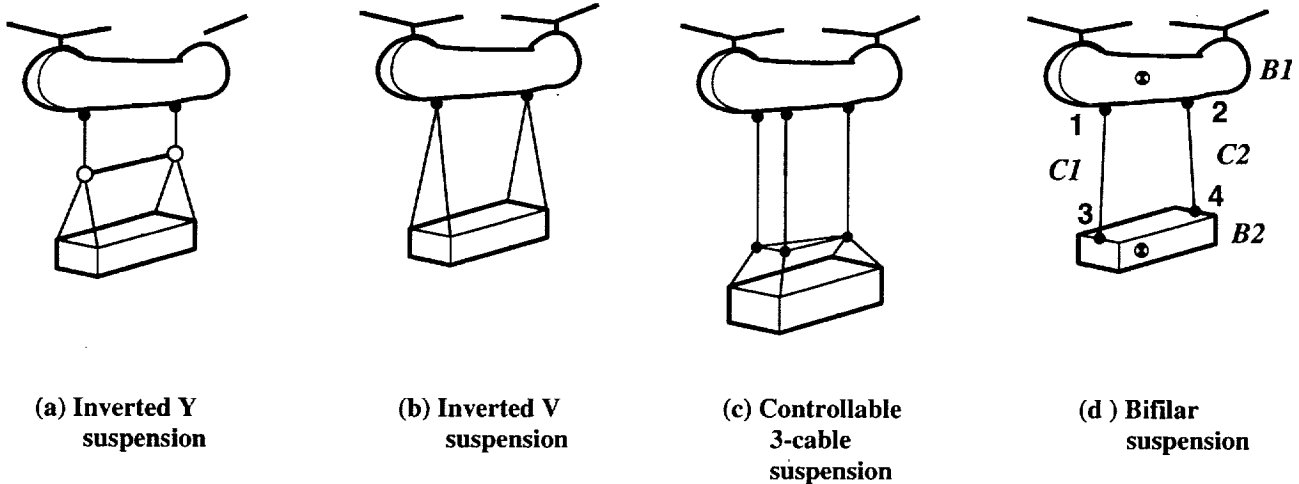
For many of these suspensions, the equations of motion are difficult to derive. The bifilar suspension is tractable by the present application method in which coordinates are selected to represent both elastic and

inelastic suspensions, but the remaining suspensions in figure 5 are not.

A simulation of the inverted-V suspension with elastic cables, obtained from equations for general elastic suspensions in which all cables connect the two rigid bodies, is reported in reference 15. The behavior of elastic and inelastic inverted-V suspensions is compared in reference 11, where it is noted that the variation of the suspension's yaw-restoring torque with relative yawing of the load depends on cable elasticity, and that this differs significantly between inelastic cables and the cables with elastic properties found in practice. Thus, cable elasticity must be considered in any accurate simulation of yawing motion. Further, one or two cables will collapse during small yawing motions of an inelastic inverted-V suspension, and this appears intractably complex to simulate as well as unrealistic. Approximate equations are given in references 11 and 12, in which the load-suspension motion is represented by three angle coordinates (load yaw and longitudinal and lateral swing angles) and cable stretching is neglected.

The inverted-Y suspension imposes one constraint when inelastic. If the spreader bar is removed, then $c = 2$. No cable or link in the suspension connects two rigid bodies, so that force balance at the bar end-points must be utilized in the simulation to locate the load relative to the helicopter regardless of elasticity. This renders the problem analytically difficult, as previously seen for the simpler system c in appendix B. No simulation equations were found in the open literature for this suspension. However, if the spreader bar is sufficiently close to the helicopter, then only small motions of the bar relative to the helicopter can occur, and the system can be approximated as an inverted-V suspension. Similarly, if the bar is sufficiently close to the load, then only small motions of the bar relative to the load can occur and the system can be approximated as a bifilar suspension, as is done in references 9 and 36.

Simulation equations for the bifilar suspension are given in references 13 and 15 for elastic suspensions



Parameters:

$m_1, J_1, R_1^*1_1, R_1^*2,$

$m_2, J_2, R_2^*3_2, R_2^*4_2$

l_{o1}, l_{o2}

Figure 5. Multipoint suspensions.

in terms of the rigid-body coordinates, and in references 36 and 44 for inelastic suspensions. Equations of motion are derived in reference 36 from Kane's equations, but the load-suspension motion coordinates appear to be ill-conditioned for ordinary small-angle motion, as discussed below. Equations for a fixed-base bifilar pendulum are derived in reference 44 from Kane's equations; this pendulum is equivalent to the load-suspension portion of the bifilar slung-load system. In addition, linearized EOMs are derived in reference 9.

In this appendix, the methods of this report are applied to the bifilar suspension of figure 5(d), by using relative motion coordinates for the load-suspension subsystem. The selection of generalized coordinates is an issue of interest. The inelastic load-suspension has four DOFs, which might be chosen variously from among the seven cable and load Euler angles, but many of these choices are ill-conditioned; that is, the relation of dependent motion variables to some sets of four DOFs becomes undefined or weakly dependent during ordinary small-angle motion. The load-suspension geometry is studied to determine well-conditioned DOFs, and simulation equations are given for one such set, including both elastic and inelastic cables. The coordinates used here are similar to those used in reference 44. An alternative, well-conditioned set is used in the linearized equations of reference 8.

A third set used in the exact equations in reference 36 is found to be ill-conditioned.

System and Constraints

The bifilar suspension is shown in figure 5(d) along with the enumeration of the bodies, cables, attachment points, and system parameters used in the derivation. The load is suspended by two cables, C1, C2, attached at distinct points, R_1, R_2 on the helicopter, B1. It is assumed that the suspension is uncontrolled ($\dot{p} = 0$) and that the line segment between load-attachment points parallels the load x-axis, $R_{34} = a i_2$. The reference cable lengths, l_{o1}, l_{o2} , refer to the unloaded lengths of elastic cables or the fixed lengths of inelastic cables.

If the cables are inelastic, then two independent holonomic constraints are imposed on the configuration position:

$$\begin{aligned}
\ell 1(r) &= |R2^*_N + T_{N,2} R2^*3_2 - R1^*_N - T_{N,1} R1^*1_1| \\
&= \ell o1 \\
&\quad (117) \\
\ell 2(r) &= |R2^*_N + T_{N,2} R2^*4_2 - R1^*_N - T_{N,1} R1^*2_1| \\
&= \ell o2
\end{aligned}$$

so that the inelastic system has 10 degrees of freedom;

$$c = 2, \quad d = 10 \quad (118)$$

Generalized Coordinates of System with Inelastic Cables

The generalized velocity coordinates of the inelastic system can be taken as the helicopter's rigid-body velocities and four coordinates that define the motion of the load and suspension:

$$u1 = \begin{pmatrix} V1^*_N \\ \omega 1_1 \\ \Omega \end{pmatrix}$$

The immediate task is to select suitable coordinates, Ω . These can be chosen from the seven cable and load Euler angles, but, as shown next, some possible choices of four coordinates are singular or ill-conditioned for ordinary small-angle motion of the system.

The suspension geometry shown in figure 5(d) is a nonplanar four-sided figure governed by the vector equation

$$\mathbf{R12} + \mathbf{R24} - \mathbf{R34} - \mathbf{R13} = \mathbf{0} \quad (119)$$

These vectors can be expressed in terms of their lengths and directions as given in table 11. The vector directions can be given in terms of the usual cable pitch and roll angles and load Euler angles described in appendix A. These angles can be taken relative to inertial space or helicopter body axes \mathcal{F}_1 . Angles relative to \mathcal{F}_1 are used here for simplicity in representing ordinary motion since these have steady values during both steady turns and straight-line flight. The angles relative to \mathcal{F}_1 are indicated by appending Δ to the usual notation. That is,

$$\left. \begin{aligned}
T_{c,1} &= E_1(\Delta\phi_c) E_2(\Delta\theta_c) \quad c \in \{c1, c2\} \\
T_{2,1} &= E_1(\Delta\phi_2) E_2(\Delta\theta_2) E_3(\Delta\psi_2)
\end{aligned} \right\} \quad (120)$$

where $T_{c,1}$ defines cable axes, $\{\mathbf{ic}, \mathbf{jc}, \mathbf{kc}\}$ such that \mathbf{kc} is in the cable direction away from the helicopter, and \mathbf{ic} is in the helicopter vertical plane of $(\mathbf{i1}, \mathbf{k1})$, as sketched in table 11. Equation (119), when expressed

in \mathcal{F}_1 coordinates, gives three scalar equations among six of the seven cable and load Euler angles in equation (120) (load roll angle does not occur), and three of these angles can be given in terms of the remaining three. However, in simulations these angles are more conveniently calculated from their rates.

The angular rates are related by the time-derivative of equation (119) as follows:

$$\dot{\mathbf{R}}12 + \dot{\mathbf{R}}24 - \dot{\mathbf{R}}34 - \dot{\mathbf{R}}13 = \mathbf{0} \quad (121)$$

The time-derivatives in equation (121) can be taken in any coordinate frame \mathcal{F}_a according to the general rule

$$\text{If } \mathbf{R} = \ell \mathbf{u} \text{ then } {}^a d\mathbf{R}/dt = \dot{\ell} \mathbf{u} + {}^a \omega^b \times \ell \mathbf{u} \quad (122)$$

where ℓ , \mathbf{u} are the length and unit direction vector of \mathbf{R} ; ${}^a d()/dt$ is the time-derivative in \mathcal{F}_a ; \mathcal{F}_b is any coordinate frame in which \mathbf{u} is a fixed vector; and ${}^a \omega^b$ is the angular velocity of \mathcal{F}_b and \mathbf{u} relative to \mathcal{F}_a . In this appendix the velocities relative to \mathcal{F}_1 are indicated by appending Δ to the usual velocity notation:

$$\Delta \mathbf{V}ij \triangleq \frac{{}^1 d}{dt} \mathbf{R}ij \quad \text{for any line segment, } \mathbf{R}ij$$

$$\Delta \omega^a \triangleq {}^1 \omega^a \quad \text{for any reference frame, } \mathcal{F}_a$$

Expressions for the velocities relative to \mathcal{F}_1 are listed in part b of table 11, and then equation (121) is expanded in terms of the load-suspension angular rates. To obtain Ω , note, first, that the relative load roll rate, $\Delta p2$, must be one of the coordinates in Ω , since it does not occur in the velocity equation and is independent of the six load-cable angular rates which do occur. Thus, Ω cannot be taken as the four cable-angle rates. An inspection of the suspension geometry in figure 5(d) confirms that the effect of load roll about the line segment $\mathbf{R34}$ on the relative position and velocity of any point in the load would be undetectable from any knowledge of the suspension geometry alone.

Secondly, scalar equations in only four of the load-suspension angular rates can be obtained from dot products of equation (121) with any vector that is perpendicular to two of the vector coefficients of the load-suspension angular rates in equation 121 as expanded in part b of table 11, that is, from dot products with $\mathbf{kc1}$, $\mathbf{kc2}$, $\mathbf{i2}$, $\mathbf{ic1} \times \mathbf{jc2}$, $\mathbf{ic1} \times \mathbf{j2}$, $\mathbf{ic1} \times \mathbf{k2}$, $\mathbf{jc1} \times \mathbf{k2}$, $\mathbf{jc2} \times \mathbf{k2}$, etc. We consider the following relations obtained from dot products, with $\mathbf{kc2}$, $\mathbf{i2}$, $\mathbf{ic1} \times \mathbf{k2}$, respectively:

$$\Delta q_2 = \left(\frac{\mathbf{j}2 \cdot \mathbf{k}c2}{\mathbf{k}2 \cdot \mathbf{k}c2} \right) \Delta r_2 + \left(\frac{\ell_1 \cos \Delta \phi_{c1} \mathbf{i}c1 \cdot \mathbf{k}c2}{a \mathbf{k}2 \cdot \mathbf{k}c2} \right) \Delta \dot{\theta}_{c1} - \left(\frac{\ell_1 \mathbf{j}c1 \cdot \mathbf{k}c2}{a \mathbf{k}2 \cdot \mathbf{k}c2} \right) \Delta \dot{\phi}_{c1} \quad (123)$$

$$\Delta \dot{\theta}_{c1} = \left(\frac{\ell_2 \cos \Delta \phi_{c2} \mathbf{i}c2 \cdot \mathbf{i}2}{\ell_1 \cos \Delta \phi_{c1} \mathbf{i}c1 \cdot \mathbf{i}2} \right) \Delta \dot{\theta}_{c2} + \left(\frac{\mathbf{j}c1 \cdot \mathbf{i}2}{\cos \Delta \phi_{c1} \mathbf{i}c1 \cdot \mathbf{i}2} \right) \Delta \dot{\phi}_{c1} - \left(\frac{\ell_2 \mathbf{j}c2 \cdot \mathbf{i}2}{\ell_1 \cos \Delta \phi_{c1} \mathbf{i}c1 \cdot \mathbf{i}2} \right) \Delta \dot{\phi}_{c2} \quad (124)$$

$$\Delta \dot{\phi}_{c1} = \left(\frac{\ell_2 \mathbf{i}c1 \times \mathbf{j}c2 \cdot \mathbf{k}2}{\ell_1 \mathbf{k}c1 \cdot \mathbf{k}2} \right) \Delta \dot{\phi}_{c2} + \left(\frac{a \mathbf{i}c1 \cdot \mathbf{i}2}{\ell_1 \mathbf{k}c1 \cdot \mathbf{k}2} \right) \Delta r_2 + \left(\frac{\ell_2 \cos \Delta \phi_{c2} \mathbf{i}c2 \times \mathbf{i}c1 \cdot \mathbf{k}2}{\ell_1 \mathbf{k}c1 \cdot \mathbf{k}2} \right) \Delta \dot{\theta}_{c2} \quad (125)$$

Use has been made of the triple-scalar and vector-product identities to obtain convenient forms.

A review of the coefficients of the angular velocities on the right-hand-side of equation (123) shows that these are much smaller than 1. That is, in steady flight (hover, straight-line, or turning flight) if $\mathbf{k}c2$ is perpendicular to $\mathbf{j}2$, $\mathbf{i}c1$, $\mathbf{j}c1$, then $\Delta q_2 = 0$ and, otherwise, for small-angle departures from these conditions, then $|\Delta q_2| \ll \max\{|\Delta r_2|, |\Delta \dot{\theta}_{c1}|, |\Delta \dot{\phi}_{c1}|\}$, assuming ℓ_1, a are of similar size. This reflects the suspension's restriction of the load relative pitch. Similarly, using the dot product of $\mathbf{k}c1$ with equation (121), it can be shown that $|\Delta q_2| \ll \max\{|\Delta r_2|, |\Delta \dot{\theta}_{c2}|, |\Delta \dot{\phi}_{c2}|\}$ near the condition that $\mathbf{k}c1$ is perpendicular to $\mathbf{j}2$, $\mathbf{i}c2$, $\mathbf{j}c2$. Consequently, any use of Δq_2 as an independent coordinate will yield equations for the dependent angle rates that are singular, or nearly so, in Δq_2 , so that Δq_2 cannot be selected as a coordinate of Ω . In that case, Ω cannot contain the load angular velocity, $\Delta \omega_{22}$.

A similar analysis of equation (124) shows that $\Delta \dot{\theta}_{c1}$ has first-order dependence on $\Delta \dot{\theta}_{c2}$ and second-order dependence on the cable roll rates. This follows after assuming that ℓ_1, ℓ_2, a are of similar size and that in the vicinity of steady flight conditions, $\mathbf{i}2$ is nearly perpendicular to $\mathbf{j}c1, \mathbf{j}c2$ and that it forms moderate angles with $\mathbf{i}c1, \mathbf{i}c2$. In that case, one of $\Delta \dot{\theta}_{c1}, \Delta \dot{\theta}_{c2}$ must be included in Ω in order to represent the effects of cable pitching motion, but not both, since these are nearly mutually dependent coordinates.

A similar analysis of equation (125) shows that the coefficients of $\Delta \dot{\phi}_{c2}, \Delta r_2$ are first order and the coefficient of $\Delta \dot{\theta}_{c2}$ is second order. This follows, assuming that ℓ_1, ℓ_2, a are of similar size, that $\mathcal{F}_{c1}, \mathcal{F}_{c2}$ are nearly parallel frames, and that $\mathbf{k}2$ forms a moderate

angle with $\mathbf{k}c1$. In that case, any two coordinates from $\{\Delta \dot{\phi}_{c1}, \Delta \dot{\phi}_{c2}, \Delta r_2\}$ can be selected to represent the cable roll-load yaw motion. The net result is that Ω must be selected to contain (1) Δp_2 , (2) two rates from $\{\Delta \dot{\phi}_{c1}, \Delta \dot{\phi}_{c2}, \Delta r_2\}$, and (3) one of $\{\Delta \dot{\theta}_{c1}, \Delta \dot{\theta}_{c2}\}$; for example,

$$\Omega = (\Delta \dot{\theta}_{c1}, \Delta \dot{\phi}_{c1}, \Delta p_2, \Delta r_2) \quad \text{or} \\ (\Delta \dot{\theta}_{c1}, \Delta \dot{\phi}_{c1}, \Delta \dot{\phi}_{c2}, \Delta p_2) \quad (126)$$

The first of these, with load roll and yaw and rear-cable angle rates, will be used below for the simulation of the relative load motion. Equations for the dependent rates, $\Delta q_2, \Delta \dot{\theta}_{c2}, \Delta \dot{\phi}_{c2}$ are included in table 11. The load-suspension generalized coordinates selected in reference 36 are

$$\Omega = (\Delta \dot{\theta}_{c1}, \Delta \dot{\phi}_{c1}, \dot{\zeta}, \Delta \dot{\phi}_2)$$

where ζ is the load pitch angle measured about $\mathbf{j}1$. This set includes a load pitch-angle rate and is nearly equivalent to the set $(\Delta \dot{\theta}_{c1}, \Delta \dot{\phi}_{c1}, \Delta q_2, \Delta p_2)$, which was shown above to be ill-conditioned. Similarly, the set in reference 36 can be shown to be ill-conditioned; that is, the equations for load yaw-angle rate and $\Delta \dot{\phi}_{c2}$ in terms of Ω are singular, or nearly singular, for ordinary small-angle motion. The coordinates used in reference 9 are equivalent to the second set in equation (126) corresponding to three cable angle rates and load roll, and are well-conditioned. The coordinates used in reference 44 are equivalent to those used here, that is, the direction angle rates of the cable and the load roll and yaw rates. The principal difference lies in the use of polar coordinates to define cable direction in reference 44, where one coordinate is undefined when the cable is vertical.

The angular velocity coordinates considered here do not exhaust the possible choices of Ω . For example, the load-suspension geometry can be viewed as consisting

of two noncoplanar triangles with sides (**R12**, **R13**) and (**R24**, **R34**). The orientation of the triangle (**R12**, **R13**) can be defined by the rear-cable angles, the orientation of the triangle (**R24**, **R34**) relative to the triangle (**R12**, **R13**) by the roll angle about the common diagonal (**R23**), and the orientation of the load relative to the triangle (**R24**, **R34**) by its roll angle about (**R34**). These four coordinates are well-conditioned but the resulting $v(u)$ is complicated.

Simulation Equations Using Generalized Load-Suspension Coordinates Relative to Helicopter Body Axes

The generalized velocity coordinates for the system with elastic cables u , are to be chosen as the generalized coordinates of the inelastic-cable system augmented by two length rates such that (1) the augmented set comprises generalized coordinates of the system with elastic cables and (2) the length rates become zero if the cables are inelastic. Here, the two cable lengths are the holonomic constraints of the inelastic cable system, and their length rates can be added to $(V1^*_N, \omega 1_1)$ along with one of the well-conditioned coordinate sets listed in equation (126) for Ω , to obtain u . Taking Ω to be the rear-cable angle rates and the load relative roll and yaw rates, then u can be taken as

$$u = \begin{pmatrix} V1^*_N \\ \omega 1_1 \\ \Delta V13_{c1} \\ \dot{\ell}2 \\ (\Delta p2, \Delta r2)^T \end{pmatrix} \quad (127)$$

where $\Delta V13$ is the relative velocity of the rear cable, which, using equations from part b of table 11, is given in terms of the cable angle and length rates by

$$\Delta V13_{c1} = (\ell 1 \Delta \dot{\theta}_{c1} \cos \Delta \phi_{c1}, -\ell 1 \Delta \dot{\phi}_{c1}, \dot{\ell}1)^T$$

The linear velocity components of $\Delta V13_{c1}$ are preferred as generalized coordinates over the cable angle rates $\Delta \dot{\theta}_{c1}, \Delta \dot{\phi}_{c1}$ owing to the simpler kinematic relation $v(u)$ obtained. Then the load c.g. inertial velocity is given from the derivative of

$$\mathbf{R2}^* = \mathbf{R1}^* + \mathbf{R1}^*1 + \mathbf{R13} + \mathbf{R32}^*$$

as

$$\mathbf{V2}^* = \mathbf{V1}^* + \omega 1 \times \mathbf{R1}^*1 + (\omega 1 \times \mathbf{R13} + \Delta \mathbf{V13}) - \omega 2 \times \mathbf{R2}^*3$$

or

$$V2^*_N = V1^*_N - T_{N,1} S(R1^*3_1) \omega 1_1 + T_{N,c1} \Delta V13_{c1} + T_{N,2} S(R2^*3_2) \omega 2_2 \quad (128)$$

The load angular velocity can be written as

$$\omega 2_2 = T_{2,1} \omega 1_1 + \Delta \omega 2_2 \quad (129)$$

It remains to determine $\Delta q2(u)$ for the case of elastic cables in order to complete the relation $v(u)$. This is obtained from the dot product of $\mathbf{kc2}$ with the velocity equation for elastic cables; the result is included in table 11.

The configuration kinematics $v(u)$, $u(v)$ are assembled in the equation summary, part a of table 12. The cable coordinates $\Delta V13_{c1}, \dot{\ell}2$ in the inverse relation, $u(v)$, are obtained by solving equation (128) for $\Delta V13_{c1}$ and solving a similar kinematic relation for the forward cable for $\dot{\ell}2$. The result for A^{-1} is seen to be simpler than for A . Additional equations for the dependent angular rates $\Delta q2(u)$, $\Delta \omega c2_{c2}(u)$ and the relative angular velocities needed to calculate $T_{2,1}, T_{c2,1}$ in a simulation are included in the equation summary for completeness.

The external forces and inertia coupling terms f_o are assembled in part b of table 12. The notation **F01**, ..., **M02** for the vector elements of f_o is introduced for brevity in later equations. These represent the sum of applied forces and moments resulting from weight ($m1g, m2g$), aerodynamics, and helicopter rotor output (**FA1**, ..., **MA2**), and inertia coupling terms from $X + \dot{A} u$. The coupling terms comprise a large number of scalar terms that are all second order in velocity coordinates from u, v , and whose computation can be organized in terms of natural vectors and matrices as given in the equation summary. If expanded to scalar expressions, a large number of terms are obtained. This is done in reference 36 where the number of such terms exceeds 300. If the relative motion is assumed sufficiently small ($|\Delta \omega c1|, |\Delta \omega 2| \ll 0.1$ rad/sec) and the cables are inelastic, then all terms in $\dot{A} u$ are negligible (of the order of 10^{-3} rad sec², $10^{-3}g$) except a term in $\omega 1 \times \mathbf{R1}^*2^* \times \omega 1$ from $\dot{A}_{22} \omega 1_1$. This greatly reduces the programming and computations required, but is inaccurate in representing the dynamics of larger relative motions.

Equations for the interaction force fc are given in part c of table 12. Each cable connects two bodies so that the interaction force can be assembled in terms of cable directions and tensions as in equation (11) by

$$fc = \sum_{j=1}^2 H_j TC_j = H TC$$

where $\{H_j\}$ are given in the equation summary. For this example, $c = m$ so that H is also a basis of the interaction force space and can be used for both elastic and inelastic cables. Note that H is identical to $-\Lambda$

given by the rows of A^{-1} corresponding to $\dot{\ell}1$ (third component of $\Delta V13_{c1}$) and $\dot{\ell}2$.

Finally, the simulation equations are listed in part d of table 12. The total specific force sf , due to $f_o + fc$, is assembled, and its vector elements are denoted $\mathbf{SF1}, \dots, \mathbf{SM2}$ for convenience. The elements of \dot{u} are obtained by expanding $A^{-1} sf$. If the cables are inelastic, then $\dot{\ell}1$ and $\dot{\ell}2$ need not be calculated, and various terms in $\dot{A} u$ containing $\dot{\ell}1, \dot{\ell}2$ are also zero in the computation of f_o .

Table 11. Generalized load-suspension velocity coordinates: bifilar suspension

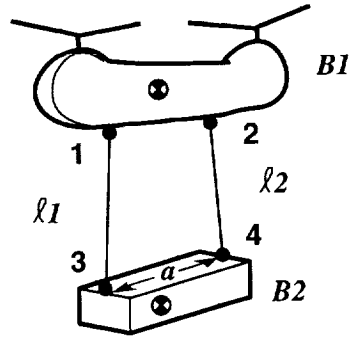
(a) Suspension geometry:

$$R_{12} + R_{24} - R_{13} - R_{34} = 0$$

$$R_{13} = \ell_1 \mathbf{k}c1$$

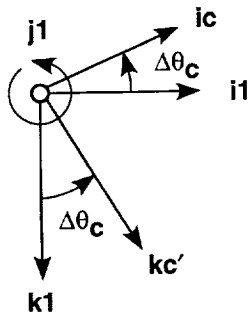
$$R_{24} = \ell_2 \mathbf{k}c2$$

$$R_{34} = a \mathbf{i}2$$

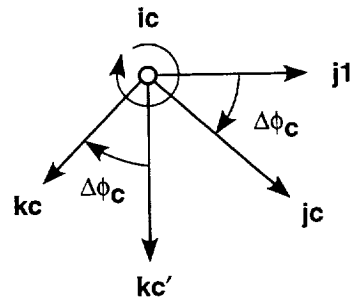


Suspension geometry.

Angles relative to \mathcal{F}_1 :



(a) Pitch rotation (about $\mathbf{j}1$)



(b) Roll rotation (about $\mathbf{i}c$)

Cable angles relative to \mathcal{F}_1 .

$$T_{c,1} = E_1(\Delta\phi_c) E_2(\Delta\theta_c) \quad c \in \{c1, c2\}$$

$$T_{2,1} = E_1(\Delta\phi_2) E_2(\Delta\theta_2) E_3(\Delta\psi_2)$$

$$\mathbf{k}c1 = \cos \Delta\phi_{c1} \sin \Delta\theta_{c1} \mathbf{i}1 - \sin \Delta\phi_{c1} \mathbf{j}1 + \cos \Delta\phi_{c1} \cos \Delta\theta_{c1} \mathbf{k}1$$

$$\mathbf{k}c2 = \cos \Delta\phi_{c2} \sin \Delta\theta_{c2} \mathbf{i}1 - \sin \Delta\phi_{c2} \mathbf{j}1 + \cos \Delta\phi_{c2} \cos \Delta\theta_{c2} \mathbf{k}1$$

$$\mathbf{i}2 = \cos \Delta\psi_2 \cos \Delta\theta_2 \mathbf{i}1 + \sin \Delta\psi_2 \cos \Delta\theta_2 \mathbf{j}1 - \sin \Delta\theta_2 \mathbf{k}1$$

Table 11. Concluded.

(b) Suspension velocity equation relative to helicopter body axes, \mathcal{F}_1 :

$$\Delta \mathbf{V}_{12} + \Delta \mathbf{V}_{24} - \Delta \mathbf{V}_{13} - \Delta \mathbf{V}_{34} = \mathbf{0}$$

Velocities relative to \mathcal{F}_1 :

$$\Delta \omega_{c1} = \Delta \dot{\phi}_{c1} \mathbf{ic1} + \Delta \dot{\theta}_{c1} (\cos \Delta \phi_{c1} \mathbf{jc1} - \sin \Delta \phi_{c1} \mathbf{kc1})$$

$$\Delta \omega_{c2} = \Delta \dot{\phi}_{c2} \mathbf{ic2} + \Delta \dot{\theta}_{c2} (\cos \Delta \phi_{c2} \mathbf{jc2} - \sin \Delta \phi_{c2} \mathbf{kc2})$$

$$\Delta \omega_2 = \Delta p_2 \mathbf{i2} + \Delta q_2 \mathbf{j2} + \Delta r_2 \mathbf{k2}$$

$$\Delta \mathbf{V}_{12} = \mathbf{0}$$

$$\Delta \mathbf{V}_{13} = \ell_1 \mathbf{kc1} + \ell_1 \Delta \omega_{c1} \times \mathbf{kc1}$$

$$\Delta \mathbf{V}_{24} = \ell_2 \mathbf{kc2} + \ell_2 \Delta \omega_{c2} \times \mathbf{kc2}$$

$$\Delta \mathbf{V}_{34} = a \Delta \omega_2 \times \mathbf{i2}$$

Velocity equation for inelastic cables:

$$\ell_2 (\Delta \dot{\theta}_{c2} \cos \Delta \phi_{c2} \mathbf{ic2} - \Delta \dot{\phi}_{c2} \mathbf{jc2}) - \ell_1 (\Delta \dot{\theta}_{c1} \cos \Delta \phi_{c1} \mathbf{ic1} - \Delta \dot{\phi}_{c1} \mathbf{jc1}) - a (\Delta r_2 \mathbf{j2} - \Delta q_2 \mathbf{k2}) = \mathbf{0}$$

Suspension angular rates in terms of $(\Delta \dot{\phi}_{c1}, \Delta \dot{\theta}_{c1}, \Delta r_2)$ for inelastic cables:

$$\Delta q_2 = \left(\frac{\mathbf{j2} \cdot \mathbf{kc2}}{\mathbf{k2} \cdot \mathbf{kc2}} \right) \Delta r_2 + \frac{\ell_1}{a \mathbf{k2} \cdot \mathbf{kc2}} (\Delta \dot{\theta}_{c1} \cos \Delta \phi_{c1} \mathbf{ic1} \cdot \mathbf{kc2} - \Delta \dot{\phi}_{c1} \mathbf{jc1} \cdot \mathbf{kc2})$$

$$\Delta \omega_{c2} \times \mathbf{kc2} = \frac{1}{\ell_2} (\ell_1 \Delta \omega_{c1} \times \mathbf{kc1} + a \Delta \omega_2 \times \mathbf{i2})$$

$$\Delta \dot{\theta}_{c2} = \Delta \omega_{c2} \times \mathbf{kc2} \cdot \mathbf{ic2} / \cos \Delta \phi_{c2}$$

$$\Delta \dot{\phi}_{c2} = -\Delta \omega_{c2} \times \mathbf{kc2} \cdot \mathbf{jc2}$$

Velocity equation and load pitch rate for elastic cables:

$$\dot{\ell}_2 \mathbf{kc2} + \ell_2 (\Delta \dot{\theta}_{c2} \cos \Delta \phi_{c2} \mathbf{ic2} - \Delta \dot{\phi}_{c2} \mathbf{jc2}) - \Delta \mathbf{V}_{13} - a (\Delta r_2 \mathbf{j2} - \Delta q_2 \mathbf{k2}) = \mathbf{0}$$

$$\Delta q_2 = \left(\frac{\mathbf{j2} \cdot \mathbf{kc2}}{\mathbf{k2} \cdot \mathbf{kc2}} \right) \Delta r_2 + \frac{\mathbf{kc2} \cdot \Delta \mathbf{V}_{13}}{a \mathbf{k2} \cdot \mathbf{kc2}} - \frac{1}{a \mathbf{k2} \cdot \mathbf{kc2}} \dot{\ell}_2$$

Table 12. Simulation equation summary: bifilar suspension

(a) Configuration kinematics:

$$v = \begin{pmatrix} V1^*_N \\ V2^*_N \\ \omega 1_1 \\ \omega 2_2 \end{pmatrix} = A u = \begin{pmatrix} I & 0 & 0 & 0 & 0 \\ I & A_{22} & A_{23} & A_{24} & A_{25} \\ 0 & I & 0 & 0 & 0 \\ 0 & A_{42} & A_{43} & A_{44} & A_{45} \end{pmatrix} \begin{pmatrix} V1^*_N \\ \omega 1_1 \\ \Delta V13_{c1} \\ \dot{\ell} 2 \\ (\Delta p 2, \Delta r 2)^T \end{pmatrix}$$

$$\Delta V13_{c1} = (\ell 1 \Delta \dot{\theta}_{c1} \cos \Delta \phi_{c1}, -\ell 1 \Delta \dot{\phi}_{c1}, \dot{\ell} 1)^T$$

Auxilliary expressions for A:

$$z0 = \mathbf{k} 2 \bullet \mathbf{k} c 2 = k 2_1^T k c 2_1$$

$$z1 = \mathbf{j} 2 \bullet \mathbf{k} c 2 = j 2_1^T k c 2_1$$

$$z\ell = -1 / a z0$$

$$zr = z1 / z0$$

$$z13_{c1} = -z\ell T_{c1,1} k c 2_1$$

$$R1^* 2^*_1 = R1^* 1_1 + \ell 1 k c 1_1 - T_{1,2} R2^* 3_2$$

$$s i_2 = (\mathbf{R} 2^* \mathbf{3} \times \mathbf{i} 2)_2 = 1^{st} \text{ column of } S(R2^* 3_2) \quad A_{44} = j 2_2 z\ell$$

$$s j_2 = (\mathbf{R} 2^* \mathbf{3} \times \mathbf{j} 2)_2 = 2^{nd} \text{ column of } S(R2^* 3_2)$$

$$s k_2 = (\mathbf{R} 2^* \mathbf{3} \times \mathbf{k} 2)_2 = 3^{rd} \text{ column of } S(R2^* 3_2)$$

$$T_{N,2} = T_{N,1} T_{1,2}$$

Submatrices of A:

$$A_{22} = -T_{N,1} S(R1^* 2^*_1)$$

$$A_{23} = T_{N,1} [T_{1,c1} + T_{1,2} s j_2 z13_{c1}^T]$$

$$A_{24} = T_{N,2} s j_2 z\ell$$

$$A_{25} = T_{N,2} [s i_2, s k_2 + z r s j_2]$$

$$A_{42} = T_{2,1}$$

$$A_{43} = j 2_2 z13_{c1}^T$$

$$A_{45} = \begin{pmatrix} 1 & 0 \\ 0 & z r \\ 0 & 1 \end{pmatrix}$$

Table 12. Continued.

$$\underline{u(v)} = \begin{pmatrix} V1^*_{N} \\ \omega 1_1 \\ \Delta V13_{c1} \\ \dot{\ell} 2 \\ (\Delta p2, \Delta r2)^T \end{pmatrix} = A^{-1} v = \begin{pmatrix} I & 0 & 0 & 0 \\ 0 & 0 & I & 0 \\ -T_{c1,N} & T_{c1,N} & B_{33} & B_{34} \\ -kc2^T_N & kc2^T_N & -\xi 12^T_1 & \xi 22^T_2 \\ 0 & 0 & B_{53} & B_{54} \end{pmatrix} \begin{pmatrix} V1^*_{N} \\ V2^*_{N} \\ \omega 1_1 \\ \omega 2_2 \end{pmatrix}$$

Submatrices of A^{-1} :

$$T_{c1,N} = T_{c1,1} T_{1,N}$$

$$B_{33} = T_{c1,1} S(R1^*1_1) + S(R13_{c1}) T_{c1,1}$$

$$B_{34} = -T_{c1,1} T_{1,2} S(R2^*3_2)$$

$$kc2_N = T_{N,1} kc2_1$$

$$\xi 12_1 = (\mathbf{R1}^*2 \times kc2)_1 = S(R1^*2_1) kc2_1$$

$$\xi 22_2 = (\mathbf{R2}^*4 \times kc2)_2 = S(R2^*4_2) T_{2,1} kc2_1$$

$$B_{53} = - \begin{pmatrix} 1 & 0 & 0 \\ 0 & 0 & 1 \end{pmatrix} T_{2,1} \quad B_{54} = \begin{pmatrix} 1 & 0 & 0 \\ 0 & 0 & 1 \end{pmatrix}$$

Relative angular velocities:

$$\Delta q2 = z\ell \dot{\ell} 2 + z13^T_{c1} \Delta V13_{c1} + zr \Delta r2$$

$$\Delta \omega 2_2 = (\Delta p2, \Delta q2, \Delta r2)^T$$

$$\Delta V24_1 = (\Delta \mathbf{V13} + \Delta \mathbf{V34})_1 = T_{1,c1} \Delta V13_{c1} + a (\Delta r2 j2_1 - \Delta q2 k2_1)$$

$$\Delta \dot{\theta}_{c2} = ic2^T_1 \Delta V24_1 / \ell 2 \cos \Delta \phi_{c2}$$

$$\Delta \dot{\phi}_{c2} = -jc2^T_1 \Delta V24_1 / \ell 2$$

$$\Delta \omega c2_2 = (\Delta \dot{\phi}_{c2}, \Delta \dot{\theta}_{c2} \cos \Delta \phi_{c2}, -\Delta \dot{\theta}_{c2} \sin \Delta \phi_{c2})^T$$

$$\Delta \omega c2_1 = \Delta \dot{\phi}_{c2} ic2_1 + \Delta \dot{\theta}_{c2} j1_1 = (\Delta \dot{\phi}_{c2} \cos \Delta \theta_{c2}, \Delta \dot{\theta}_{c2}, -\Delta \dot{\phi}_{c2} \sin \Delta \theta_{c2})^T$$

Table 12. Continued.

(b) External forces and inertia coupling terms:

$$f_o = fg + fa - X - D \dot{A} u$$

$$f_o = \begin{pmatrix} F01_N \\ F02_N \\ M01_1 \\ M02_2 \end{pmatrix} = \begin{pmatrix} m1 g_N + FA1_N \\ m2 g_N + FA2_N - m2(\dot{A}_{22} \omega_{11} + \dot{A}_{23} \Delta V13_{c1} + \dot{A}_{24} \dot{\ell}2 + \dot{A}_{25} (\Delta p2, \Delta r2)^T) \\ MA1_1 - S(\omega_{11}) J1 \omega_{11} \\ MA2_2 - S(\omega_{22}) J2 \omega_{22} - J2 (\dot{A}_{42} \omega_{11} + \dot{A}_{43} \Delta V13_{c1} + \dot{A}_{44} \dot{\ell}2 + \dot{A}_{25} (\Delta p2, \Delta r2)^T) \end{pmatrix}$$

Auxilliary expressions for \dot{A} :

$$\omega_{22} = T_{2,1} \omega_{11} + \Delta\omega_{22}$$

$$\omega_{c1_1} = \omega_{11} + \Delta\omega_{c1_1}$$

$$\omega_{2c2_2} = \Delta\omega_{22} - T_{2,1} \Delta\omega_{c2_1}$$

$$\omega_{c2c1_{c1}} = T_{c1,1} (\Delta\omega_{c2_1} - \Delta\omega_{c1_1})$$

$$\dot{z}0 = \mathbf{kc}2 \bullet (\Delta\omega_{22} - \Delta\omega_{c2_2}) \times \mathbf{k}2$$

$$= kc2_1^T T_{1,2} S(\omega_{2c2_2}) k_{22}$$

$$\dot{z}1 = \mathbf{kc}2 \bullet (\Delta\omega_{22} - \Delta\omega_{c2_2}) \times \mathbf{j}2$$

$$= kc2_1^T T_{1,2} S(\omega_{2c2_2}) j_{22}$$

$$\dot{z}\ell = -z\ell \dot{z}0/z0$$

$$\dot{z}r = (\dot{z}1 - zr \dot{z}0)/z0$$

$$\dot{z}13_{c1} = -(\dot{z}\ell \mathbf{kc}2 + z\ell(\Delta\omega_{c2_2} - \Delta\omega_{c1_1}) \times \mathbf{kc}2)_{c1} = [\dot{z}\ell/z\ell I + S(\omega_{c2c1_{c1}})] z13_{c1}$$

$$\dot{R}1^*2^*_1 = T_{1,c1} \Delta V13_{c1} + T_{1,2} S(R2^*3_2) \Delta\omega_{22}$$

Submatrices of \dot{A} :

$$\dot{A}_{22} = -T_{N,1}[S(\omega_{11}) S(R1^*2^*_1) + S(\dot{R}1^*2^*_1)]$$

$$\dot{A}_{23} = T_{N,1}[S(\omega_{c1_1}) T_{1,c1} + T_{1,2} (S(\omega_{22}) sj_2 z13_{c1}^T + sj_2 \dot{z}13_{c1}^T)]$$

$$\dot{A}_{24} = T_{N,2}[\dot{z}\ell I + z\ell S(\omega_{22})]sj_2$$

$$\dot{A}_{25} = T_{N,2} [\mu_{12}, \mu_{22}]$$

$$\mu_{12} = S(\omega_{22}) si_2$$

$$\mu_{22} = S(\omega_{22}) (sk_2 + zr sj_2) + \dot{z}r sj_2$$

$$\dot{A}_{42} = -S(\Delta\omega_{22}) T_{2,1}$$

$$\dot{A}_{43} = j_{22} \dot{z}13_{c1}^T$$

$$\dot{A}_{44} = \dot{z}\ell j_{22}$$

$$\dot{A}_{45} = \begin{pmatrix} 0 & 0 \\ 0 & \dot{z}r \\ 0 & 0 \end{pmatrix}$$

Table 12. Continued.

(c) Suspension forces:

$$f_c = [H1, H2] \begin{pmatrix} TC1 \\ TC2 \end{pmatrix} = \begin{pmatrix} kc1_N & kc2_N \\ -kc1_N & -kc2_N \\ \xi11_1 & \xi12_1 \\ -\xi21_2 & -\xi22_2 \end{pmatrix} \begin{pmatrix} TC1 \\ TC2 \end{pmatrix}$$

$$kc1_N = T_{N,1} kc1_1$$

$$kc2_N = T_{N,1} kc2_1$$

$$\xi11_1 = (\mathbf{R1}^* \mathbf{1} \times \mathbf{kc1})_1 = S(R1^*1_1) kc1_1$$

$$\xi21_2 = (\mathbf{R2}^* \mathbf{3} \times \mathbf{kc1})_2 = S(R2^*3_2) T_{2,1} kc1_1$$

$$\xi12_1 = (\mathbf{R1}^* \mathbf{2} \times \mathbf{kc2})_1 = S(R1^*2_1) kc2_1$$

$$\xi22_2 = (\mathbf{R2}^* \mathbf{4} \times \mathbf{kc2})_2 = S(R2^*4_2) T_{2,1} kc2_1$$

Cable tensions for elastic cables:

$$TCj = \max\{0, Kj (\ell_j - \ell_{oj})\} \quad j = 1, 2$$

Cable tensions for inelastic cables:

$$\begin{pmatrix} TC1 \\ TC2 \end{pmatrix} = -[H^T D^{-1} H]^{-1} H^T D^{-1} f_o$$

$$H1^T D^{-1} f_o = kc1_N^T (F01_N/m1 - F02_N/m2) + \xi11_1^T J1^{-1} M01_1 - \xi21_2^T J2^{-1} M02_2$$

$$H2^T D^{-1} f_o = kc2_N^T (F01_N/m1 - F02_N/m2) + \xi12_1^T J1^{-1} M01_1 - \xi22_2^T J2^{-1} M02_2$$

$$H1^T D^{-1} H1 = \mu12 + \xi11_1^T J1^{-1} \xi11_1 + \xi21_2^T J2^{-1} \xi21_2$$

$$H2^T D^{-1} H2 = \mu12 + \xi12_1^T J1^{-1} \xi12_1 + \xi22_2^T J2^{-1} \xi22_2$$

$$H1^T D^{-1} H2 = \mu12 kc1_N^T kc2_N + \xi11_1^T J1^{-1} \xi12_1 + \xi21_2^T J2^{-1} \xi22_2$$

where

$$\mu12 = (m1 + m2)/m1 m2$$

Table 12. Concluded.

(d) Simulation equations:

$$sf = \begin{pmatrix} SF1_N \\ SF2_N \\ SM1_1 \\ SM2_2 \end{pmatrix} = D^{-1} (fo + fc)$$

$$\dot{u} = A^{-1} sf$$

$$\dot{V}1^*_N = SF1_N$$

$$\dot{\omega}1_1 = SM1_1$$

$$\Delta \dot{V}13_{c1} = T_{c1,N} (SF2_N - SF1_N) + B_{33} SM1_1 + B_{34} SM2_2$$

$$\ddot{\ell}2 = -H2^T sf$$

$$\begin{pmatrix} \Delta \dot{p}2 \\ \Delta \dot{r}2 \end{pmatrix} = \begin{pmatrix} 1 & 0 & 0 \\ 0 & 0 & 1 \end{pmatrix} (SM2_2 - T_{2,1} SM1_1)$$

100



APPENDIX D

SIMULATION EQUATIONS FOR DUAL-LIFT SYSTEMS

INTRODUCTION

Simulation equations are derived in this appendix for the three dual-lift configurations shown in figure 6.

Rigid loads that are sufficiently long to allow safe separation of the two helicopters can be suspended directly below the helicopters (fig. 6(a)). Several isolated civil operations have used this configuration (ref. 4), including a load carried with a separation of 1.5 rotor diameters. Shorter loads can be carried by various configurations considered in the early studies (refs. 1 and 2). Flight tests and control-system analyses have focused principally on the arrangement shown in figure 6(c), which uses a spreader bar (refs. 3-7, 17, 20, and 21). Limited flight tests were conducted using a relatively heavy spreader bar that was 2 rotor diameters long in order to ensure safe helicopter separation. Control automation is expected to result in minimum separations of 1.25 rotor diameters and a spreader-bar weight penalty of about 5% of payload (ref. 4). Although this weight is small relative to the other masses in this system, it is included in the equations of motion, and the configuration is represented as a system of four rigid bodies. An alternative three-body configuration without a spreader bar (fig. 6(b)) has also been considered in references 18 and 19. The stabilization of difficult loads has not been considered in the suspension designs of figure 6 and may lead to new suspensions in the future.

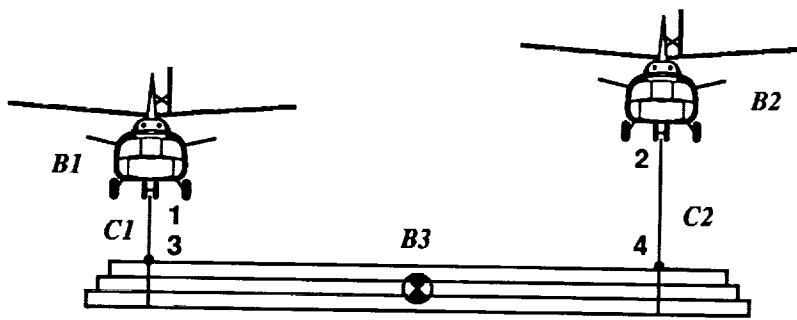
Until recently, work on the equations of motion of dual-lift systems was limited to approximate models tractable for control studies of these complex systems. The cables have been assumed inelastic in all cases. In reference 17, the slung-load systems are approximated as point masses linked by fixed-length cables in tension, and general equations of motion for these systems are given from d'Alembert's principle. The general equations required inversion of a $d \times d$ matrix analogous to that in equation (14), but analytical inversion did not appear feasible for a 12-DOF point-mass model of the system in figure 6(c). In later work on this system at Princeton University (refs. 6 and 7) Lagrange's equations were used, assuming a

point-mass load and thin-rod spreader bar (16 DOFs). Linearized equations specialized to hover are obtained (ref. 7) and the results include a real-time simulation of two-dimensional motion (seven DOFs, ref. 6). More recently, nonlinear equations of two-dimensional motion have been given for a point-mass approximation of the three-body system shown in figure 6(b), which has four DOFs (ref. 18). General nonlinear EOMs for the dual-lift system with spreader bar similar to those given here were initially reported in reference 8; nonlinear EOMs in terms of the rigid body velocity coordinates for the same system with inelastic suspension are given in references 19 and 20.

Simulation equations are derived in this appendix for the three dual-lift configurations of figure 6 using the methods of this report. The results accommodate elastic or inelastic cables and dissimilar helicopters. All three dual-lift systems can be integrated in to a single set of simulation equations. In addition, equations are given for an approximate model of the dual-lift system with spreader bar, using point-mass helicopters and load, and a thin-rod spreader bar. With elastic cables, this system has 14 DOFs; with inelastic cables it has 10 DOFs. Cables, rigid bodies, attachment points, and system parameters are enumerated in figure 6. The system parameters are the masses, inertia matrices, and body-axis coordinates of the cable attachment points for each body, and the reference cable lengths, $\{l_{0j}\}$, which refer to the unloaded lengths of elastic cables or the fixed lengths of inelastic cables.

Dual-Lift System for Long Loads

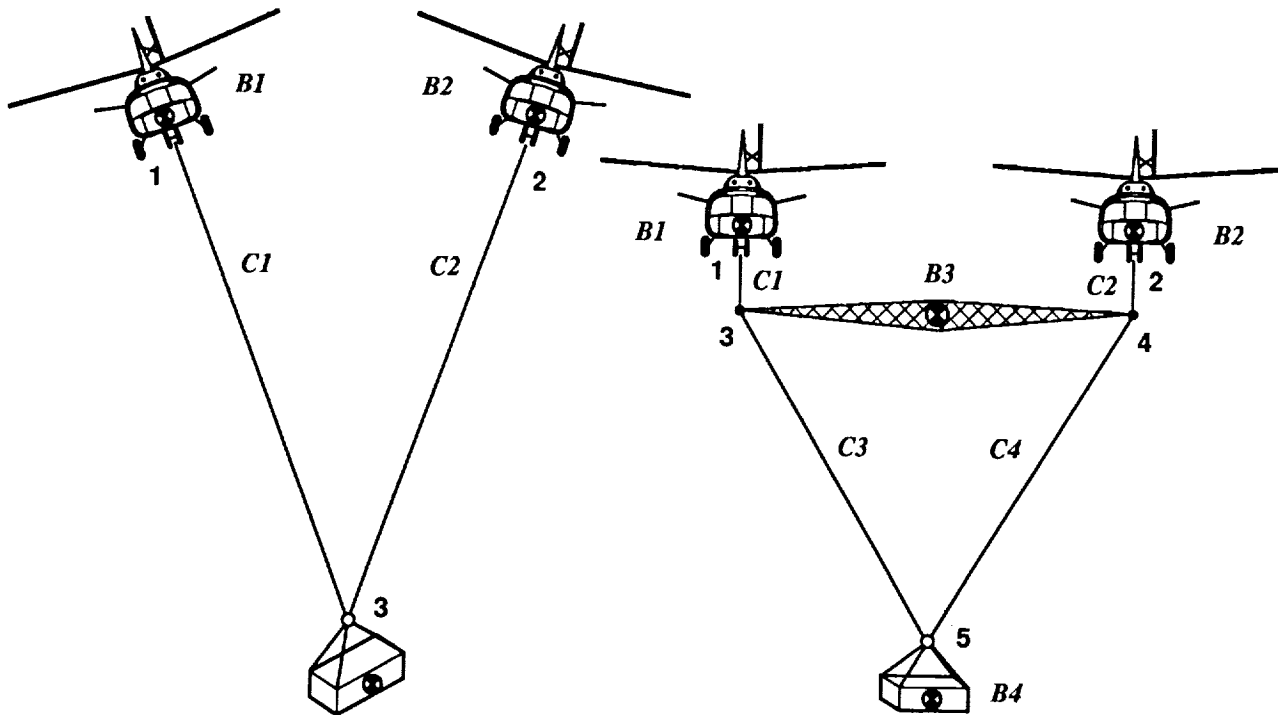
System and constraints- The configuration in figure 6(a) accommodates long loads and consists of three rigid bodies B_1, B_2, B_3 connected by two cables, C_1, C_2 , attached at R_1, \dots, R_4 . If the cables are inelastic then each imposes one holonomic constraint on the configuration motion by fixing the distances



Parameters:

- $m_1, J_1, R_1^{*1},$
- m_2, J_2, R_2^{*2}
- $m_3, J_3, R_3^{*3}, R_3^{*4}$
- l_{o1}, l_{o2}

(a) Long loads



Parameters:

- $m_1, J_1, R_1^{*1},$
- m_2, J_2, R_2^{*2}
- m_3, J_3, R_3^{*3}
- l_{o1}, l_{o2}

(b) Pendant suspension

Parameters:

- $m_1, J_1, R_1^{*1},$
- m_2, J_2, R_2^{*2}
- $m_3, J_3, R_3^{*3}, R_3^{*4}$
- m_4, J_4, R_4^{*5}
- $l_{o1}, l_{o2}, l_{o3}, l_{o4} = l_{o3}$

(c) Spread bar suspension

Figure 6. Dual-lift suspensions and system parameters.

R13, R24:

$$\left. \begin{aligned} \ell 1(r) &= |R3^*_N + T_{N,3} R3^*3_3 - R1^*_N \\ &\quad - T_{N,1} R1^*1_1| = \ell o 1 \\ \ell 2(r) &= |R3^*_N + T_{N,3} R3^*4_3 - R2^*_N \\ &\quad - T_{N,2} R2^*2_2| = \ell o 2 \end{aligned} \right\} \quad (130)$$

and then, for inelastic cables;

$$c = 2, \quad d = 16 \quad (131)$$

Generalized velocity coordinates and configuration kinematics— The generalized velocity coordinates u are to be selected so as to separate motion caused by cable stretching from motion with invariant cable lengths. This is readily done by extension of the single-cable example of appendix B. First, assume that the c.g. velocity of B1 and the angular velocities of all bodies ($V1^*_N, \omega 1_1, \omega 2_2, \omega 3_3$) can be included in u , and then observe that the c.g. velocities of B2, B3 can be given from the derivatives of

$$\left. \begin{aligned} R3^*_N &= R1^*_N + T_{N,1} R1^*1_1 + R13_N \\ &\quad - T_{N,3} R3^*3_3 \\ R2^*_N &= R3^*_N + T_{N,3} R3^*4_3 - R24_N \\ &\quad - T_{N,2} R2^*2_2 \end{aligned} \right\} \quad (132)$$

as

$$\left. \begin{aligned} V3^*_N &= V1^*_N - T_{N,1} S(R1^*1_1) \omega 1_1 \\ &\quad + T_{N,c1} V13_{c1} + T_{N,3} S(R3^*3_3) \omega 3_3 \\ V2^*_N &= V3^*_N - T_{N,3} S(R3^*4_3) \omega 3_3 \\ &\quad - T_{N,c2} V24_{c2} + T_{N,2} S(R2^*2_2) \omega 2_2 \end{aligned} \right\} \quad (133)$$

where $V13_{c1}, V24_{c2}$ are the inertial cable velocities referred to cable axes $\mathcal{F}_{c1}, \mathcal{F}_{c2}$. As described in appendix A, these axes are obtained by defining inertial pitch and roll angles for each cable $(\phi_{c1}, \theta_{c1}), (\phi_{c2}, \theta_{c2})$, and then cable axes $\mathcal{F}_{c1}, \mathcal{F}_{c2}$ are obtained from the inertial axes by

$$T_{c,N} = E_1(\phi_c) E_2(\theta_c) \quad c = c1, c2 \quad (134)$$

where $\mathbf{kc1}, \mathbf{kc2}$ are along the cables, **R13, R24**; and $\mathbf{ic1}, \mathbf{ic2}$ are in the inertial vertical plane of $(\mathbf{iN}, \mathbf{kN})$. For these axes

$$\omega c = \dot{\phi}_c \mathbf{ic} + \dot{\theta}_c (\cos \phi_c \mathbf{jc} - \sin \phi_c \mathbf{kc}) \quad c = c1, c2 \quad (135)$$

and then

$$\left. \begin{aligned} V13_{c1} &= \dot{\ell} 1 \mathbf{kc1}_{c1} + (\omega c1 \times \mathbf{kc1})_{c1} \ell 1 \\ &= (\ell 1 \dot{\theta}_{c1} \cos \phi_{c1}, -\ell 1 \dot{\phi}_{c1}, \dot{\ell} 1)^T \\ V24_{c2} &= (\ell 2 \dot{\theta}_{c2} \cos \phi_{c2}, -\ell 2 \dot{\phi}_{c2}, \dot{\ell} 2)^T \end{aligned} \right\} \quad (136)$$

These velocity coordinates separate the cable rotational and stretching motion, and, together with $(V1^*_N, \omega 1_1, \omega 2_2, \omega 3_3)$, make up 24 generalized coordinates for the system with elastic cables which contains a subset of 16 coordinates for the system with inelastic cables.

The configuration kinematics $v(u)$ are assembled in the equation summary of table 13. The 18×18 matrix, A , contains 6 rows representing equations (133), and 12 rows from the unit matrix for the coordinates that are in both u and v . The reverse relation, $v(u)$, is readily given after obtaining $V13_{c1}(v), V24_{c2}(v)$ from equations (133). Only transformations and skew-symmetric matrices representing Coriolis terms occur in A, A^{-1} .

External forces and inertia coupling— The external forces on the configuration and the coupling terms, f_o , are assembled in part b of table 13. The vector elements of f_o are denoted $(\mathbf{F01}, \dots, \mathbf{M03})$ for brevity in later equations. The f_o contains the forces and moments on the rigid bodies due to weight, aerodynamics, and rotor output, along with the coupling terms, $X + D\dot{A}u$, which are all second order in velocity coordinates from u, v . The submatrices of \dot{A} require only time-derivatives of transformations (appendix A), and $\dot{A}u$ yields terms which are recognized as centrifugal and Coriolis accelerations of the forms $\omega \times \omega \times \mathbf{R}$ and $\omega \times \mathbf{V}$.

Suspension forces— The resultant forces and moments applied by the suspension to the configuration of rigid bodies, f_c , is given in part c of table 13. Here, each cable connects two rigid bodies so that f_c can be given from equation (11) in the case of elastic cables. Since the number of cables and constraints is equal, the configuration vectors of the cable tensions $\{H1, H2\}$, given in table 13, comprise a basis of the suspension force space which can be used with equations (18) and (19) to give f_c for inelastic cables. The results are given in table 13. This basis is identical to the formal basis, $-\Lambda$, given by the rows of A^{-1} corresponding to the stretching-motion coordinates $\dot{\ell} 1(v), \dot{\ell} 2(v)$. The suspension force parameters for inelastic cables are the two cable tensions, and the equations for elastic and inelastic cables differ only in the calculation of these tensions.

Simulation equations— Finally, the equations for \dot{u} , are assembled in part d of table 13 from $A^{-1} sf$, where sf refers to the applied specific forces and moments on the configuration due to $f_o + f_c$. The vector

elements of sf are denoted $\mathbf{SF1}, \dots, \mathbf{SM3}$ for convenience. The equations for $\dot{V}1^*_N, \dot{\omega}1_1, \dot{\omega}2_2, \dot{\omega}3_3$ are identical to those usually obtained from the Newton-Euler equations. The equations for the (relative) cable accelerations $\dot{V}13_{c1}, \dot{V}24_{c2}$, depend solely on differences of specific forces and moments on the connected bodies. For inelastic cables, the third components of $\dot{V}13_{c1}, \dot{V}24_{c2}$, namely, $\dot{\ell}1, \dot{\ell}2$ are theoretically zero.

Dual-Lift System with Pendant Suspension

The system shown in figure 6(b) consists of three rigid bodies with the load suspended by two cables $C1, C2$ connected at a common point $\mathbf{R3}$. The load and the hardware attaching it at $\mathbf{R3}$ are regarded as a single rigid body, $B3$. This system is simply a specialization of the previous configuration to one with a single attachment point at the load, $\mathbf{R3}$. Analysis and simulation equations are identical to those of the previous case except for replacing $\mathbf{R4}$ with $\mathbf{R3}$ throughout. An equation summary is therefore omitted. Equations for this system are also included in the results for the multilift system with m -helicopters and pendant suspension that is treated in appendix E.

Dual-Lift System with Spreader Bar

System description and constraints— The dual-lift system shown in figure 6(c) consists of four rigid bodies: the two helicopters, $B1, B2$, are connected by tether cables, $C1, C2$ to a spreader bar $B3$, and the load is suspended from the spreader bar by the bridle cables, $C3, C4$, attached at a common point, $\mathbf{R5}$. The load and the hardware attaching it to $\mathbf{R5}$ are regarded as a single rigid body, $B4$.

It is unnecessary to make any specializing assumptions about the system parameters, but it is noted that existing designs are characterized by bridle cables of equal length with an angle from the spreader bar in the range $45^\circ - 60^\circ$, with a spreader bar length in the range of 1.25 to 1.5 rotor diameters, and a spreader-bar weight that is about 5% of the system payload (ref. 4). Identical helicopters with equal loading are usually considered, but the present results accommodate dissimilar helicopters and unequal loading.

If the four cables are inelastic, they impose four independent holonomic constraints on the configuration by fixing the following distances:

$$\begin{aligned} \ell 1(r) &= |R3^*_N + T_{N,3} R3^*3_3 \\ &\quad - R1^*_N - T_{N,1} R1^*1_1| = \ell o1 \\ \ell 2(r) &= |R3^*_N + T_{N,3} R3^*4_3 \\ &\quad - R2^*_N - T_{N,2} R2^*2_2| = \ell o2 \end{aligned} \tag{137}$$

$$\begin{aligned} \ell 3(r) &= |R4^*_N + T_{N,4} R4^*5_4 \\ &\quad - R3^*_N - T_{N,3} R3^*3_3| = \ell o3 \end{aligned}$$

$$\begin{aligned} \ell 4(r) &= |R4^*_N + T_{N,4} R4^*5_4 \\ &\quad - R3^*_N - T_{N,3} R3^*4_3| = \ell o4 \end{aligned}$$

Then, for inelastic cables,

$$c = 4, \quad d = 20 \tag{138}$$

Generalized velocity coordinates and configuration kinematics— The generalized velocity coordinates u are to be selected so as to separate motion caused by cable stretching (four coordinates) from motion caused by invariant cable lengths (20 coordinates). First, note that the subsystem that consists of helicopters, tether cables, and spreader bar is identical to the system in figure 6(a) and can be represented by the identical 18 coordinates ($V1^*_N, \omega1_1, \omega2_2, \omega3_3, V13_{c1}, V24_{c2}$). As before, inertial cable angles $(\phi_{c1}, \theta_{c1}), (\phi_{c2}, \theta_{c2})$ and cable axes $\mathcal{F}_{c1}, \mathcal{F}_{c2}$ are defined (eq. (134)), and then the inertial velocities, $V13_{c1}, V24_{c2}$ separate the tether cable stretching and rotational motions (eq. (136)), and the rigid body velocities $V3^*_N, V2^*_N$ are given in terms of the generalized coordinates by equation (133).

Secondly, the load motion remains to be given in suitable coordinates. The load c.g. velocity is obtained from the derivative of

$$R4^*_N = R3^*_N + R3^*5_N - T_{N,4} R4^*5_4$$

as

$$V4^*_N = V3^*_N + V3^*5_N + T_{N,4} S(R4^*5_4) \omega4_4 \tag{139}$$

Assume that $\omega4_4$ can be included in u . It then remains to develop appropriate coordinates for $V3^*5_N$. This development is given in table 14.

The inertial velocity, $\mathbf{V3^*5}$, results from the inertial velocities of the two cables $C3, C4$. These cables always form a triangle with the spreader-bar longitudinal axis $\mathbf{i3}$, and axes \mathcal{F}_t can be attached to the plane of the triangle with longitudinal axis along the spreader

bar, $\mathbf{i3}$, and normal axis, \mathbf{kt} , perpendicular to $\mathbf{i3}$ in the plane of $C3$, $C4$. This plane can have any roll angle, ϕ_t , about $\mathbf{i3}$, and then $\mathbf{R3}^*5$ has components $(\ell3x, \ell3z)$ in this plane. For elastic cables, $(\ell3x, \ell3z)$ are arbitrary; for inelastic cables, they have fixed values. The coordinates $\{\dot{\phi}_t, \dot{\ell}3x, \dot{\ell}3z\}$ are appropriate velocity coordinates which separate the stretching and rotational motion of $\mathbf{R3}^*5$. To isolate these coordinates in $\mathbf{V3}^*5$, define the modified spreader-bar reference frame $\mathbf{F}_{3'}$, from the spreader-bar Euler angles $\{\psi_3, \theta_3\}$, and then give the inertial velocity of $\mathbf{R3}^*5$ as the sum of its velocity relative to $\mathbf{F}_{3'}$ (\mathbf{VT} in part a of table 14) and the effect of the inertial rotation of $\mathbf{F}_{3'}$ ($\Delta\mathbf{VT}$ in part a of table 14). As seen in table 14, the motion of $\mathbf{R3}^*5$ caused by cable stretching and $\dot{\phi}_t$ is isolated in VT_t and the remaining motion, $\Delta\mathbf{VT}$ depends only on the spreader-bar angular velocity.

Appropriate generalized coordinates for the system can now be given by augmenting the 18 coordinates previously used for the system of figure 6(a) with $(VT_t, \omega4_4)$; $V4^*_N$ is given in terms of these coordinates by

$$V4^*_N = V3^*_N + T_{N,t} (VT_t + BT \omega3_3) + T_{N,4} S(R4^*5_4) \omega4_4 \quad (140)$$

Finally, the kinematic relations $v(u)$, $u(v)$ are assembled in table 14, by using equations (133) and (140) to obtain $V2^*_N(u)$, $V3^*_N(u)$, $V4^*_N(u)$ and then rearranging these same equations to obtain $V13_{c1}(v)$, $V24_{c2}(v)$, $VT_t(v)$. The remaining 15 rows of A , A^{-1} are all from the unit matrix, since the corresponding coordinates are in both u, v . The nontrivial submatrices of A , A^{-1} are all coordinate transformations and skew-symmetric matrices representing Coriolis terms.

Applied forces and inertia coupling— These terms, f_o , are assembled in part c of table 14. The vector elements of f_o are denoted $\mathbf{F01}, \dots, \mathbf{M04}$ for brevity in later equations. The configuration vector f_o contains the sum of applied forces due to weight ($m1 \mathbf{g}, \dots, m4 \mathbf{g}$), aerodynamic and helicopter rotor forces and moments ($\mathbf{FA1}, \dots, \mathbf{MA4}$), and the inertia coupling $X + \dot{A} u$. The submatrices of A are defined in part b of table 14 except that BT is given in part a. Their time-derivatives are obtained principally from derivatives of coordinate transformations. A general expression from appendix A is repeated here along with expressions for the cable-axis angular velocities in the required reference frames, $\omega c1_{c1}, \omega c2_{c2}, \omega t_t$, and expressions for the nontrivial terms of $\dot{A} u$. The time-derivative of BT is obtained routinely, but a formula is omitted for brevity.

Suspension forces— Equations for the suspension force f_c are assembled in part d of table 14. Each of the four cables $C1, C2, C3, C4$ connects two rigid bodies so that f_c can be given as in equation (11) by

$$f_c = \sum_{j=1}^4 H_j TC_j = H TC \quad (141)$$

The matrix H is given in table 14. Its columns also form a basis of the suspension force space since $c = m = 4$, so that equation (141) can be used for both elastic and inelastic cables, the cable tensions being calculated from cable stretch or from equations (18) and (19) in the two cases, respectively. Expressions for both cases are listed in the table. The table includes formulas for calculating cable line segments from u , and these suffice to determine H and the elastic cable tensions.

Alternatively, a basis can be given as the rows of A^{-1} corresponding to the cable-stretching coordinates (rows 6, 9, 10, 12). This basis is given as Λ in part d of table 14. The corresponding constraint force parameters s can be identified as $TC1, TC2$, and the \mathcal{F}_t components of the suspension force, \mathbf{FT} , which acts on the triangle at $\mathbf{R5}$. Note that these components can be given from the cable tensions and, conversely, so that Λ can also be used to assemble f_c for both elastic and inelastic cables.

Simulation equations— The total specific force applied to the configuration, sf , is assembled in part e of table 14 from the vector elements of the external forces f_o and the interaction forces f_c . The vector elements of sf are denoted $\mathbf{SF1}, \dots, \mathbf{SM4}$ for convenience. Finally, the simulation equations for the vector elements of \dot{u} are given by expanding $\dot{u} = A^{-1} sf$, and these represent either elastic or inelastic cables. For inelastic cables, the four cable-stretching coordinates (coordinates 6, 9, 10, 12 of \dot{u}) are all theoretically zero.

Remarks— The three dual-lift systems can be integrated into a single simulation. The three-body system in figure 6(a) is a subsystem of the four-body system c. That is, system a is obtained from system c by dropping the load and bridle cables and by regarding the spreader bar as the load and assigning it appropriate parameter values. System a can be represented by a subset of the generalized velocity coordinates and equations for system c, obtained by deleting the six load-triangle coordinates and the load forces and moments. Further, as previously noted, the pendant

suspension system in figure 6(b) is a simple specialization of system *a* to coincident load-attachment points ($\mathbf{R4} = \mathbf{R3}$).

The EOMs for the rigid-body velocities, v , given in reference 20 for dual lift with spreader bar and inelastic suspension can be obtained by the procedure outlined in section 3, equations (142)-(146), by using generalized coordinates, u , which are reference point coordinates like those in part b of table 14, except that the reference point is taken at the spreader bar c.g. These coordinates also result in a simpler kinematic relation, $v = Au$, than in part b of table 14 and are of interest as an alternate set of generalized coordinates for the simulation equations.

Dual-Lift System with Spreader Bar: Degenerate-Body Approximation

In this section the system is represented by point-mass helicopters and load, and a rigid-rod spreader bar, as illustrated in part a of table 15. The system with elastic cables has 14 DOFs. Inelastic cables impose four holonomic constraints as in equation (137), in which case $d = 10$.

The formulation of EOMs for systems with degenerate bodies is outlined in section 5. To account for the point masses, $B1, B2, B4$, it is only necessary to modify the equations in table 14 to remove the angular velocities from v, u , along with the associated rows and columns of A, A^{-1} , and the associated moments in f_o, f_c . A 15-DOF system is obtained.

The rigid-rod spreader bar has two attitude degrees of freedom, represented by its inertial heading and pitch angles. The spreader-bar body axes \mathcal{F}_3 are now coincident with the special axis frame $\mathcal{F}_{3'}$, defined in table 14, and the attachment points on the spreader bar are on the $\mathbf{i3}$ -axis (table 15).

To account for the rigid-rod spreader bar $B3$, define the reduced configuration velocity \bar{v} , in which ω_{33} is replaced by the spreader-bar's pitch and heading rates, $\bar{\alpha}\bar{3} = (\dot{\theta}_3, \dot{\psi}_3)^T$, and make the same replacement in the generalized coordinates, u :

$$\bar{v} = (V1^*_N, V2^*_N, V3^*_N, V4^*_N, \bar{\alpha}\bar{3})^T$$

$$u = (V1^*_N, V13_{c1}, V24_{c2}, VT_t, \bar{\alpha}\bar{3})^T$$

The required kinematic relation,

$$\omega_{33} = j_{33} \dot{\theta}_3 + k_{N3} \dot{\psi}_3 = \overline{W}_{33} \bar{\alpha}\bar{3}$$

is expanded in table 15. The cable velocities $\mathbf{V13}, \mathbf{V24}, \mathbf{VT}$ were defined previously in equation (136) and part a of table 14. The 14 coordinates of u contain four scalar coordinates $\dot{\ell}1, \dot{\ell}2, \dot{\ell}3x, \dot{\ell}3z$, that represent cable stretching and 10 coordinates that represent motion with invariant cable lengths. The kinematic relations $\bar{v}(u), u(\bar{v})$ are obtained by specializing equations (133) and (140) to the degenerate bodies. The results are assembled in part b of table 15. The submatrices of \bar{A}, \bar{A}^{-1} are coordinate transformations and cross products with the spreader-bar's axes of pitch and heading rotations.

Equations for the applied forces and inertia reactions f_o , are given in part c of table 15. The configuration vector f_o is expanded routinely except to note that A in $\dot{A}u$ is from the relation $v(u) = \overline{W} \bar{A} u$, where \overline{W} maps Euler-angle rates to angular velocities (eq. (32)). The inertia reactions consist of Coriolis velocities due to transformation rates, centrifugal accelerations due to spreader-bar angular velocity, and an effect, $\mathbf{z1}$, of the Euler-angle rate coordinates.

The suspension forces (table 15) can be given in terms of cable tensions as in table 14, $f_c = H TC$, where H here is obtained from H in table 14 by deleting the elements that generate moments on the point-mass bodies. The moment action vectors $\{\xi_{3j}\}$ were defined previously in table 14 along with equations for calculating cable line segments. For elastic cables, TC is calculated from the cable lengths as usual. For inelastic cables, first obtain the reduced basis in 14-dimensional space, $\bar{H} = \overline{W}^T H$, and then the cable tensions are given by equation (37). Inversion of a 4×4 matrix ($\bar{H}^T D^{-1} \bar{H}$) is again required. Expressions for its elements are routinely obtained by expansion of the matrix. The alternative basis, \bar{A} from the rows of A^{-1} corresponding to the cable stretching coordinates, can also be used in equation (37) to obtain $\bar{f}_c = \bar{A} s = \overline{W}^T f_c$. The cable tensions can be obtained from s as given in part d of table 14.

Finally, the simulation equations (36) are assembled in part c of table 15. The reduced specific force, $\bar{s}\bar{f} = \overline{D}^{-1} \overline{W}^T (f_o + f_c)$, contains the specific forces, $\mathbf{SF1}, \dots, \mathbf{SF4}$, and the *reduced specific moment* on the spreader bar, $\mathbf{SM3}$; the latter contains the components of the moment sum, $\mathbf{M03} + \mathbf{MC3}$, along the pitch and heading axes of rotation, $\mathbf{j3}, \mathbf{kN}$. Last, the simulation equations for \dot{u} are given by expanding equation (36).

Table 13. Simulation equation summary: dual lift for long loads

(a) Kinematics:

$$v = \begin{pmatrix} V1^*_{N} \\ V2^*_{N} \\ V3^*_{N} \\ \omega_{11} \\ \omega_{22} \\ \omega_{33} \end{pmatrix} = A u = \begin{pmatrix} I & 0 & 0 & 0 & 0 & 0 \\ I & T_{N,c1} & -T_{N,c2} & A_{24} & A_{25} & A_{26} \\ I & T_{N,c1} & 0 & A_{24} & 0 & A_{36} \\ 0 & 0 & 0 & I & 0 & 0 \\ 0 & 0 & 0 & 0 & I & 0 \\ 0 & 0 & 0 & 0 & 0 & I \end{pmatrix} \begin{pmatrix} V1^*_{N} \\ V13_{c1} \\ V24_{c2} \\ \omega_{11} \\ \omega_{22} \\ \omega_{33} \end{pmatrix}$$

$$u = \begin{pmatrix} V1^*_{N} \\ V13_{c1} \\ V24_{c2} \\ \omega_{11} \\ \omega_{22} \\ \omega_{33} \end{pmatrix} = A^{-1} v = \begin{pmatrix} I & 0 & 0 & 0 & 0 & 0 \\ -T_{c1,N} & 0 & T_{c1,N} & B_{24} & 0 & B_{26} \\ 0 & -T_{c2,N} & T_{c2,N} & 0 & B_{35} & B_{36} \\ 0 & 0 & 0 & I & 0 & 0 \\ 0 & 0 & 0 & 0 & I & 0 \\ 0 & 0 & 0 & 0 & 0 & I \end{pmatrix} \begin{pmatrix} V1^*_{N} \\ V2^*_{N} \\ V3^*_{N} \\ \omega_{11} \\ \omega_{22} \\ \omega_{33} \end{pmatrix}$$

$$V13_{c1} = (\ell_1 \dot{\theta}_{c1} \cos \phi_{c1}, -\ell_1 \dot{\phi}_{c1}, \dot{\ell}_1)^T$$

$$V24_{c2} = (\ell_2 \dot{\theta}_{c2} \cos \phi_{c2}, -\ell_2 \dot{\phi}_{c2}, \dot{\ell}_2)^T$$

$$A_{24} = -T_{N,1} S(R1^*1_1)$$

$$B_{24} = -T_{c1,N} A_{24}$$

$$A_{25} = T_{N,2} S(R2^*2_2)$$

$$B_{26} = -T_{c1,N} A_{36}$$

$$A_{26} = -T_{N,3} S(R3^*3_3)$$

$$B_{35} = T_{c2,N} A_{25}$$

$$A_{36} = T_{N,3} S(R3^*3_3)$$

$$B_{36} = -T_{c2,N} T_{N,3} S(R3^*4_3)$$

Table 13. Continued.

(c) Suspension forces:

$$f_c = \begin{pmatrix} FC1_N \\ FC2_N \\ FC3_N \\ MC1_1 \\ MC2_2 \\ MC3_3 \end{pmatrix} = H1 TC1 + H2 TC2 = \begin{pmatrix} kc1_N & | & 0 \\ 0 & | & kc2_N \\ -kc1_N & | & -kc2_N \\ \xi11_1 & | & 0 \\ 0 & | & \xi22_2 \\ -\xi31_3 & | & -\xi32_3 \end{pmatrix} \begin{pmatrix} TC1 \\ TC2 \end{pmatrix}$$

$$\xi11_1 = (\mathbf{R1}^* \mathbf{1} \times \mathbf{kc1})_1 = S(R1^* 1_1) T_{1,N} kc1_N$$

$$\xi31_3 = (\mathbf{R3}^* \mathbf{3} \times \mathbf{kc1})_3 = S(R3^* 3_3) T_{3,N} kc1_N$$

$$\xi22_2 = (\mathbf{R2}^* \mathbf{2} \times \mathbf{kc2})_2 = S(R2^* 2_2) T_{2,N} kc2_N$$

$$\xi32_3 = (\mathbf{R3}^* \mathbf{4} \times \mathbf{kc2})_3 = S(R3^* 4_3) T_{3,N} kc2_N$$

Elastic cable tensions:

$$TCj = \max\{0, Kj (\ell_j - \ell_{oj})\} \quad j = 1, 2$$

Inelastic cable tensions:

$$\begin{pmatrix} TC1 \\ TC2 \end{pmatrix} = -(H^T D^{-1} H)^{-1} H^T D^{-1} f_o$$

$$H_1^T D^{-1} f_o = kc1_N^T \left[\frac{F01_N}{m1} - \frac{F03_N}{m3} \right] + \xi11_1^T J1^{-1} M01_1 - \xi31_3^T J3^{-1} M03_3$$

$$H_2^T D^{-1} f_o = kc2_N^T \left[\frac{F02_N}{m2} - \frac{F03_N}{m3} \right] + \xi22_2^T J2^{-1} M02_2 - \xi32_3^T J3^{-1} M03_3$$

$$H_1^T D^{-1} H_1 = \frac{m1+m3}{m1 m3} + \xi11_1^T J1^{-1} \xi11_1 + \xi31_3^T J3^{-1} \xi31_3$$

$$H_2^T D^{-1} H_2 = \frac{m2+m3}{m2 m3} + \xi22_2^T J2^{-1} \xi22_2 + \xi32_3^T J3^{-1} \xi32_3$$

$$H_1^T D^{-1} H_2 = kc1_N^T kc2_N / m3 + \xi31_3^T J3^{-1} \xi32_3$$

Table 13. Concluded.

(d) Simulation equations:

$$sf = D^{-1}(fo + fc) = \begin{pmatrix} SF1_N \\ SF2_N \\ SF3_N \\ SM1_1 \\ SM2_2 \\ SM3_3 \end{pmatrix} = \begin{pmatrix} (F01_N + FC1_N)/m1 \\ (F02_N + FC2_N)/m2 \\ (F03_N + FC3_N)/m3 \\ J1^{-1}(M01_1 + MC1_1) \\ J2^{-1}(M02_2 + MC2_2) \\ J3^{-1}(M03_3 + MC3_3) \end{pmatrix}$$

$$\dot{u} = A^{-1} sf$$

$$\dot{V}1^*_N = SF1$$

$$\dot{V}13_{c1} = T_{c1,N}(SF3_N - SF1_N - A_{24} SM1_1 - A_{36} SM3_3)$$

$$\dot{V}24_{c2} = T_{c2,N}(SF3_N - SF2_N + A_{25} SM2_2 - T_{N,3} S(R3^*4_3) SM3_3)$$

$$\dot{\omega}1_1 = SM1_1$$

$$\dot{\omega}2_2 = SM2_2$$

$$\dot{\omega}3_3 = SM3_3$$

Table 14. Simulation equation summary: dual-lift system with spreader bar

(a) Generalized velocity coordinates for bridle cables ($C3, C4$):

$$\mathcal{F}_t = \{\mathbf{i}_3, \mathbf{j}_t, \mathbf{k}_t\}$$

\mathbf{i}_3 = spreader bar longitudinal axis, along $\mathbf{R43}$

\mathbf{k}_t = perpendicular to \mathbf{i}_3 in plane of $C3, C4$

$$R3^*5_t = (\ell3x, 0, \ell3z)^T$$

$$\mathcal{F}_{3'} = \{\mathbf{i}_3, \mathbf{j}_{3'}, \mathbf{k}_{3'}\}$$

$$T_{3',N} = E_2(\theta_3)E_3(\psi_3)$$

$$T_{t,3'} = E_1(\phi_t)$$

$$V3^*5_t \triangleq T_{t,N} \dot{R}3^*5_N = VT_t + \Delta VT_t$$

$$R3^*5_{3'} = T_{3',t} R3^*5_t = (\ell3x, -\ell3z \sin \phi_t, \ell3z \cos \phi_t)^T$$

$$VT_t \triangleq T_{t,3'} \dot{R}3^*5_{3'} = (\dot{\ell}3x, -\ell3z \dot{\phi}_t, \dot{\ell}3z)^T$$

$$\omega_{3'} = \dot{\psi}_3 \mathbf{k}_N + \dot{\theta}_3 \mathbf{j}_{3'} = [\mathbf{j}_{3'} \mathbf{j}_{3'} + \mathbf{k}_N \mathbf{k}_{3'} / \cos \theta_3] \bullet \omega_3$$

$$\Delta VT = -R3^*5 \times \omega_{3'}$$

$$\Delta VT_t = BT \omega_{3'}$$

$$BT = \begin{pmatrix} 0 & \ell3z \cos \Delta \phi & \ell3z \sin \Delta \phi \\ 0 & -\ell3x \sin \Delta \phi + \ell3z \sin \phi_3 \tan \theta_3 & \ell3x \cos \Delta \phi + \ell3z \cos \phi_3 \tan \theta_3 \\ 0 & -\ell3x \cos \Delta \phi & -\ell3x \sin \Delta \phi \end{pmatrix}$$

where

$$\Delta \phi \triangleq \phi_t - \phi_3$$

Table 14. Continued.

(b) Configuration kinematics:

$$v = \begin{pmatrix} V1^*_N \\ V2^*_N \\ V3^*_N \\ V4^*_N \\ \omega_{11} \\ \omega_{22} \\ \omega_{33} \\ \omega_{44} \end{pmatrix} = A u = \begin{pmatrix} I & 0 & 0 & 0 & 0 & 0 & 0 & 0 \\ I & T_{N,c1} & -T_{N,c2} & 0 & A_{25} & A_{26} & A_{27} & 0 \\ I & T_{N,c1} & 0 & 0 & A_{25} & 0 & A_{37} & 0 \\ I & T_{N,c1} & 0 & T_{N,t} & A_{25} & 0 & A_{47} & A_{48} \\ 0 & 0 & 0 & 0 & I & 0 & 0 & 0 \\ 0 & 0 & 0 & 0 & 0 & I & 0 & 0 \\ 0 & 0 & 0 & 0 & 0 & 0 & I & 0 \\ 0 & 0 & 0 & 0 & 0 & 0 & 0 & I \end{pmatrix} \begin{pmatrix} V1^*_N \\ V13_{c1} \\ V24_{c2} \\ VT_t \\ \omega_{11} \\ \omega_{22} \\ \omega_{33} \\ \omega_{44} \end{pmatrix}$$

$$u = \begin{pmatrix} V1^*_N \\ V13_{c1} \\ V24_{c2} \\ VT_t \\ \omega_{11} \\ \omega_{22} \\ \omega_{33} \\ \omega_{44} \end{pmatrix} = A^{-1}v = \begin{pmatrix} I & 0 & 0 & 0 & 0 & 0 & 0 & 0 \\ -T_{c1,N} & 0 & T_{c1,N} & 0 & B_{25} & 0 & B_{27} & 0 \\ 0 & -T_{c2,N} & T_{c2,N} & 0 & 0 & B_{36} & B_{37} & 0 \\ 0 & 0 & -T_{t,N} & T_{t,N} & 0 & 0 & -BT & B_{48} \\ 0 & 0 & 0 & 0 & I & 0 & 0 & 0 \\ 0 & 0 & 0 & 0 & 0 & I & 0 & 0 \\ 0 & 0 & 0 & 0 & 0 & 0 & I & 0 \\ 0 & 0 & 0 & 0 & 0 & 0 & 0 & I \end{pmatrix} \begin{pmatrix} V1^*_N \\ V2^*_N \\ V3^*_N \\ V4^*_N \\ \omega_{11} \\ \omega_{22} \\ \omega_{33} \\ \omega_{44} \end{pmatrix}$$

$$A_{25} = -T_{N,1}S(R1^*1_1)$$

$$A_{26} = T_{N,2}S(R2^*2_2)$$

$$A_{37} = T_{N,3}S(R3^*3_3)$$

$$A'_{27} = T_{N,3} S(R3^*4_3)$$

$$A_{27} = A_{37} - A'_{27} = -T_{N,3} S(R3_4_3)$$

$$A_{47} = A_{37} + T_{N,t}BT$$

$$A_{48} = T_{N,4}S(R4^*5_4)$$

$$B_{25} = -T_{c1,N}A_{25}$$

$$B_{36} = T_{c2,N}A_{26}$$

$$B_{27} = -T_{c1,N}A_{37}$$

$$B_{37} = -T_{c2,N} A'_{27}$$

$$B_{48} = -T_{t,N}A_{48}$$

Table 14. Continued.

(c) Applied forces and inertia couplings:

$$f_o = fg + fa - X - D \dot{A} u$$

$$= \begin{pmatrix} F01_N \\ F02_N \\ F03_N \\ F04_N \\ M04_1 \\ M02_2 \\ M03_3 \\ M04_4 \end{pmatrix} = \begin{pmatrix} m1 g_N + FA1_N \\ m2 g_N + FA2_N - m2[\dot{T}_{N,c1} V13_{c1} - \dot{T}_{N,c2} V24_{c2} + \dot{A}_{25} \omega_{11} \\ + \dot{A}_{26} \omega_{22} + \dot{A}_{27} \omega_{33}] \\ m3 g_N + FA3_N - m3[\dot{T}_{N,c1} V13_{c1} + \dot{A}_{25} \omega_{11} + \dot{A}_{37} \omega_{33}] \\ m4 g_N + FA4_N - m4[\dot{T}_{N,c1} V13_{c1} + \dot{T}_{N,t} VT_t + \dot{A}_{25} \omega_{11} + \dot{A}_{47} \omega_{33} + \dot{A}_{48} \omega_{44}] \\ MA1_1 - S(\omega_{11}) J1 \omega_{11} \\ MA2_2 - S(\omega_{22}) J2 \omega_{22} \\ MA3_3 - S(\omega_{33}) J3 \omega_{33} \\ MA4_4 - S(\omega_{44}) J4 \omega_{44} \end{pmatrix}$$

$$\dot{T}_{N,c} = T_{N,c} S(\omega_{c_c}) \quad c = 1, 2, 3, 4, c1, c2, t$$

$$\omega_{c_c} = (\dot{\phi}_c, \dot{\theta}_c \cos \phi_c, -\dot{\theta}_c \sin \phi_c)^T \quad c = c1, c2$$

$$\omega t = \mathbf{i3} \dot{\phi}_t + \omega \mathbf{3}'$$

$$\omega t_t = \begin{pmatrix} 1 & -\sin \phi_3 \tan \theta_3 & -\cos \phi_3 \tan \theta_3 \\ 0 & \cos \Delta \phi & \sin \Delta \phi \\ 0 & -\sin \Delta \phi & \cos \Delta \phi \end{pmatrix} \begin{pmatrix} \dot{\phi}_t \\ \omega_{33}(2) \\ \omega_{33}(3) \end{pmatrix}$$

$$\dot{A}_{25} \omega_{11} = -T_{N,1} S(\omega_{11}) S(R1^*1_1) \omega_{11} = T_{N,1} S^2(\omega_{11}) R1^*1_1$$

$$\dot{A}_{26} \omega_{22} = -T_{N,2} S^2(\omega_{22}) R2^*2_2$$

$$\dot{A}_{27} \omega_{33} = -T_{N,3} S^2(\omega_{33}) (R3^*3_3 - R3^*4_3)$$

$$\dot{A}_{37} \omega_{33} = -T_{N,3} S^2(\omega_{33}) R3^*3_3$$

$$\dot{A}_{47} \omega_{33} = -T_{N,3} S^2(\omega_{33}) R3^*3_3 + T_{N,t} S(\omega t_t) BT \omega_{33} + T_{N,t} \dot{B}T \omega_{33}$$

$$\dot{A}_{48} \omega_{44} = -T_{N,4} S^2(\omega_{44}) R4^*5_4$$

Table 14. Continued.

(d) Suspension force:

$$f_c = H TC = \begin{pmatrix} kc1_N & 0 & 0 & 0 \\ 0 & kc2_N & 0 & 0 \\ -kc1_N & -kc2_N & kc3_N & kc4_N \\ 0 & 0 & -kc3_N & -kc4_N \\ \xi11_1 & 0 & 0 & 0 \\ 0 & \xi22_2 & 0 & 0 \\ -\xi31_3 & -\xi32_3 & \xi33_3 & \xi34_3 \\ 0 & 0 & -\xi43_4 & -\xi44_4 \end{pmatrix} \begin{pmatrix} TC1 \\ TC2 \\ TC3 \\ TC4 \end{pmatrix}$$

$$f_c = \Lambda s = \begin{pmatrix} kc1_N & 0 & 0 & 0 \\ 0 & kc2_N & 0 & 0 \\ -kc1_N & -kc2_N & i3_N & kt_N \\ 0 & 0 & -i3_N & -kt_N \\ \xi11_1 & 0 & 0 & 0 \\ 0 & \xi22_2 & 0 & 0 \\ -\xi31_3 & -\xi32_3 & \xi3x_3 & \xi3z_3 \\ 0 & 0 & -\xi4x_4 & -\xi4z_4 \end{pmatrix} \begin{pmatrix} TC1 \\ TC2 \\ FTx \\ FTz \end{pmatrix}$$

$TC1, \dots, TC4 =$ cable tensions for $C1, \dots, C4$

$Ft = kc3 TC3 + kc4 TC4 = i3 FTx + kt FTz$

$$\begin{array}{lll} \xi11 = R1^*1 \times kc1 & \xi33 = R3^*3 \times kc3 & \xi3x = \ell3z jt \\ \xi31 = R3^*3 \times kc1 & \xi43 = R4^*5 \times kc3 & \xi4x = R4^*5 \times i3 \\ \xi22 = R2^*2 \times kc2 & \xi34 = R3^*4 \times kc4 & \xi3z = -\ell3x jt \\ \xi32 = R3^*4 \times kc2 & \xi44 = R4^*5 \times kc4 & \xi4z = R4^*5 \times kt \end{array}$$

Table 14. Continued.

$$R13_N = \ell_1 kc1_N = \int T_{N,c1} V13_{c1} dt$$

$$R24_N = \ell_2 kc2_N = \int T_{N,c2} V24_{c2} dt$$

$$R3^*5_N = \int T_{N,t} (VT_t + \Delta VT_t) dt$$

$$R35_N = \ell_3 kc3_N = R3^*5_N + \int T_{N,3} S(R3^*3_3) \omega3_3 dt$$

$$R45_N = \ell_4 kc4_N = R3^*5_N + \int T_{N,3} S(R3^*4_3) \omega3_3 dt$$

Elastic cable tensions:

$$TC_j = \max\{0, K_j (\ell_j - \ell_{oj})\} \quad j = 1, \dots, 4$$

Constraint force parameters for inelastic cables:

$$s = TC = -[H^T D^{-1} H]^{-1} H^T D^{-1} f_o$$

$$H1^T D^{-1} f_o = kc1_N^T (F01_N/m1 - F03_N/m3) + \xi11_1^T J1^{-1} M01_1 - \xi31_3^T J3^{-1} M03_3$$

$$H2^T D^{-1} f_o = kc2_N^T (F02_N/m2 - F03_N/m3) + \xi22_2^T J2^{-1} M02_2 - \xi32_3^T J3^{-1} M03_3$$

$$H3^T D^{-1} f_o = kc3_N^T (F03_N/m3 - F04_N/m4) + \xi33_3^T J3^{-1} M03_3 - \xi43_4^T J4^{-1} M04_4$$

$$H4^T D^{-1} f_o = kc4_N^T (F03_N/m3 - F04_N/m4) + \xi34_3^T J3^{-1} M03_3 - \xi44_4^T J4^{-1} M04_4$$

$$H1^T D^{-1} H1 = \mu_{13} + \xi11_1^T J1^{-1} \xi11_1 + \xi31_3^T J3^{-1} \xi31_3$$

$$H2^T D^{-1} H2 = \mu_{23} + \xi22_2^T J2^{-1} \xi22_2 + \xi32_3^T J3^{-1} \xi32_3$$

$$H3^T D^{-1} H3 = \mu_{34} + \xi33_3^T J3^{-1} \xi33_3 + \xi43_4^T J4^{-1} \xi43_4$$

$$H4^T D^{-1} H4 = \mu_{34} + \xi34_3^T J3^{-1} \xi34_3 + \xi44_4^T J4^{-1} \xi44_4$$

$$H1^T D^{-1} H2 = kc1_N^T kc2_N/m3 + \xi31_3^T J3^{-1} \xi32_3$$

$$H1^T D^{-1} H3 = -(kc1_N^T kc3_N/m3 + \xi31_3^T J3^{-1} \xi33_3)$$

$$H1^T D^{-1} H4 = -(kc1_N^T kc4_N/m3 + \xi31_3^T J3^{-1} \xi34_3)$$

$$H2^T D^{-1} H3 = -(kc2_N^T kc3_N/m3 + \xi32_3^T J3^{-1} \xi33_3)$$

$$H2^T D^{-1} H4 = -(kc2_N^T kc4_N/m3 + \xi32_3^T J3^{-1} \xi34_3)$$

$$H3^T D^{-1} H4 = \mu_{34} kc3_N^T kc4_N + \xi33_3^T J3^{-1} \xi34_3 + \xi43_4^T J4^{-1} \xi44_4$$

where

$$\mu_{13} = (m1 + m3)/m1 m3$$

$$\mu_{23} = (m2 + m3)/m2 m3$$

$$\mu_{34} = (m3 + m4)/m3 m4$$

Table 14. Concluded.

(e) Simulation equations:

$$sf = D^{-1}(fo + fc) = \begin{pmatrix} SF1_N \\ SF2_N \\ SF3_N \\ SF4_N \\ SM1_1 \\ SM2_2 \\ SM3_3 \\ SM4_4 \end{pmatrix} = \begin{pmatrix} (F01_N + FC1_N)/m1 \\ (F02_N + FC2_N)/m2 \\ (F03_N + FC3_N)/m3 \\ (F04_N + FC4_N)/m4 \\ J1^{-1}(M01_1 + MC1_1) \\ J2^{-1}(M02_2 + MC2_2) \\ J3^{-1}(M03_3 + MC3_3) \\ J4^{-1}(M04_4 + MC4_4) \end{pmatrix}$$

$$\dot{u} = A^{-1} sf$$

$$\dot{V}1^*_N = SF1_N$$

$$\dot{\omega}1_1 = SM1_1$$

$$\dot{\omega}2_2 = SM2_2$$

$$\dot{\omega}3_3 = SM3_3$$

$$\dot{\omega}4_4 = SM4_4$$

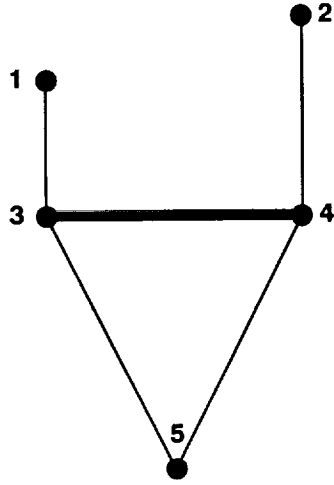
$$\dot{V}13_{c1} = T_{c1,N}[SF3_N - SF1_N - A_{25} SM1_1 - A_{37} SM3_3]$$

$$\dot{V}24_{c2} = T_{c2,N}[SF3_N - SF2_N + A_{26} SM2_2 - A'_{27} SM3_3]$$

$$\dot{V}T_t = T_{t,N}[SF4_N - SF3_N - A_{48} SM4_4] - BT SM3_3$$

Table 15. Simulation Equations: Degenerate-Body Approximation of Dual-Lift System with Spreader Bar

(a) System and spreader-bar kinematics:



Parameters:

- m1
- m2
- m3, J3 = J3' diag {0,1,1}
- m4
- l_{o1}, l_{o2}, l_{o3}, l_{o4} = l_{o3}, R3*3, R3*4

Degenerate-body dual-lift system.

i_3 = spreader-bar longitudinal axis

$$(R_{34}, R_{3^*4}, R_{3^*3}) = (-R_{34} i_3, -R_{3^*4} i_3, +R_{3^*3} i_3)$$

$$T_{3,N} = E_2(\theta_3) E_3(\psi_3)$$

$$T_{l,3} = E_1(\phi_l)$$

$$\omega_{33} = (j_{33}, k_{N3}) \begin{pmatrix} \dot{\theta}_3 \\ \dot{\psi}_3 \end{pmatrix} = \begin{pmatrix} 0 & -\sin \theta_3 \\ 1 & 0 \\ 0 & \cos \theta_3 \end{pmatrix} \begin{pmatrix} \dot{\theta}_3 \\ \dot{\psi}_3 \end{pmatrix} = \overline{W}_{33} \dot{\alpha}_3$$

Table 15. Continued.

(b) Kinematics:

$$\bar{v} = \begin{pmatrix} V1^*_N \\ V2^*_N \\ V3^*_N \\ V4^*_N \\ \frac{\dot{\alpha}3}{\alpha^3} \end{pmatrix} = \bar{A} u = \begin{pmatrix} I & 0 & 0 & 0 & 0 \\ I & T_{N,c1} & -T_{N,c2} & 0 & A_{25} \\ I & T_{N,c1} & 0 & 0 & A_{35} \\ I & T_{N,c1} & 0 & T_{N,t} & A_{45} \\ 0 & 0 & 0 & 0 & I \end{pmatrix} \begin{pmatrix} V1^*_N \\ V13_{c1} \\ V24_{c2} \\ VT_t \\ \frac{\dot{\alpha}3}{\alpha^3} \end{pmatrix}$$

$$u = \begin{pmatrix} V1^*_N \\ V13_{c1} \\ V24_{c2} \\ VT_t \\ \frac{\dot{\alpha}3}{\alpha^3} \end{pmatrix} = \bar{A}^{-1} \bar{v} = \begin{pmatrix} I & 0 & 0 & 0 & 0 \\ -T_{c1,N} & 0 & T_{c1,N} & 0 & B_{25} \\ 0 & -T_{c2,N} & T_{c2,N} & 0 & B_{35} \\ 0 & 0 & -T_{t,N} & T_{t,N} & -\overline{BT}_t \\ 0 & 0 & 0 & 0 & I \end{pmatrix} \begin{pmatrix} V1^*_N \\ V2^*_N \\ V3^*_N \\ V4^*_N \\ \frac{\dot{\alpha}3}{\alpha^3} \end{pmatrix}$$

Auxiliary expressions:

$$A'_{25} = +T_{N,3} S(i3_3) \overline{W3}_3 = (+k3_N, -\cos \theta_3 j3_N) = \begin{pmatrix} +\sin \theta_3 \cos \psi_3 & +\cos \theta_3 \sin \psi_3 \\ +\sin \theta_3 \sin \psi_3 & -\cos \theta_3 \cos \psi_3 \\ +\cos \theta_3 & 0 \end{pmatrix}$$

Submatrices of \bar{A}, \bar{A}^{-1} :

$$A_{25} = -T_{N,3} S(R34_3) \overline{W3}_3 = R34 A'_{25}$$

$$A_{35} = T_{N,3} S(R3^*3_3) \overline{W3}_3 = R3^*3 A'_{25}$$

$$A_{45} = -T_{N,3} S(R35_3) \overline{W3}_3 = -T_{N,3} S(-R3^*3_3 + R3^*5_3) \overline{W3}_3$$

$$B_{25} = -T_{c1,N} A_{35}$$

$$B_{35} = -T_{c2,N} T_{N,3} S(R3^*4_3) \overline{W3}_3 = R3^*4 T_{c2,N} A'_{25}$$

$$\Delta VT_t = -(\mathbf{R3}^*5 \times \omega \mathbf{3}')_t = \overline{BT}_t \frac{\dot{\alpha}3}{\alpha^3}$$

$$\overline{BT}_t = -S(R3^*5_t) T_{t,3} \overline{W3}_3 = \begin{pmatrix} \ell 3z \cos \phi_t & \ell 3z \sin \phi_t \cos \theta_3 \\ -\ell 3x \sin \phi_t & \ell 3z \sin \theta_3 + \ell 3x \cos \phi_t \cos \theta_3 \\ -\ell 3x \cos \phi_t & -\ell 3x \sin \phi_t \cos \theta_3 \end{pmatrix}$$

Table 15. Continued.

(c) Applied forces and inertia reactions:

$$f_o = fg + fa - X - D \dot{A} u$$

$$A = \bar{W} \bar{A} = \text{diag}\{I, I, I, I, \bar{W}3_3\} \bar{A}$$

$$f_o = \begin{pmatrix} F01_N \\ F02_N \\ F03_N \\ F04_N \\ M03_3 \end{pmatrix} = \begin{pmatrix} m1 g_N + FA1_N \\ m2 g_N + FA2_N - m2(\dot{T}_{N,c1} V13_{c1} - \dot{T}_{N,c2} V24_{c2} + \dot{A}_{25} \bar{\alpha}3) \\ m3 g_N + FA3_N - m3(\dot{T}_{N,c1} V13_{c1} + \dot{A}_{35} \bar{\alpha}3) \\ m4 g_N + FA4_N - m4(\dot{T}_{N,c1} V13_{c1} + \dot{T}_{N,t} VT_t + \dot{A}_{45} \bar{\alpha}3) \\ MA3_3 - S(\omega3_3) J3 \omega3_3 - J3 \bar{W}3_3 \dot{\bar{\alpha}}3 \end{pmatrix}$$

Transformation rates:

$$\dot{T}_{N,c} = T_{N,c} S(\omega c_c) \quad c = c1, c2, t$$

$$\omega c_c = (\dot{\phi}_c, \dot{\theta}_c \cos \phi_c, -\dot{\theta}_c \sin \phi_c)^T \quad c = c1, c2$$

$$\omega t_t = \begin{pmatrix} 1 & 0 & -\sin \theta_3 \\ 0 & \cos \phi_t & \sin \phi_t \cos \theta_3 \\ 0 & -\sin \phi_t & \cos \phi_t \cos \theta_3 \end{pmatrix} \begin{pmatrix} \dot{\phi}_t \\ \dot{\theta}_3 \\ \dot{\psi}_3 \end{pmatrix} = W t_t \dot{\alpha} t$$

Other submatrices of $\dot{A} u$:

$$z1_3 = \bar{W}3_3 \dot{\bar{\alpha}}3 = -\dot{\theta}_3 \dot{\psi}_3 (\cos \theta_3, 0, \sin \theta_3)^T$$

$$z2_N = \dot{A}'_{25} \dot{\bar{\alpha}}3 = T_{N,3} [S^2(\omega3_3) + S(z1_3)] i3_3$$

$$= \begin{pmatrix} -\dot{\theta}_3^2 \cos \theta_3 \cos \psi_3 + 2\dot{\theta}_3 \dot{\psi}_3 \sin \theta_3 \sin \psi_3 - \dot{\psi}_3^2 \cos \theta_3 \cos \psi_3 \\ -\dot{\theta}_3^2 \cos \theta_3 \sin \psi_3 - 2\dot{\theta}_3 \dot{\psi}_3 \sin \theta_3 \cos \psi_3 - \dot{\psi}_3^2 \cos \theta_3 \sin \psi_3 \\ -\dot{\theta}_3^2 \sin \theta_3 \end{pmatrix}$$

$$\dot{A}_{25} \dot{\bar{\alpha}}3 = R34 z2_N$$

$$\dot{A}_{35} \dot{\bar{\alpha}}3 = R3^*3 z2_N$$

$$\dot{A}_{45} \dot{\bar{\alpha}}3 = T_{N,3} [(S^2(\omega3_3) + S(z1_3)) R35_3 + S(\omega3_3) R\dot{3}5_3]$$

where

$$R35_3 = -R3^*3_3 + R3^*5_3$$

$$R\dot{3}5_3 = T_{3,t} VT_t$$

Table 15. Continued.

(d) Suspension forces:

$$f_c = H TC = \begin{pmatrix} kc1_N & 0 & 0 & 0 \\ 0 & kc2_N & 0 & 0 \\ -kc1_N & -kc2_N & kc3_N & kc4_N \\ 0 & 0 & -kc3_N & -kc4_N \\ -\xi31_3 & -\xi32_3 & \xi33_3 & \xi34_3 \end{pmatrix} \begin{pmatrix} TC1 \\ TC2 \\ TC3 \\ TC4 \end{pmatrix}$$

Elastic cables:

$$TCj = \max\{0, Kj (\ell_j - \ell_{oj})\} \quad j = 1, \dots, 4$$

Inelastic cables:

$$\bar{H} = \bar{W}^T H = \begin{pmatrix} kc1_N & 0 & 0 & 0 \\ 0 & kc2_N & 0 & 0 \\ -kc1_N & -kc2_N & kc3_N & kc4_N \\ 0 & 0 & -kc3_N & -kc4_N \\ -\bar{\xi}31_3 & -\bar{\xi}32_3 & +\bar{\xi}33_3 & +\bar{\xi}34_3 \end{pmatrix}$$

$$\bar{\xi}3j_3 = \bar{W}3_3^T \xi3j_3 \quad j = 1, \dots, 4$$

$$TC = -[\bar{H}^T \bar{D}^{-1} \bar{H}]^{-1} \bar{H}^T \bar{D}^{-1} \bar{W}^T f_o$$

$$\bar{W} = \text{diag}\{I, I, I, I, \bar{W}3_3\}$$

$$\bar{D} = \bar{W}^T D \bar{W} = \text{diag}\{m1 I, m2 I, m3 I, m4 I, \bar{J}3\}$$

$$\bar{J}3 = \bar{W}3_3^T J3 \bar{W}3_3 = J3' \text{diag}\{1, \cos^2 \theta_3\}$$

Table 15. Concluded.

(e) Simulation equations:

$$\overline{sf} = \overline{D}^{-1} \overline{W}^T (fo + fc) = \begin{pmatrix} SF1_N \\ SF2_N \\ SF3_N \\ SF4_N \\ \overline{SM3} \end{pmatrix} = \begin{pmatrix} (F01_N + FC1_N)/m1 \\ (F02_N + FC2_N)/m2 \\ (F03_N + FC3_N)/m3 \\ (F04_N + FC4_N)/m4 \\ \overline{J3}^{-1} \overline{W3}_3^T (M03_3 + MC3_3) \end{pmatrix}$$

$$\dot{u} = \overline{A}^{-1} \overline{sf}$$

$$\dot{V}1^*_N = SF1_N$$

$$\dot{V}13_{c1} = T_{c1,N}(SF3_N - SF1_N - R3^*3 A'_{25} \overline{SM3})$$

$$\dot{V}24_{c2} = T_{c2,N}(SF3_N - SF2_N + R3^*4 A'_{25} \overline{SM3})$$

$$\dot{V}T_t = T_{t,N}(SF4_N - SF3_N) - \overline{BT}_t \overline{SM3}$$

$$\ddot{\overline{\alpha 3}} = \overline{SM3}$$



APPENDIX E

SIMULATION EQUATIONS FOR A MULTILIFT SYSTEM WITH PENDANT SUSPENSION

INTRODUCTION

This appendix gives simulation equations for the multilift system shown in figure 7, in which m helicopters support a load with a single cable attaching the load to each helicopter. This system was suggested in discussions by P. K. A. Menon (ref. 18) as one of potential interest using remotely controlled helicopters. These equations can be obtained by extension of the results for a single helicopter with single-cable suspension. Results are also given for the special case in which all attachments are at the c.g.'s of the rigid bodies; these include the equations for the point-mass approximation of the system.

System and constraints— The n -body system shown in figure 7 consists of a load B_n suspended, pendant-style, from $m = n - 1$ helicopters, B_1, \dots, B_m , by cables C_1, \dots, C_m attached to the helicopters at $\mathbf{R}_1, \dots, \mathbf{R}_m$. The load and short cables and the hardware attaching the load to the pendant vertex at \mathbf{R}_n are considered a single rigid body. If the cables are inelastic, then each imposes one holonomic constraint on the motion of a helicopter relative to the load by fixing the distance

$$\begin{aligned} \ell_j(r) &= |\mathbf{R}_j \mathbf{n}| \\ &= |\mathbf{R}_n^* \mathbf{n}_N + T_{N,n} \mathbf{R}_n^* \mathbf{n}_n - \mathbf{R}_j^* \mathbf{n}_N - T_{N,j} \mathbf{R}_j^* \mathbf{j}_j| = \ell_{0j} \end{aligned} \quad (142)$$

For inelastic cables

$$c = m = n - 1 \quad \text{and} \quad d = 6n - m \quad (143)$$

Generalized velocity coordinates— The generalized velocity coordinates u , are to be selected so as to separate motion caused by cable stretching from motion with invariant cable lengths. This is readily done by extension of the treatment of a single-cable suspension from a single helicopter given in appendix B. The coordinates u consist of the c.g. velocity of a reference body, taken as the load in this case, $V n^*_N$, and the m cable velocities given by their components in

cable axes, $\{V j n_{c_j} \quad j = 1, \dots, m\}$. These are augmented by the angular velocities of all n rigid bodies to obtain $6n$ coordinates for the elastic suspension. For the inelastic suspension, the cable-stretching coordinate ℓ_j of each cable velocity is nulled, leaving $6n - m$ coordinates.

To assemble the kinematic relations $v(u), u(v)$ note that the c.g. position of each helicopter is given by

$$\mathbf{R}_j^* \mathbf{n}_N = \mathbf{R}_n^* \mathbf{n}_N + \mathbf{R}_n^* \mathbf{n}_n - \mathbf{R}_j^* \mathbf{n}_N - \mathbf{R}_j^* \mathbf{j}_j \quad j = 1, \dots, m \quad (144)$$

whence its c.g. velocity is given in terms of coordinates from u as

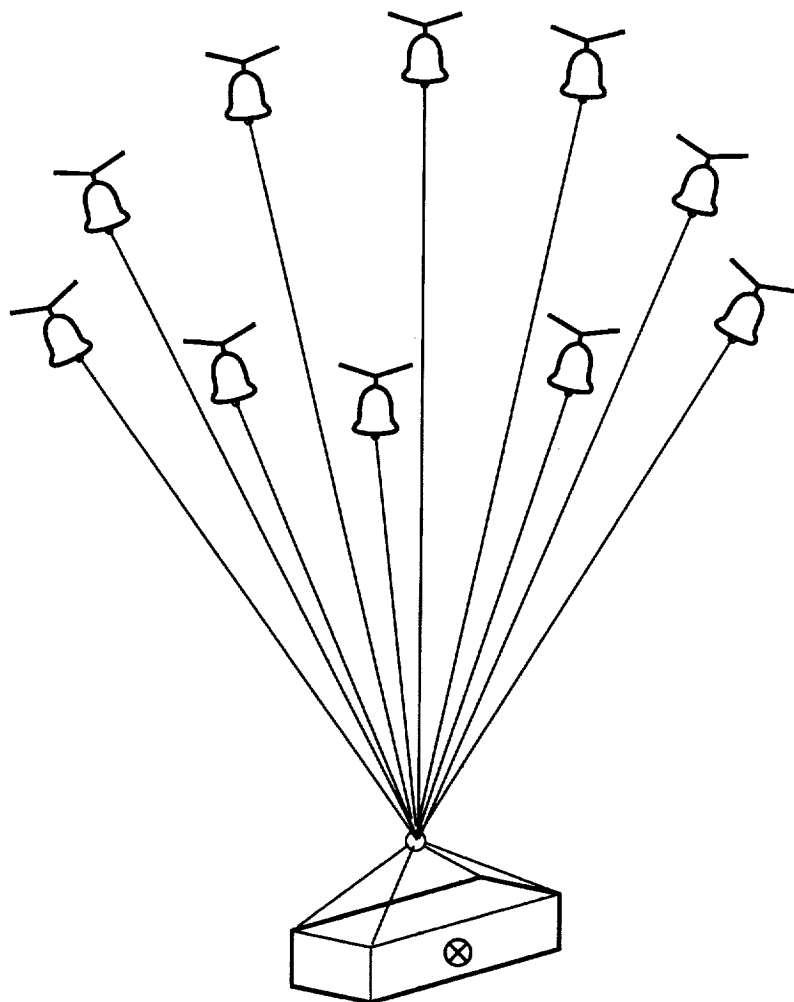
$$\begin{aligned} V j^* \mathbf{n}_N &= V n^* \mathbf{n}_N - T_{N,n} S(\mathbf{R}_n^* \mathbf{n}_n) \omega n_n - T_{N,c_j} V j n_{c_j} \\ &\quad + T_{N,j} S(\mathbf{R}_j^* \mathbf{j}_j) \omega j_j \quad j = 1, \dots, m \end{aligned} \quad (145)$$

This can be rearranged to give the cable velocities in terms of the coordinates of v as

$$\begin{aligned} V j n_{c_j} &= T_{c_j, N} (V n^* \mathbf{n}_N - V j^* \mathbf{n}_N + T_{N,j} S(\mathbf{R}_j^* \mathbf{j}_j) \omega j_j \\ &\quad - T_{N,n} S(\mathbf{R}_n^* \mathbf{n}_n) \omega n_n) \quad j = 1, \dots, m \end{aligned} \quad (146)$$

The kinematics $v(u), u(v)$ can be obtained from equations (145) and (146), and are presented in part a of table 16. The coefficient matrices A, A^{-1} contain $3(n+1)$ rows from the unit matrix, corresponding to coordinates that are in both u, v , and the remaining rows contain only transformations and cross products from Coriolis velocities.

External forces and inertia coupling— The external forces and moments on the configuration, f_0 , are assembled in part b of table 16. Its vector elements are denoted $(\mathbf{F}0_1, \dots, \mathbf{M}0_n)$ for convenience in later equations. The f_0 term contains forces and moments on the rigid bodies due to weight, $(m_1 \mathbf{g}, \dots, m_n \mathbf{g})$, aerodynamics and helicopter rotor output, $(\mathbf{F}A_1, \dots, \mathbf{M}A_n)$, and the inertia coupling terms $X + D\dot{A}u$. The submatrices of \dot{A} require only time-derivatives of transformations, and the corresponding terms in f_0 due to $\dot{A}u$ are all Coriolis accelerations of the cables $\omega c_j \times V j n$, and centrifugal accelerations of the c.g. attachment-point moment arms for all the bodies, $\omega j \times (\omega j \times \mathbf{R}_j^* \mathbf{j}_j)$.



B_1, \dots, B_n

Rigid bodies

C_1, \dots, C_m

Cables, $m = n - 1$

$(m_j, J_j, R_j^*j_j), j = 1, \dots, n$

Rigid body parameters

$\lambda_{0j}, j = 1, \dots, m$

Reference cable lengths

Figure 7. Multilift pendant suspension.

Suspension forces— The resultant forces and moments applied by the suspension to the rigid bodies of the configuration fc , is given in part c of table 16. Since the number of cables and constraints is equal, the configuration vectors for the cable tensions $\{H1, \dots, Hm\}$ comprise a basis of the suspension force space which can also be used to give fc for inelastic cables; as a result, only the cable-tension formulas differ for the elastic and inelastic cable models. For inelastic cables, it is necessary to invert the $m \times m$ matrix $H^T D^{-1} H$.

Simulation equations— Finally, the equations for \dot{u} are assembled in part d of table 16 from $\dot{u} = A^{-1} sf$. Here, sf refers to the specific forces and moments on the configuration due to $fo + fc$. Its vector elements are denoted $SF1, \dots, SMn$ for convenience. The equations for Vn^*_N and $\{\omega_{j_j}, j = 1, \dots, n\}$ are identical to those obtained from the Newton-Euler equations; the cable-velocity equations depend on differences of specific forces and moments.

Special case of c.g. attachments on point-mass bodies— A simpler set of equations is obtained if all cable attachments are assumed to be made at the helicopter and load c.g.'s ($Rj^*j = 0, j = 1, \dots, n$). Results are listed in table 17 and are obtained by imposing the c.g. attachment-point condition on the results given in table 16. The matrices A, A^{-1} become block diagonal for the linear and angular velocity coordinates; this accounts in part for the separation of

these coordinates into independent subsystems. Furthermore, since the suspension can apply no moments to any body ($MCj = 0, j = 1, \dots, n$), the attitude dynamics of each rigid body are independent of all other coordinates of the configuration motion, except through the aerodynamic moments, and are defined by the usual Euler equation for independent rigid bodies (table 17).

The remaining equations in table 17 govern the linear velocity coordinates and are also simulation equations for the point-mass approximation of the system. The c.g. velocities now depend only on cable velocities in equations (145) and (146), and in the assembled velocity kinematics given in table 17. The applied forces have no coupling with the rigid-body angular velocities through $\dot{A}u$, although such a coupling can occur in the aerodynamics. The interaction forces for the inelastic suspension are now independent of the applied moments on any body. The corresponding cable tensions still require the inverse of an $m \times m$ matrix. This is given in table 17 as a sum of a diagonal matrix of mass ratios and the positive semidefinite Grammian of the cable directions, and can be inverted without computational difficulty. The final result is almost as simple as the elastic suspension formulation using rigid body coordinates. It uses cable-velocity coordinates and accommodates both inelastic and elastic suspensions with explicit calculation of cable tensions in both cases.

Table 16. Simulation equation summary: multilift with pendant suspension

(a) Configuration kinematics:

$$v = A u$$

$$\begin{pmatrix} V1^*_N \\ V2^*_N \\ \cdot \\ \cdot \\ Vm^*_N \\ Vn^*_N \\ - \\ \omega 1_1 \\ \omega 2_2 \\ \cdot \\ \cdot \\ \omega m_n \\ \omega n_n \end{pmatrix} = \begin{pmatrix} -T_{N,c1} & 0 & \cdot & \cdot & 0 & I & | & A_{1,n+1} & 0 & \cdot & \cdot & 0 & A_{1,2n} \\ 0 & -T_{N,c2} & \cdot & \cdot & 0 & I & | & 0 & A_{2,n+2} & \cdot & \cdot & 0 & A_{1,2n} \\ \cdot & \cdot & \cdot & \cdot & \cdot & \cdot & | & \cdot & \cdot & \cdot & \cdot & \cdot & \cdot \\ \cdot & \cdot & \cdot & \cdot & \cdot & \cdot & | & \cdot & \cdot & \cdot & \cdot & \cdot & \cdot \\ Vm^*_N & 0 & 0 & \cdot & -T_{N,cm} & I & | & 0 & 0 & \cdot & \cdot & A_{m,n+m} & A_{1,2n} \\ Vn^*_N & 0 & 0 & \cdot & 0 & I & | & 0 & 0 & \cdot & \cdot & 0 & 0 \\ - & - & - & - & - & - & | & - & - & - & - & - & - \\ \omega 1_1 & & & & & & | & & & & & & & \omega 1_1 \\ \omega 2_2 & & & & & & | & & & & & & & \omega 2_2 \\ \cdot & & & 0 & & & | & & & I & & & & \cdot \\ \cdot & & & & & & | & & & & & & & \cdot \\ \omega m_n & & & & & & | & & & & & & & \omega m_n \\ \omega n_n & & & & & & | & & & & & & & \omega n_n \end{pmatrix} \begin{pmatrix} V1n_{c1} \\ V2n_{c2} \\ \cdot \\ \cdot \\ Vmn_{cm} \\ Vn^*_N \\ - \\ \omega 1_1 \\ \omega 2_2 \\ \cdot \\ \cdot \\ \omega m_n \\ \omega n_n \end{pmatrix}$$

$$u = A^{-1} v$$

$$\begin{pmatrix} V1n_{c1} \\ V2n_{c2} \\ \cdot \\ \cdot \\ Vmn_{cm} \\ Vn^*_N \\ - \\ \omega 1_1 \\ \omega 2_2 \\ \cdot \\ \cdot \\ \omega m_n \\ \omega n_n \end{pmatrix} = \begin{pmatrix} -T_{c1,N} & 0 & \cdot & \cdot & 0 & T_{c1,N} & | & B_{1,n+1} & 0 & \cdot & \cdot & 0 & B_{1,2n} \\ 0 & -T_{c2,N} & \cdot & \cdot & 0 & T_{c2,N} & | & 0 & B_{2,n+2} & \cdot & \cdot & 0 & B_{2,2n} \\ \cdot & \cdot & \cdot & \cdot & \cdot & \cdot & | & \cdot & \cdot & \cdot & \cdot & \cdot & \cdot \\ \cdot & \cdot & \cdot & \cdot & \cdot & \cdot & | & \cdot & \cdot & \cdot & \cdot & \cdot & \cdot \\ Vmn_{cm} & 0 & 0 & \cdot & -T_{cm,N} & T_{cm,N} & | & 0 & 0 & \cdot & \cdot & B_{m,n+m} & B_{m,2n} \\ Vn^*_N & 0 & 0 & \cdot & 0 & I & | & 0 & 0 & \cdot & \cdot & 0 & 0 \\ - & - & - & - & - & - & | & - & - & - & - & - & - \\ \omega 1_1 & & & & & & | & & & & & & & \omega 1_1 \\ \omega 2_2 & & & & & & | & & & & & & & \omega 2_2 \\ \cdot & & & 0 & & & | & & & I & & & & \cdot \\ \cdot & & & & & & | & & & & & & & \cdot \\ \omega m_n & & & & & & | & & & & & & & \omega m_n \\ \omega n_n & & & & & & | & & & & & & & \omega n_n \end{pmatrix} \begin{pmatrix} V1^*_N \\ V2^*_N \\ \cdot \\ \cdot \\ Vm^*_N \\ Vn^*_N \\ - \\ \omega 1_1 \\ \omega 2_2 \\ \cdot \\ \cdot \\ \omega m_n \\ \omega n_n \end{pmatrix}$$

$$A_{j,n+j} = T_{N,j} S(Rj^*j_j) \quad j = 1, \dots, m$$

$$A_{1,2n} = -T_{N,n} S(Rn^*n_n)$$

$$B_{j,n+j} = T_{c_j,N} A_{j,n+j} \quad j = 1, \dots, m$$

$$B_{j,2n} = T_{c_j,N} A_{1,2n} \quad j = 1, \dots, m$$

Table 16. Continued.

(b) Applied forces and inertia coupling:

$$f_0 = f_g + f_a - X - D\dot{A}u = \begin{pmatrix} F01_n \\ \cdot \\ \cdot \\ \cdot \\ F0m_N \\ F0n_N \\ M01_1 \\ \cdot \\ \cdot \\ \cdot \\ M0n_n \end{pmatrix} = \begin{pmatrix} m1 g_N + FA1_N - m1 \dot{A}_1 u \\ \cdot \\ \cdot \\ \cdot \\ mm g_N + FA m_N - mm \dot{A}_m u \\ mn g_N + FA n_N \\ MA1_1 - S(\omega 1_1) J1 \omega 1_1 \\ \cdot \\ \cdot \\ \cdot \\ MA n_n - S(\omega n_n) Jn \omega n_n \end{pmatrix}$$

where:

$$A_j = j^{\text{th}} \text{row of } A$$

$$\dot{A}_j u = -T_{N,cj} S(\omega c_{cj}) V j n_{cj} - T_{N,j} S^2(\omega j_j) R j^* j_j + T_{N,n} S^2(\omega n_n) R n^* n_n \quad j = 1, \dots, m$$

$$\omega c_{cj} = (\dot{\phi}_{cj}, \dot{\theta}_{cj} \cos \phi_{cj}, -\dot{\theta}_{cj} \sin \phi_{cj}) \quad j = 1, \dots, m$$

Table 16. Continued.

(c) Suspension forces:

$$f_c = H TC = \begin{pmatrix} kc1_N & 0 & \dots & 0 \\ 0 & kc2_N & \dots & 0 \\ \cdot & \cdot & & \cdot \\ \cdot & \cdot & & \cdot \\ \cdot & \cdot & & \cdot \\ 0 & 0 & \dots & kcm_N \\ -kc1_N & -kc2_N & \dots & -kcm_N \\ \xi11_1 & 0 & \dots & 0 \\ 0 & \xi22_2 & \dots & 0 \\ \cdot & \cdot & & \cdot \\ \cdot & \cdot & & \cdot \\ \cdot & \cdot & & \cdot \\ 0 & 0 & \dots & \xi mm_m \\ -\xi n1_n & -\xi n2_n & & -\xi nm_n \end{pmatrix} \begin{pmatrix} TC1 \\ TC2 \\ \cdot \\ \cdot \\ TCm \end{pmatrix}$$

$$\left. \begin{aligned} \xi jj_j &= (\mathbf{Rj}^* \mathbf{j} \times \mathbf{kcj})_j = S(Rj^* j_j) T_{j,N} kcj_N \\ \xi nj_n &= (\mathbf{Rn}^* \mathbf{n} \times \mathbf{kcj})_n = S(Rn^* n_n) T_{n,N} kcj_N \end{aligned} \right\} j = 1, \dots, m$$

$$TC = \begin{cases} (\max\{0, K_j (\ell_j - \ell_{0j})\}, j = 1, \dots, m)^T & \text{(Elastic cables)} \\ -[H^T D^{-1} H]^{-1} H^T D^{-1} f_o & \text{(Inelastic cables)} \end{cases}$$

Table 16. Concluded.

(d) Simulation equations:

$$sf = D^{-1}(fo + fc) = \begin{pmatrix} SF1_N \\ \cdot \\ \cdot \\ SFn_N \\ SM1_1 \\ \cdot \\ \cdot \\ \cdot \\ SMn_n \end{pmatrix} = \begin{pmatrix} (F01_N + FC1_N)/m1 \\ \cdot \\ \cdot \\ (F0n_N + FCn_N)/mn \\ J1^{-1}(M01_1 + MC1_1) \\ \cdot \\ \cdot \\ \cdot \\ Jn^{-1}(M0n_n + MCn_n) \end{pmatrix}$$

$$\dot{u} = A^{-1} sf$$

$$\dot{V}jn_{cj} = T_{cj,N}[SFn_N - SFj_N + A_{j,n+j} SMj_j + A_{1,2n} SMn_n] \quad j = 1, \dots, m$$

$$\dot{V}n^*_N = SFn_N$$

$$\dot{\omega}j_j = SMj_j \quad j = 1, \dots, n$$

Table 17. Simulation equation summary for c.g. attachments:
multilift with pendant suspension

c.g. Attachments: $R_j^* j = 0 \quad j = 1, \dots, n$

Angular velocity coordinates:

$$\dot{\omega} j_j = J_j^{-1} [M A j_j - S(\omega j_j) J j \omega j_j] \quad j = 1, \dots, n$$

Linear velocity coordinates

(a) Configuration kinematics:

$$\begin{pmatrix} V1^*_N \\ V2^*_N \\ \cdot \\ \cdot \\ Vm^*_N \\ Vn^*_N \end{pmatrix} = \begin{pmatrix} -T_{N,c1} & 0 & \cdot & \cdot & \cdot & 0 & I \\ 0 & -T_{N,c2} & \cdot & \cdot & \cdot & 0 & I \\ \cdot & \cdot & \cdot & \cdot & \cdot & \cdot & \cdot \\ \cdot & \cdot & \cdot & \cdot & \cdot & \cdot & \cdot \\ 0 & 0 & \cdot & \cdot & \cdot & -T_{N,cm} & I \\ 0 & 0 & \cdot & \cdot & \cdot & 0 & I \end{pmatrix} \begin{pmatrix} V1n_{c1} \\ V2n_{c2} \\ \cdot \\ \cdot \\ Vmn_{cm} \\ Vn^*_N \end{pmatrix}$$

$$\begin{pmatrix} V1n_{c1} \\ V2n_{c2} \\ \cdot \\ \cdot \\ Vmn_{cm} \\ Vn^*_N \end{pmatrix} = \begin{pmatrix} -T_{c1,N} & 0 & \cdot & \cdot & \cdot & 0 & T_{c1,N} \\ 0 & -T_{c2,N} & \cdot & \cdot & \cdot & 0 & T_{c2,N} \\ \cdot & \cdot & \cdot & \cdot & \cdot & \cdot & \cdot \\ \cdot & \cdot & \cdot & \cdot & \cdot & \cdot & \cdot \\ 0 & 0 & \cdot & \cdot & \cdot & -T_{cm,N} & T_{cm,N} \\ 0 & 0 & \cdot & \cdot & \cdot & 0 & I \end{pmatrix} \begin{pmatrix} V1^*_N \\ V2^*_N \\ \cdot \\ \cdot \\ Vm^*_N \\ Vn^*_N \end{pmatrix}$$

(b) Applied forces and inertia coupling:

$$f_o = \begin{pmatrix} F01_N \\ \cdot \\ \cdot \\ \cdot \\ F0n_N \end{pmatrix}$$

$$\left. \begin{aligned} F0j_N &= m_j g_N + F A j_N - m_j T_{N,cj} S(\omega c j_c j) V j n_{c j} \\ \omega c j_c j &= (\dot{\phi}_{c j}, \dot{\theta}_{c j} \cos \phi_{c j}, -\dot{\theta}_{c j} \sin \phi_{c j}) \\ F0n_N &= m n g_N + F A n_N \end{aligned} \right\} j = 1, \dots, m$$

Table 17. Concluded.

(c) Suspension forces:

$$fc = \begin{pmatrix} FC1_N \\ FC2_N \\ \cdot \\ \cdot \\ FCm_N \\ \cdot \\ FCn_N \end{pmatrix} = H TC = \begin{pmatrix} kc1_N & 0 & \cdot & \cdot & \cdot & 0 \\ 0 & kc2_N & \cdot & \cdot & \cdot & 0 \\ \cdot & \cdot & \cdot & \cdot & \cdot & \cdot \\ \cdot & \cdot & \cdot & \cdot & \cdot & \cdot \\ \cdot & \cdot & \cdot & \cdot & \cdot & \cdot \\ 0 & 0 & \cdot & \cdot & \cdot & kcm_N \\ -kc1_N & -kc2_N & \cdot & \cdot & \cdot & -kcm_N \end{pmatrix} \begin{pmatrix} TC1 \\ TC2 \\ \cdot \\ \cdot \\ \cdot \\ TCm \end{pmatrix}$$

or

$$FCj_N = kcj_N TCj \quad j=1, \dots, m$$

$$FCn_N = -\sum_{j=1}^m kcj_N TCj$$

$$TC = \begin{cases} (\max\{0, K_j (\ell_j - \ell_{0j})\}, j = 1, \dots, m)^T & \text{(Elastic cables)} \\ -[H^T D^{-1} H]^{-1} H^T D^{-1} fo & \text{(Inelastic cables)} \end{cases}$$

$$H^T D^{-1} fo = \begin{pmatrix} kc1_N^T (F01_N/m1 - F0n_N/mn) \\ \cdot \\ \cdot \\ \cdot \\ kcm_N^T (F0m_N/mm - F0n_N/mn) \end{pmatrix}$$

$$H^T D^{-1} H = \frac{1}{mn} [\text{diag}\{\frac{mn}{mj}, j = 1, \dots, m\} + K^T K]$$

$$K = [kc1_N, kc2_N, \dots, kcm_N]$$

(d) Simulation equations:

$$sf = D^{-1}(fo + fc) = \begin{pmatrix} SF1_N \\ \cdot \\ \cdot \\ \cdot \\ SFn_N \end{pmatrix} = \begin{pmatrix} (F01_N + FC1_N)/m1 \\ \cdot \\ \cdot \\ \cdot \\ (F0n_N + FCn_N)/mn \end{pmatrix}$$

$$\dot{u} = A^{-1} sf$$

$$\dot{V}n_N^* = SFn_N$$

$$\dot{V}jn_{cj} = T_{cj,N} (SFn_N - SFj_N) \quad j = 1, \dots, m$$



APPENDIX F LINEARIZED EQUATIONS FOR DUAL-LIFT SYSTEM WITH SPREADER BAR

INTRODUCTION

Linearized equations of motion (LEOMs) are given for the dual-lift system with spreader bar for static equilibrium reference flight conditions and assuming inelastic suspension. These are derived from the non-linear EOMs, equation (14); LEOMs for general slung-load systems and for general reference flight conditions are given in table 4, and these are specialized to static equilibrium in equation (41). The dual-lift system geometry and details of the nomenclature are given in appendix D (fig. 6), and notation for the configuration vectors and matrices in the LEOMs follows that established in section 6. Standard linearized aerodynamics are assumed for each body axis as stated in section 6. Various secondary effects are neglected, including interbody interferences.

Coordinates and kinematics—Coordinates are often selected for linear analysis to exploit any natural decomposition of the perturbations into nearly decoupled subsystems of forces, controls, and motion variables. For a single-symmetric aeronautical body aligned with the air-velocity vector, motions in the plane of symmetry containing ($\mathbf{V}_a, \mathbf{i}_b, \mathbf{k}_b$) are nearly decoupled from its lateral-directional motions. For the multibody dual-lift system in hover, all mass lies in or near a plane defined by the spreader bar and local vertical ($\mathbf{i}_3, \mathbf{k}_N$), and the system modes of motion in this plane are nearly decoupled from its yawing and pendulum modes of motion lateral to this plane. These two decompositions can be made coincident at hover by aligning the helicopters in or perpendicular to the plane of the suspension; this is done in references 6 and 7 where a comprehensive description of the natural modes is given. In static equilibrium at cruise speeds, the spreader-bar heading may be at an angle to the flight path, with the helicopters arranged as in formation flying, and with the load-bar triangle swept back to moderate angles from the local vertical, if there is significant load specific drag (fig. 8). In this case, the aerodynamics can couple the motion in and lateral to the plane of the load and spreader bar.

For the present work, the coordinates are selected to maximize the longitudinal-lateral aerodynamic decoupling; this is expected to be a satisfactory starting set for analysis of the natural modes. The generalized velocity coordinates u , and the kinematics $v(q, u)$ are given in part a of table 18. These differ from those in appendix D in the use of body axis coordinates of the reference-point velocity relative to the mean wind, $VA1_1^*$, and tether cable velocities relative to body axes, $\Delta V13_{c1}, \Delta V24_{c2}$, where

$$\Delta \mathbf{V13} = \mathbf{V13} - \omega_1 \times \mathbf{R13}$$

$$\Delta \mathbf{V24} = \mathbf{V24} - \omega_2 \times \mathbf{R24}$$

These cable velocities and the cable axis transformations are given in terms of cable angles relative to helicopter body axes as given in part a of table 18, and discussed in appendix A. Note that u contains all 24 velocity coordinates of the system with elastic suspension. This allows an easier statement of results. Results for the 20 coordinates of the system with inelastic suspension are obtained by deleting columns 6, 9, 10, and 12 from A corresponding to the scalar coordinates $\Delta \mathbf{V13} \bullet \mathbf{k}c1, \Delta \mathbf{V24} \bullet \mathbf{k}c2, \mathbf{V}T \bullet \mathbf{i}3, \mathbf{V}T \bullet \mathbf{k}t$ of u , or by deleting appropriate rows and columns from the coefficient matrices of the LEOMs derived from A for the system of 24 coordinates, as is done at the end of this analysis.

The generalized position coordinates q and the kinematic relation $u(q, \dot{q})$ are included in part a of table 18, for the 20 coordinates of the inelastic system. The coordinates u, q selected here are reference-point coordinates consisting of the c.g. position, and velocity of body B1, $\int VA1_1^* dt, VA1_1^*$, plus additional position coordinates $\bar{q} = \{\Delta \alpha c1, \dots, \alpha 4\}$, which are fixed in static equilibrium, and velocity coordinates $\bar{u} = \{\Delta \mathbf{V13} \bullet \mathbf{i}c1, \dots, \omega 4\}$, which are zero in static equilibrium. The cable angles $\Delta \alpha c1, \Delta \alpha c2$ in \bar{q} are angles relative to helicopter body axes. The reference-point position coordinates, $\int VA1_1^* dt$ in q , have no useful physical meaning, and they do not occur in the LEOMs. Their derivatives, $VA1_1^*$, do occur, and these are meaningful and convenient in aeronautical work.

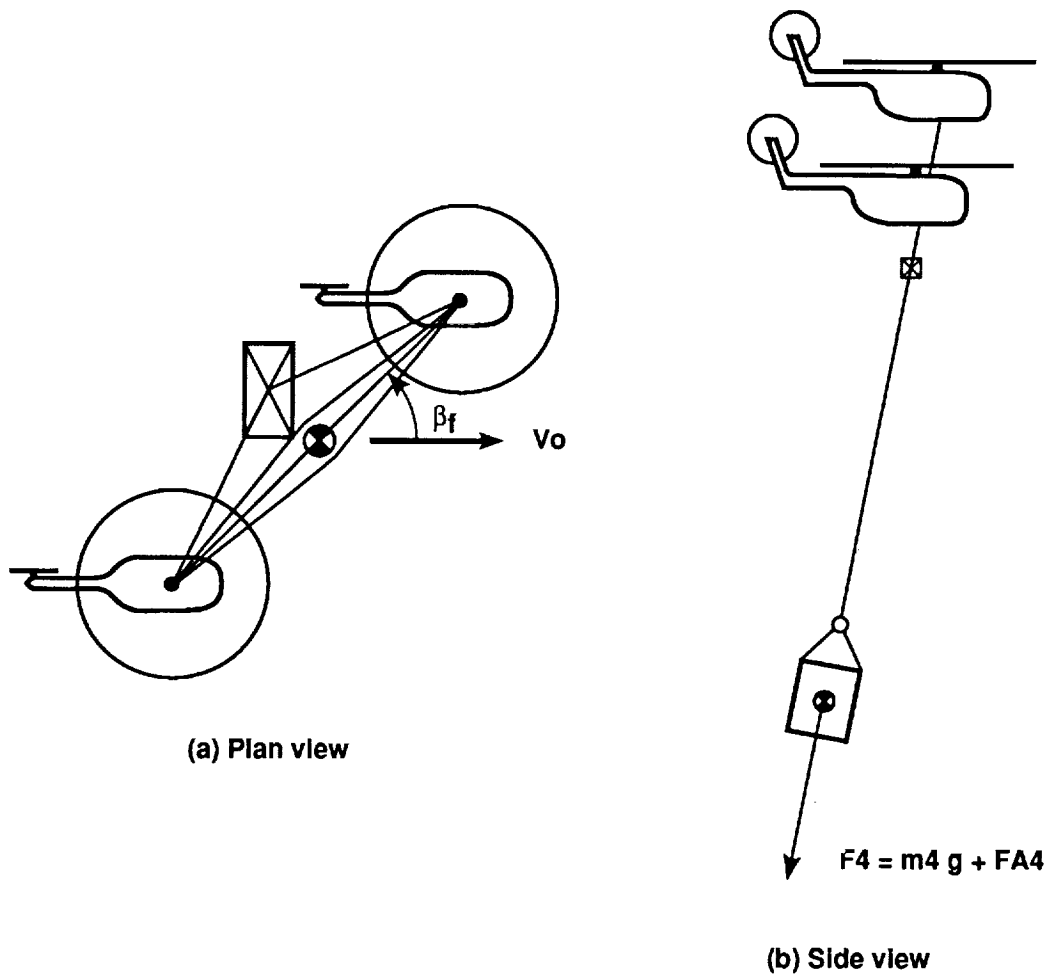


Figure 8. Dual-lift configuration in static equilibrium.

Linearized EOMs for static equilibrium– The LEOMs are listed in part b of table 18, for both the state equation for $(\delta q, \delta u)$ and the second-order differential equation for δq . These repeat equations (46b) and (47), which were obtained by specializing the equations in table 4 for general slung-load systems and general (accelerating) reference flight conditions to static equilibrium and for reference-point coordinates, q, u . The primitive configuration vectors, matrices, and perturbations $va, fba, T, Fb_\delta, Fb_{va}, \delta q, \delta u, \delta \dot{u}$, Δ are defined in section 6. The stability and control derivatives Fb_δ, Fb_{va} are assumed to be given, along with the reference flight condition and the corresponding values of va_o, fba_o, T_o . The matrix, ξ_u , is defined in table 4 and has one nonzero column for static equilibrium and reference-point coordinates (eq. (46a)).

Results for the coefficient matrices of the state equation, M_o, Q_δ, Q'_u, Q_q , for the dual-lift system are given in parts c-h of table 18. These matrices are expanded to a working form; that is, they are partitioned into submatrices corresponding to the subdivision of the coordinates q, u in part a of table 18, and the submatrices are given in terms of natural vectors and matrices using coordinate frames and formulations as they would be found in a working nonlinear simulation based on appendix D. MACSYMA was used to carry out routine matrix product expansions.

Acceleration coefficient matrix– Results for the symmetric acceleration coefficient matrix, $M_o = A_o^T D A_o$ are given in part c of table 18. The matrix M_o^{-1} serves the general function of mapping perturbation forces and moments from $(Q'_u \delta u + Q_q \delta q + Q_\delta \Delta)$ to perturbation accelerations $\delta \dot{u}$. Details of the map describing the sources of effects on each element of $\delta \dot{u}$ are inaccessible analytically but can be given from numerical inverses of M_o in specific cases.

Control term– The control term $Q_\delta \Delta = A_o^T T_o Fb_\delta \Delta$ is given in part d of table 18, and contains all control derivatives. Controls for the two helicopters $\delta 1, \delta 2$ are represented. Load controls are omitted but can be added routinely if these are of interest. The matrix T_o transforms the derivatives of the body axis components of force in Fb_δ to derivatives of their inertial components, and the matrix A_o does bookkeeping on the coordinate frames and takes cross products with moment arms to generate the perturbation moments due to perturbation forces. The vector elements of $Q_\delta \Delta$ and the sum, $Q'_u \delta u + Q_q \delta q + Q_\delta \Delta$ are perturbation forces and moments with units and coordinate frames consistent with the usual listing of

forces and moments in the configuration force vectors fa, fc , etc.

Velocity coefficient matrix– The velocity coefficient matrix Q'_u in part e of table 18, contains all the stability derivatives of the system, along with terms in the reference velocity. The matrix $F_{vaN} = T_o Fb_{va} T_o^T$ transforms Fb_{va} to gradients of the inertial components of the forces relative to the inertial components of the air velocity vectors. Its submatrices are conveniently indicated by the notation $FA1N_{VN}, \dots, MA44_w$ defined in part e of table 18. The matrix A_o in Q'_u does bookkeeping on coordinate frames and applied moment arms. Every submatrix of Q'_u maps an input perturbation from a vector element of δu to an output perturbation force or moment corresponding to the elements of fa , and has units and input-output reference frames consistent with this function. Every column is associated with an element of δu , as indicated in part e of table 18, and this defines the input reference frame and input units for all its submatrices. Every row is associated with an element of $Q_\delta \Delta$, and this defines the output reference frame and output units for all its submatrices.

Position coefficient matrix– The position coefficient matrix Q_q is given as a sum of two parts, $Q1_q$ (part f of table 18), which contains the reference trajectory forces fg, fba_o ; and $Q2_q$ (part g of table 18) which contains a combination of stability derivatives and the reference velocity. The nonzero submatrices of Q_q map angle perturbations from δq to perturbation forces and moments corresponding to the vector elements of fa , and their units and output reference frames are consistent with this function. Each column of Q_q gives the effect of an element from δq ; the reference point position perturbation has no effect on the system motion, and all other elements of δq have a nontrivial effect.

The position coefficient matrix requires the gradients of several configuration vectors containing $A(q), T(q)$, and these entail gradients of coordinate transformations and the matrix BT . A general formula for the gradient of coordinate transformations is given in appendix A. A treatment of the gradient of BT is appended in part h of table 18. This matrix occurs solely in the submatrix A_{47} of A and contributes to the seventh row of $Q1_q$ in the derivatives of μ_{13} , where μ_{13} is a moment due to load external forces, $F4 = m4 g + FA4$, and is given in \mathcal{F}_3 coordinates by

$$\begin{aligned} \mu_{13} &= BT^T T_{t,N} F4_N \\ &= ([j3' j3' + kN k3' \sec \theta_3] R3^* 5 \times F4)_3 \end{aligned}$$

A convenient scalar form is given in part h of table 18. The unit vectors $\{\mathbf{j3}', \mathbf{k3}'\}$ are associated with the spreader bar, and their coordinates in $\mathcal{F}_3, \mathcal{F}_N$ are noted in part h of table 18. The vector, μ_{13} is seen to be a function of the variables $\{\phi_1, \phi_3, \theta_3, \psi_3\}$ from q , and the required derivatives are obtained routinely, and are given in part h of table 18.

For static equilibrium, the reference trajectory forces in Q_{1q} , satisfy

$$\mathbf{F1} + \mathbf{F2} + \mathbf{F3} + \mathbf{F4} = \mathbf{0}$$

where \mathbf{Fi} is the total applied external force on Bi (eq. (38)). This has been used to simplify several submatrices of Q_{1q} . The load and spreader-bar aerodynamics occur only in Q_{17}, Q_{18} in columns 7 and 8, corresponding to $\delta\alpha_3, \delta\alpha_4$. In sufficiently low-speed flight these can be neglected, and most terms in columns 7 and 8 drop out, leaving only load-bar weight effects. An approximate view of the equilibrium forces on each body is given by assuming that the load-bar aerodynamic forces are dominated by drag, and that each helicopter supports its share of the load-bar weight and aerodynamic force:

$$\mathbf{F3} = m_3 \mathbf{g} + \mathbf{FA3} \approx m_3 \mathbf{g} - D_3 \mathbf{iva}$$

$$\mathbf{F4} = m_4 \mathbf{g} + \mathbf{FA4} \approx m_4 \mathbf{g} - D_4 \mathbf{iva}$$

$$\mathbf{L} = \mathbf{F3} + \mathbf{F4} \approx (m_3 + m_4)\mathbf{g} - (D_3 + D_4) \mathbf{iva}$$

$$\mathbf{F1} = m_1 \mathbf{g} + \mathbf{FA1} = -\mathbf{FC1} = -TC1 \mathbf{kc1} \approx -\rho \mathbf{L}$$

$$\mathbf{F2} = m_2 \mathbf{g} + \mathbf{FA2} = -\mathbf{FC2} = -TC2 \mathbf{kc2} \approx -(1-\rho)\mathbf{L}$$

where \mathbf{iva} is the direction of the reference air-velocity vector, $\mathbf{VA0}$; \mathbf{L} is the load to be supported by the two helicopters, and is transmitted to them by means of the tether cable forces, $\mathbf{FC1}, \mathbf{FC2}$; and ρ is the load fraction supported by the helicopter B1. If these are substituted in Q_{1q} , then only the load-bar weight and drag are present. In general, cable forces $\mathbf{FC1}, \mathbf{FC2}$ can include mutually cancelling tugging of the helicopters against each other through the spreader bar, but is not present in the optimized reference configuration assumed in the expressions above. The net external forces on the helicopters are directed opposite the cables in equilibrium. Finally, it is noted that all moments $\mathbf{MA1}, \dots, \mathbf{MA4}$ drop out of the gradient in Q_{1q} . The terms in $Q_{1q} \delta q$ are perturbation forces and moments. A typical perturbation force is illustrated by the contribution from the submatrix in row 2, column 5:

$$T_{c1,N} S(F_{1N}) W_{1N} \delta\alpha_1 = (\mathbf{F1} \times \mathbf{d}\alpha_1)_{c1}$$

$$\mathbf{d}\alpha_1 = \mathbf{i1} \delta\phi_1 + \mathbf{j1}' \delta\theta_1 + \mathbf{kN} \delta\psi_1$$

$$\mathbf{F1} \approx -\rho \mathbf{L}$$

This is seen to be the cable-axis components of the cross product of the net external force on B1 with the total attitude perturbation of B1. The load-bar drag at cruise speeds appears in \mathbf{L} . A typical perturbation moment is illustrated by the contribution from the submatrix in row 5, column 5.

$$-A_{25}^T S(F_{1N}) W_{1N} \delta\alpha_1 = -(\mathbf{R1}^* \mathbf{3} \times (\mathbf{F1} \times \mathbf{d}\alpha_1))_1$$

which is the moment about the c.g. of B1 of the perturbation force described above applied at the tether cable attachment point, $\mathbf{R3}$, and given in \mathcal{F}_1 components.

The second term, Q_{2q} , contains the stability derivatives of all bodies except the reference body, B1, in combination with the reference air-velocity vector, $\mathbf{VA0}$, and is zero in hover. More generally, its terms can be rationalized by forming the vector $Q_{2q} \delta q$. In the result, all terms have the same form; for example, the third element is

$$T_{c2,N} FA_{2N} S(VA_{0N}) [W_{1N} \delta\alpha_1 - W_{2N} \delta\alpha_2]$$

$$= T_{c2,N} FA_{2N} (\mathbf{VA0} \times (\mathbf{d}\alpha_1 - \mathbf{d}\alpha_2))_N$$

$$\approx T_{c2,N} FA_{2N}$$

$$\times [k_N VA_0 \delta(\theta_2 - \theta_1) - j h_N VA_0 \delta(\psi_2 - \psi_1)]$$

where $\mathbf{d}\alpha_1, \mathbf{d}\alpha_2$ are attitude perturbations of B1, B2 as above, \mathbf{jh} is perpendicular to the reference velocity in the horizontal plane, and the expanded approximate result assumes that the body and level-heading axes $\mathcal{F}_1, \mathcal{F}_2, \mathcal{F}_H$ are nearly parallel. The result is an aerodynamic perturbation force due to the perturbation velocities $\mathbf{kN} VA_0 \delta(\theta_2 - \theta_1)$, $\mathbf{jh} VA_0 \delta(\psi_2 - \psi_1)$. All terms in $Q_{2q} \delta q$ similarly consist of aerodynamic perturbation forces and moments from bodies B_i , $i = 2, 3, 4$ due to the perturbation velocities $\mathbf{kN} VA_0 \delta(\theta_i - \theta_1)$, $\mathbf{jh} VA_0 \delta(\psi_i - \psi_1)$, which are perpendicular to the flight path and depend on differences in attitude perturbations from those of the reference body.

Second-order ODE— Finally, the state equation is reduced to the 20 coordinates of the system with inelastic suspensions by deleting the rows of M_o, Q'_u, Q_q, Q_δ and the columns of M_o, Q'_u corresponding to the cable-stretching coordinates of u (scalar coordinates 6, 9, 10, and 12). The second-order ODE for δq is obtained from this result as defined in part b of table 18; that is, M_o, Q'_u are post-multiplied by the block-diagonal matrix, U (part a of table 18).

This modifies the columns of these matrices to convert from the linear cable velocities and angular velocities of $\delta u, \delta \dot{u}$ to the Euler-angle rates of $\delta \dot{q}, \delta \ddot{q}$.

Table 18. Linearized equations of motion for dual-lift system

(a) Coordinates and kinematics:

$$v = \begin{pmatrix} V1^*_N \\ V2^*_N \\ V3^*_N \\ V4^*_N \\ \omega_{11} \\ \omega_{22} \\ \omega_{33} \\ \omega_{44} \end{pmatrix} = A u + w = \begin{pmatrix} T_{N,1} & 0 & 0 & 0 & 0 & 0 & 0 & 0 \\ T_{N,1} & T_{N,c1} & -T_{N,c2} & 0 & A_{25} & A_{26} & A_{27} & 0 \\ T_{N,1} & T_{N,c1} & 0 & 0 & A_{25} & 0 & A_{37} & 0 \\ T_{N,1} & T_{N,c1} & 0 & T_{N,t} & A_{25} & 0 & A_{47} & A_{48} \\ & & & & I & & & \\ & & & & & I & & \\ & & & & & & I & \\ & & & & & & & I \end{pmatrix} \begin{pmatrix} VA1^*_1 \\ \Delta V13_{c1} \\ \Delta V24_{c2} \\ VT_t \\ \omega_{11} \\ \omega_{22} \\ \omega_{33} \\ \omega_{44} \end{pmatrix} + \begin{pmatrix} I \\ I \\ I \\ I \\ 0 \\ 0 \\ 0 \\ 0 \end{pmatrix} W0_N$$

Cable velocity coordinates:

$$T_{c1,N} = E_1(\Delta\phi_{c1}) E_2(\Delta\theta_{c1}) T_{1,N}$$

$$T_{c2,N} = E_1(\Delta\phi_{c2}) E_2(\Delta\theta_{c2}) T_{2,N}$$

$$V13_{c1} = T_{c1,N} \dot{R}13_N = \Delta V13_{c1} - (\mathbf{R}13 \times \omega 1)_{c1}$$

$$V24_{c2} = T_{c2,N} \dot{R}24_N = \Delta V24_{c2} - (\mathbf{R}24 \times \omega 2)_{c2}$$

$$\Delta V13_{c1} = T_{c1,1} \dot{R}13_1 = (\ell_1 \Delta\dot{\theta}_{c1} \cos \Delta\phi_{c1}, -\ell_1 \Delta\dot{\phi}_{c1}, \dot{\ell}_1)^T \quad A_{47} = A_{37} + T_{N,t} BT$$

$$\Delta V24_{c1} = T_{c2,N} \dot{R}24_2 = (\ell_2 \Delta\dot{\theta}_{c2} \cos \Delta\phi_{c2}, -\ell_2 \Delta\dot{\phi}_{c2}, \dot{\ell}_2)^T \quad A_{48} = T_{N,4} S(R4^*5_4)$$

$$VT_t = (\dot{\ell}_3 x, -\dot{\ell}_3 z \dot{\phi}_t, \dot{\ell}_3 z)^T$$

$$BT = -S(R3^*5_t) [j3'_t j3'^T_3 + kN_t k3'^T_3 \sec \theta_3]$$

Submatrices of A:

$$A_{25} = -T_{N,1} S(R1^*1_1 + \ell_1 kc1_1)$$

$$A_{26} = T_{N,2} S(R2^*2_2 + \ell_2 kc2_2)$$

$$A_{27} = -T_{N,3} S(R34_3)$$

$$A_{37} = T_{N,3} S(R3^*3_3)$$

Notes: Scalar elements of BT are given in appendix D, table 14.

$W0$ is the mean wind.

Table 18. Continued.

Generalized position coordinates (inelastic suspension):

$$u = \begin{pmatrix} VA1^*_1 \\ \Delta V13 \bullet ic1 \\ \Delta V13 \bullet jc1 \\ \Delta V24 \bullet ic2 \\ \Delta V24 \bullet jc2 \\ VT \bullet jt \\ \omega_{11} \\ \omega_{22} \\ \omega_{33} \\ \omega_{44} \end{pmatrix} = U(q) \dot{q} = U(q) \begin{pmatrix} VA1^*_1 \\ \Delta \dot{\alpha}c1 \\ \Delta \dot{\alpha}c2 \\ \dot{\phi}_t \\ \dot{\alpha}1 \\ \dot{\alpha}2 \\ \dot{\alpha}3 \\ \dot{\alpha}4 \end{pmatrix}$$

$$\dot{q} = U^{-1} u$$

$$\Delta \alpha c1 = (\Delta \phi_{c1}, \Delta \theta_{c1})^T$$

$$\Delta \alpha c2 = (\Delta \phi_{c2}, \Delta \theta_{c2})^T$$

$$U(q) = \text{diag}\{I, U_{22}, U_{33}, -\ell 3z, W_{11}, W_{22}, W_{33}, W_{44}\}$$

$$U^{-1}(q) = \text{diag}\{I, U_{22}^{-1}, U_{33}^{-1}, -1/\ell 3z, W_{11}^{-1}, W_{22}^{-1}, W_{33}^{-1}, W_{44}^{-1}\}$$

$$U_{22} = \begin{pmatrix} 0 & \ell 1 \cos \Delta \phi_{c1} \\ -\ell 1 & 0 \end{pmatrix}$$

$$U_{33} = \begin{pmatrix} 0 & \ell 2 \cos \Delta \phi_{c2} \\ -\ell 2 & 0 \end{pmatrix}$$

Note: $\{W_{i_i}, W_{i_i}^{-1} \quad i = 1, 2, 3, 4\}$ defined in appendix A, equations (67) and (68)

Table 18. Continued.

(b) LEOMs for static equilibrium:

$$\delta \dot{q} = U_o^{-1} \delta u$$

$$\delta \ddot{u} = M_o^{-1} (Q'_u \delta u + Q_q \delta q + Q_\delta \Delta)$$

or

$$M'_o \delta \ddot{q} - Q'_q \delta \dot{q} - Q_q \delta q = Q_\delta \Delta$$

where

$$M_o = A_o^T D A_o$$

$$Q'_u = A_o^T F_{vaN} A_o - A_o^T D \xi_u$$

$$Q_q = Q1_q + Q2_q$$

$$Q1_q = [\nabla_q^T A^T(q) (fg + fa_o) + A_o^T \nabla_q^T T(q) fba_o]_{q_o}$$

$$Q2_q = A_o^T F_{vaN} [\nabla_q^T (T_o T(q)^T (v_o - w) + A(q) u_o)]_{q_o}$$

$$Q_\delta = A_o^T T_o Fb_\delta$$

$$F_{vaN} = T_o Fb_{va} T_o^T$$

ξ_u : defined in equation (46) for static equilibrium.

and

$$M'_o = M_o U_o$$

$$Q'_q = Q'_u U_o$$

$$U_o = U(q_o)$$

Table 18. (continued)

(c) Acceleration coefficient matrix: $M_o = A_o^T D A_o$:

$$\begin{pmatrix} m_{1234} I & m_{234} T_{1,N} T_{N,c1} & -m_2 T_{1,N} T_{N,c2} & m_4 T_{1,N} T_{N,t} & m_{234} T_{1,N} A_{25} & m_2 T_{1,N} A_{26} & T_{1,N} M_{17} & m_4 T_{1,N} A_{48} \\ m_{234} I & -m_2 T_{c1,N} T_{N,c2} & m_4 T_{c1,N} T_{N,t} & m_{234} T_{c1,N} A_{25} & m_2 T_{c1,N} A_{26} & T_{c1,N} M_{17} & m_4 T_{c1,N} A_{48} \\ m_2 I & 0 & m_4 I & -m_2 T_{c2,N} A_{25} & -m_2 T_{c2,N} A_{26} & -m_2 T_{c2,N} A_{27} & 0 \\ m_4 I & m_4 I & J1 - m_{234} S^2(R1^*3_1) & m_4 T_{t,N} A_{25} & m_2 A_{25}^T A_{26} & m_4 T_{t,N} A_{47} & m_4 T_{t,N} A_{48} \\ J2 - m_2 S^2(R2^*4_2) & J1 - m_{234} S^2(R1^*3_1) & m_2 A_{25}^T A_{26} & m_2 A_{25}^T A_{26} & m_2 A_{26}^T A_{27} & A_{25}^T M_{17} & m_4 A_{25}^T A_{48} \\ 0 & 0 & 0 & 0 & 0 & m_2 A_{26}^T A_{27} & 0 \\ J3 + m_4 A_{47}^T A_{47} & -m_3 S^2(R3^*3_3) & -m_2 S^2(R34_3) & J3 + m_4 A_{47}^T A_{47} & -m_3 S^2(R3^*3_3) & -m_2 S^2(R34_3) & m_4 A_{47}^T A_{48} \\ -m_2 S^2(R4^*5_4) & -m_2 S^2(R4^*5_4) \end{pmatrix}$$

$$m_{234} = m_2 + m_3 + m_4$$

$$m_{1234} = m_1 + m_{234}$$

$$M_{17} = m_2 A_{27} + m_3 A_{37} + m_4 A_{47}$$

Note: $A_{25}, \dots, A_{48}, BT$ defined in part a of table 18.

Table 18. Continued.

(d) Control vector: $Q_\delta \Delta = A_o^T T_o F b_\delta \Delta$:

$$Q_\delta \Delta = \begin{pmatrix} \nabla_{\delta_1}^T F A_{11} \\ 0 \\ 0 \\ 0 \\ \nabla_{\delta_1}^T M A_{11} \\ 0 \\ 0 \\ 0 \end{pmatrix} \Delta_1 + \begin{pmatrix} T_{1,N} \\ T_{c1,N} \\ -T_{c2,N} \\ 0 \\ A_{25}^T \\ A_{26}^T \\ A_{27}^T \\ 0 \end{pmatrix} T_{N,2} \nabla_{\delta_2}^T F A_{22} + \begin{pmatrix} 0 \\ 0 \\ 0 \\ 0 \\ 0 \\ \nabla_{\delta_2}^T M A_{22} \\ 0 \\ 0 \end{pmatrix} \Delta_2$$

Note: Δ_1, Δ_2 = control perturbations for helicopter #1, #2.

Table 18. Continued.

(e) Velocity coefficient matrix: $Q'_u = A_0^T F_{uaN} A_0 - A_0^T D \xi_u$:

$\delta V1^*_1$	$\delta V13_{c1}$	$\delta V24_{c2}$	δVT_i	$\delta\omega1_1$	$\delta\omega2_2$	$\delta\omega3_3$	$\delta\omega4_4$
$T_{1,N} DF1234 T_{N,1}$	$T_{1,N} DF234 T_{N,c1}$	$T_{1,N} C_{13}$	$T_{1,N} C_{14}$	$T_{1,N}(FA1N_\omega + C_{15})$	$T_{1,N} C_{16}$	$T_{1,N} C_{17}$	$T_{1,N} C_{18}$
$T_{c1,N} DF234 T_{N,1}$	$T_{c1,N} DF234 T_{N,c1}$	$T_{c1,N} C_{13}$	$T_{c1,N} C_{14}$	$T_{c1,N} C_{25}$	$T_{c1,N} C_{16}$	$T_{c1,N} C_{17}$	$T_{c1,N} C_{18}$
$-T_{c2,N} FA2NVN T_{N,1}$	$-T_{c2,N} FA2NVN T_{N,c1}$	$-T_{c2,N} C_{13}$	0	$-T_{c2,N}(FA2NVN A_{25} + m_2 SV0)$	$-T_{c2,N} C_{16}$	$-T_{c2,N} FA2NVN A_{27}$	0
$T_{i,N} FA4NVN T_{N,1}$	$T_{i,N} FA4NVN T_{N,c1}$	0	$T_{i,N} C_{14}$	$T_{i,N}(FA4NVN A_{25} + m_4 SV0)$	0	$T_{i,N} FA4NVN A_{47}$	$T_{i,N} C_{18}$
$(MA11VN + A_{25}^T DF234) T_{N,1}$	$A_{25}^T DF234 T_{N,c1}$	$A_{25}^T C_{13}$	$A_{25}^T C_{14}$	$MA11_\omega + A_{25}^T C_{25}$	$A_{25}^T C_{16}$	$A_{25}^T C_{17}$	$A_{25}^T C_{18}$
$C_{61} T_{N,1}$	$C_{61} T_{N,c1}$	$-C_{61} T_{N,c2}$	0	$C_{61} A_{25}$	C_{66}	$C_{61} A_{27}$	0
$C_{71} T_{N,1}$	$C_{71} T_{N,c1}$	$A_{27}^T C_{13}$	$A_{27}^T C_{14}$	$C_{71} A_{25}$	$A_{27}^T C_{16}$	C_{77}	$A_{27}^T C_{18}$
$C_{81} T_{N,1}$	$C_{81} T_{N,c1}$	0	$C_{81} T_{N,t}$	$C_{81} A_{25}$	0	$C_{81} A_{47}$	C_{88}

Submatrices of $F_{uaN} = T_0 F_{ua} T_0^T$

$$FA1NVN = T_{N,1} [\nabla_{VA1}^T, FA1, |T_{1,N} \quad FA1N_\omega = T_{N,1} [\nabla_{VA1}^T, FA1, | \quad MA11VN = [\nabla_{VA1}^T, MA1, |T_{1,N} \quad MA11_\omega = \nabla_{\omega 1,1}^T MA1, |$$

$$\vdots \quad \vdots \quad \vdots \quad \vdots \quad \vdots \quad \vdots \quad \vdots \quad \vdots$$

$$FA4NVN = T_{N,4} [\nabla_{VA4}^T, FA4, |T_{4,N} \quad FA4N_\omega = T_{N,4} [\nabla_{VA4}^T, FA4, | \quad MA44VN = [\nabla_{VA4}^T, MA4, |T_{4,N} \quad MA44_\omega = \nabla_{\omega 4,4}^T MA4, |$$

$$DF234 = FA2NVN + FA3NVN + FA4NVN$$

$$DF1234 = FA1NVN + DF234$$

$$SV0 = T_{N,1} S(VA0_1)$$

$$C_{61} = MA22VN + A_{26}^T FA2NVN$$

$$C_{66} = MA22_\omega + MA22VN A_{26} + A_{26}^T C_{16}$$

$$C_{71} = MA33VN + A_{27}^T FA2NVN + A_{27}^T FA3NVN + A_{27}^T FA4NVN$$

$$C_{77} = MA33_\omega + MA33VN A_{37} + A_{37}^T FA4NVN A_{37} + A_{37}^T (FA3N_\omega + FA3NVN A_{37} + FA3NVN A_{37} + FA3NVN A_{37} + FA4NVN A_{48}$$

$$C_{81} = MA44VN + A_{48}^T FA4NVN$$

$$C_{88} = MA44_\omega + MA44VN A_{48} + A_{48}^T C_{18}$$

Note: $A_{27}, \dots, A_{48}, m_{234}, M_{17}$ defined in parts a and c of table 18

Table 18. Concluded.

(h) Derivatives of μ_{13} : $\partial\mu_{13}/\partial\phi_t$, $\nabla_{\alpha_3}^T \mu_{13}$:

$$\mu_{13} = BT^T T_{t,N} F_{4N} = -[j3'_3 j3_N'^T + k3'_3 kN_N^T \sec\theta_3] S(F_{4N}) T_{N,t} R3^*5_t$$

where:

$$\mathbf{j3}' = -\sin\psi_3 \mathbf{iN} + \cos\psi_3 \mathbf{jN} = \cos\phi_3 \mathbf{j3} - \sin\phi_3 \mathbf{k3}$$

$$\mathbf{k3}' = \sin\phi_3 \mathbf{j3} + \cos\phi_3 \mathbf{k3}$$

then:

$$\partial\mu_{13}/\partial\phi_t = Z1_3$$

$$\nabla_{\alpha_3}^T \mu_{13} = [\frac{\partial\mu_{13}}{\partial\phi_3}, \frac{\partial\mu_{13}}{\partial\theta_3}, \frac{\partial\mu_{13}}{\partial\psi_3}]$$

$$\partial\mu_{13}/\partial\phi_3 = [-j3'_3 kN_N^T \sec\theta_3 + k3'_3 j3_N'^T] \mu_{2N}$$

$$\partial\mu_{13}/\partial\theta_3 = Z2_3 - \sec\theta_3 \tan\theta_3 k3'_3 kN_N^T \mu_{2N}$$

$$\partial\mu_{13}/\partial\psi_3 = Z3_3 + j3'_3 i3_N''^T \mu_{2N}$$

where:

$$\mathbf{i3}'' = \cos\psi_3 \mathbf{iN} + \sin\psi_3 \mathbf{jN}$$

$$\mu_{2N} = S(F_{4N}) T_{N,t} R3^*5_t$$

$$BT1 = j3'_3 j3_N'^T + k3'_3 kN_N^T \sec\theta_3$$

$$[Z1_3, Z2_3, Z3_3] = BT1 S(F_{4N}) T_{N,t} S(R3^*5_t) Wt_t$$

and: $Wt_t = [it_t, j3'_t, kN_t]$ (appendix A, eq. (77))

REFERENCES

1. Feasibility Study for Multiple Helicopter Heavy Lift Systems. Report R-136, VERTOL Aircraft Corp., Philadelphia, Pa. Oct. 1957. (For U.S. Army Applied Technology Laboratory, Ft. Eustis, Va., Contract DA44-177-TC-391.)
2. Maciolek, J. R.: Preliminary Multilift Feasibility Study. Sikorsky Engineering Report SER 64460 (proprietary), Sikorsky Aircraft Co., Stratford, Conn., May 1969.
3. Meek, T.; and Chesley, G. B.: Twin Helicopter Lift System Study and Feasibility Demonstration. Sikorsky Engineering Report SER 64323, Sikorsky Aircraft Co., Stratford, Conn., Dec. 1970. (For U.S. Army Air Materiel Directorate, Ft. Eustis, Va., Contract DAAJ02-70-C-0013.)
4. Carter, E. S.: Implication of Heavy Lift Helicopter Size Effect Trends and Multilift Options for Filling the Need. Proceedings of the 8th European Rotorcraft Forum, Aix-en-Provence, France, Sept. 1982.
5. Cicolani, L. S.; and Kanning, G.: General Equilibrium Characteristics of a Dual-Lift Helicopter System. NASA TP-2615, 1986.
6. Curtiss, H. C.; and Warburton, F. W.: Stability and Control of the Twin Lift Helicopter System. J. Am. Helicopter Soc., April 1985.
7. Curtiss, H. C.: Studies of the Dynamics of the Twin Lift System 1983-1987. MAE TR No. 1840., Department of Mechanical and Aerospace Engineering, Princeton University, Princeton, N.J., Oct. 1988.
8. Cicolani, L. S.; and Kanning, G.: Equations of Motion of Slung Load Systems with Results for Dual Lift. NASA TM-102246, Feb. 1990, Ames Research Center, Moffett Field, CA.
9. Abzug, M. J.: Dynamics and Control of Helicopters with Two-Cable Sling Loads. AIAA Paper 70-929, 1970.
10. Nagabhushan, B. L.: Systematic Investigation of Models of Helicopters with a Slung Load. Ph.D. Thesis, Virginia Polytechnic Institute, Blacksburg, Va., 1977.
11. Prabhakar, A.: A Study of the Effects of an Underslung Load on the Dynamic Stability of a Helicopter. Ph.D. Thesis, Royal Military College of Science, Shrivenham, U.K., 1976. (Also, Paper No. 16, Third European Rotorcraft and Powered Lift Aircraft Forum. Aix-en-Provence, France, Sept. 1977. Also, *Vertica*, vol. 2, 1978, pp. 121-143.)
12. Weber, J. M.; Liu, T. Y.; and Chung, W.: A Math Simulation Model of a CH-47B Helicopter. vols. 1 and 2, NASA TM-84351, 1984.
13. Briczinski, S. J.; and Karas, G. R.: Criteria for Externally Suspended Helicopter Loads. USAAMRDL TR 71-61, U.S. Army Mobility Research and Development Laboratory, Ft. Eustis, Va., Nov. 1971.
14. Shaughnessy, J. D.; Deaux, T. N.; and Yenni, K. R.: Development and Validation of a Piloted Simulation of an Helicopter and External Sling Load. NASA TP-1285, 1979.
15. Sampath, P.: Dynamics of a Helicopter Slung-Load System. Ph.D. Thesis, Department of Aerospace Engineering, University of Maryland, College Park, Md., April 1980.
16. Ronen, T.: Dynamics of a Helicopter with a Sling Load. Ph.D. Thesis, Stanford University, Stanford, Calif., Aug. 1985. (Also, AIAA Paper 86-2288-CP, Williamsburg, Va., Aug. 1986.)

17. Lewis, J.; and Martin, C.: Models and Analysis for Twin Lift Helicopter Systems. American Control Conference, San Francisco, Calif., June 1983. Proceedings of the IEEE, vol. 3, 1983, pp. 1324-1325.
18. Menon, P. K. A.; Schrage, D. P.; and Prasad, J. W. R.: Nonlinear Control of a Twin-Lift Helicopter. AIAA Paper 88-4051-CP, Minneapolis, Minn., Aug. 1988.
19. Mittal, M.: Modeling and Control of a Twin-Lift Helicopter System. Ph.D. Thesis, School of Aerospace Engineering, Georgia Institute of Technology, Atlanta, Ga., Nov. 1991.
20. Mittal, M.; and Prasad, J. V. R.: Input-Output Linearization of a Three Dimensional Model of a Twin-Lift Helicopter System. Paper 91-2754, Proceedings, AIAA Guidance, Navigation and Control Conference, New Orleans, La., Aug. 1991.
21. Prasad, J. V. R.; Mittal, M.; and Schrage, D. P.: Control of a Twin Lift Helicopter System Using Nonlinear State Feedback. J. Am. Helicopter Soc., Oct. 1991.
22. Schiehlen, W. O.; and Kreuzer E. J.: Symbolic Computerized Derivation of Equations of Motion. Dynamics of Multibody Systems, K. Magnus, ed., Springer-Verlag, New York, 1978.
23. Kreuzer, E. J.; and Schiehlen, W. O.: Generation of Symbolic Equations of Motion for Complex Spacecraft Using Formalism NEWEUL. Amer. Astronautical Soc. Advances in the Astronautical Sciences, H. Jacobs, ed., vol. 54, 1983, pp. 21-35.
24. Schiehlen, W. O.: Computer Generation of Equations of Motion. NATO Institute on Computer Aided Analysis and Optimization of Mechanical System Dynamics, E. J. Haug, ed., Springer-Verlag, New York, 1984.
25. Jerkovsky, W.: The Structure of Multibody Dynamics Equations. J. Guidance Control, vol. 1, May 1978, pp. 173-182.
26. Wittenburg, J.: Dynamics of Systems of Rigid Bodies. Teubner, Stuttgart, Germany, 1977.
27. Haug, E. J.: Elements and Methods of Computational Dynamics. NATO Institute on Computer Aided Analysis and Optimization of Mechanical System Dynamics, E. J. Haug, ed., Springer-Verlag, New York, 1984.
28. Schwertassek, R.; and Roberson, R. E.: A Perspective on Computer-Oriented Multibody Dynamical Formalisms and Their Implementations. IUTAM/IFTToMM Symposium on the Dynamics of Multibody Systems, Udine, 1985. Bianchi, W. Schiehlen, ed., Springer-Verlag, New York, 1986.
29. MACSYMA Reference Manual. Mathlab Group, Laboratory for Computer Science, MIT, Cambridge, Mass., Version Ten, vols. 1 and 2, Jan. 1983.
30. Hussain, M. A.; and Noble, B.: Application of Symbolic Computation to the Analysis of Mechanical Systems, Including Robot Arms. NATO Institute on Computer Aided Analysis and Optimization of Mechanical System Dynamics, E. J. Haug, ed., Springer-Verlag, New York, 1984.
31. Lancashire, T.; Lytwyn, R. T., Wilson, G.; and Nording, D.: Investigation of the Mechanics of Cargo Handling by Aerial Crane-Type Aircraft. USAAVLABS Technical Report 66-63, U.S. Army Aviation. Material Laboratory, Fort Eustis, Va., Aug. 1966.
32. Garnett, T. S.; Smith, J. H.; and Lane, R.: Design and Flight Test of the Active Arm External Load Stabilization System. Proceedings of the 32nd Annual National Forum of the American Helicopter Society, May 1976.
33. Asseo, S. J.; and Whitbeck, R. F.: Control Requirements for Slung-Load Stabilization in Heavy Lift Helicopters. J. Am. Helicopter Soc., vol. 18, July 1973, pp. 23-31.

34. Gabel, R.; and Wilson, G. J.: Test Approaches to External Sling Load Instabilities. *J. Am. Helicopter Soc.*, vol. 13, no. 3, July 1968.
35. Bierman, G. J.: Factorization Methods for Discrete Sequential Estimation. Academic Press, New York, 1977.
36. Weber, J. M.; and Grief, R.: A Lagrange-d'Alembert Formulation of the Equations of Motion of a Helicopter Carrying an Externally Suspended Load. NASA TM-85864, 1985.
37. Hess, A. R.; and Tran, M. T.: Pilot/Vehicle Analysis of a Twin Lift Helicopter Configuration in Hover. *JGCD*, Sept. 1988.
38. Rodriguez, A. A.; and Athans, M.: Multivariable Control of a Twin Lift Helicopter System Using the LQG/LTR Methodology. Proceedings of American Control Conference, Seattle, Wash., June 1986, pp. 1325-1332.
39. Cicolani, L. S.; and Kanning, G.: A Comprehensive Estimate of the Static Aerodynamic Forces and Moments of the 8- by 8- by 20-foot Cargo Container. NASA TM-89433, 1987.
40. Kane, T. R.: Dynamics. Third ed., Stanford University, Stanford, Calif., Jan. 1978.
41. Etkin, B.: Dynamics of Atmospheric Flight. Wiley and Sons, New York, 1972.
42. Hutto, A. J.: Qualitative Report on Flight Test of a Two-Point External Load Suspension System. 26th Annual National Forum of the American Helicopter Society, June 1970.
43. Sheldon, D. F.: An Appreciation of the Dynamics Problems Associated with the External Transportation of Loads from a Helicopter. *Vertica*, vol. 1, 1977, pp. 281-290.
44. Kane, T. R.; and Tseng, G.: Dynamics of a Bifilar Pendulum. *Int. J. Mech. Sci.*, vol. 9, 1967, pp. 83-86.

REPORT DOCUMENTATION PAGE			Form Approved OMB No. 0704-0188	
Public reporting burden for this collection of information is estimated to average 1 hour per response, including the time for reviewing instructions, searching existing data sources, gathering and maintaining the data needed, and completing and reviewing the collection of information. Send comments regarding this burden estimate or any other aspect of this collection of information, including suggestions for reducing this burden, to Washington Headquarters Services, Directorate for Information Operations and Reports, 1215 Jefferson Davis Highway, Suite 1204, Arlington, VA 22202-4302, and to the Office of Management and Budget, Paperwork Reduction Project (0704-0188), Washington, DC 20503.				
1. AGENCY USE ONLY (Leave blank)	2. REPORT DATE November 1992	3. REPORT TYPE AND DATES COVERED Technical Publication		
4. TITLE AND SUBTITLE Equations of Motion of Slung-Load Systems, Including Multilift Systems			5. FUNDING NUMBERS 505-66-01	
6. AUTHOR(S) Luigi S. Cicolani and Gerd Kanning				
7. PERFORMING ORGANIZATION NAME(S) AND ADDRESS(ES) Ames Research Center Moffett Field, CA 94035-1000			8. PERFORMING ORGANIZATION REPORT NUMBER A-91099	
9. SPONSORING/MONITORING AGENCY NAME(S) AND ADDRESS(ES) National Aeronautics and Space Administration Washington, DC 20546-0001			10. SPONSORING/MONITORING AGENCY REPORT NUMBER NASA TP-3280	
11. SUPPLEMENTARY NOTES Point of Contact: Luigi S. Cicolani, Ames Research Center, MS 210-3, Moffett Field, CA 94035-1000 (415) 604-5446				
12a. DISTRIBUTION/AVAILABILITY STATEMENT Unclassified-Unlimited Subject Category - 08			12b. DISTRIBUTION CODE	
13. ABSTRACT (Maximum 200 words) General simulation equations are derived for the rigid body motion of slung-load systems. This work is motivated by an interest in trajectory control for slung loads carried by two or more helicopters. An approximation of these systems consists of several rigid bodies connected by straight-line cables or links. The suspension can be assumed elastic or inelastic. Equations for the general system are obtained from the Newton-Euler rigid-body equations with the introduction of generalized velocity coordinates. Three forms are obtained: two generalize previous case-specific results for single-helicopter systems with elastic and inelastic suspensions, respectively, and the third is a new formulation for inelastic suspensions. The latter is derived from the elastic suspension equations by choosing the generalized coordinates so that motion induced by cable stretching is separated from motion with invariant cable lengths, and by then nulling the stretching coordinates to get a relation for the suspension forces. The result is computationally more efficient than the conventional formulation, is readily integrated with the elastic suspension formulation, and is easily applied to the complex dual-lift and multilift systems. Results are given for two-helicopter systems; three configurations are included and these can be integrated in a single simulation. Equations are also given for some single-helicopter systems, for comparison with the previous literature, and for a multilift system. Equations for degenerate-body approximations (point masses, rigid rods) are also formulated and results are given for dual-lift and multilift systems. Finally, linearized equations of motion are given for general slung-load systems are presented along with results for the two-helicopter system with a spreader bar.				
14. SUBJECT TERMS Slung-load equations of motion, Multilift equations of motion, Dual lift, Helicopters			15. NUMBER OF PAGES 132	
			16. PRICE CODE A07	
17. SECURITY CLASSIFICATION OF REPORT Unclassified	18. SECURITY CLASSIFICATION OF THIS PAGE Unclassified	19. SECURITY CLASSIFICATION OF ABSTRACT	20. LIMITATION OF ABSTRACT	